Distribution Agreement

In presenting this thesis or dissertation as a partial fulfillment of the requirements for an advanced degree from Emory University, I hereby grant to Emory University and its agents the non-exclusive license to archive, make accessible, and display my thesis or dissertation in whole or in part in all forms of media, now or hereafter known, including display on the world wide web. I understand that I may select some access restrictions as part of the online submission of this thesis or dissertation. I retain all ownership rights to the copyright of the thesis or dissertation. I also retain the right to use in future works (such as articles or books) all or part of this thesis or dissertation.

_____

Emily L. Hunter Date

IDA3-mediated IFT Transport of the Ciliary Inner Dynein Arm I1

By

Emily L. Hunter
Doctor of Philosophy
Graduate Division of Biological and Biomedical Science
Biochemistry, Cell and Developmental Biology

Winfield S. Sale, Ph.D.

Advisor

Tamara Caspary, Ph.D.

Committee Member

Victor Faundez, MD, Ph.D.

Committee Member

Steven W. L'Hernault

Committee Member

James Q. Zheng

Committee Member

Accepted:

Lisa A. Tedesco, Ph.D.
Dean of the James T. Laney School of Graduate Studies

Date

IDA3-mediated IFT Transport of the Ciliary Inner Dynein Arm I1

By

Emily L. Hunter

B.A. Biology, Connecticut College, 2012

Advisor: Winfield S. Sale, Ph.D.

An Abstract of
A dissertation submitted to the Faculty of the
James T. Laney School of Graduate Studies of Emory University
in partial fulfillment of the requirements for the degree of
Doctor of Philosophy in the Graduate Division of Biological and Biomedical Science
Biochemistry, Cell and Developmental Biology
2018

Abstract

IDA3-mediated IFT Transport of the Ciliary Inner Dynein Arm I1 Dynein
By Emily L. Hunter

Motile cilia, also termed flagella, play a vital role in development, cell signaling, and organ function. The motility of the cilium is dependent upon the conserved axonemal dynein motors that assemble in the cytoplasm prior to transport to the distal tip of the cilium by Intraflagellar Transport (IFT). Defective assembly of the axonemal dyneins results in numerous human diseases including Primary Cilia Dyskinesia (PCD). We are just beginning to understand the key proteins and mechanisms required to assemble and transport ciliary dyneins, as well as other axonemal complexes. Here, I take advantage of the *Chlamydomonas* mutant *ida3* to study the transport and assembly of the conserved inner dynein arm I1/f dynein. The *ida3* mutant properly assembles I1 dynein in the cytoplasm but I1 dynein fails to enter the cilium for assembly in the axoneme, resulting in a slow swimming phenotype. Cryo-ET confirms I1 dynein is the only structural defect present in *ida3* axonemes. From my dissertation work, we now know the *IDA3* gene encodes a conserved ~115kD coiled-coil protein that primarily enters the cilium during ciliary growth. Live-cell imaging and biochemical analyses reveal that during cilium growth, IDA3, along with I1 dynein, is transported by anterograde IFT to the tip of the cilium. At the tip, IDA3 detaches from IFT and diffuses within the ciliary compartment. IFT transport of IDA3 decreases as cilia lengthen and subsides once full-length is achieved. Presence of the I1 dynein cargo is essential to permit processive IFT transport of IDA3 to the distal tip of the cilium. I conclude *IDA3* encodes a highly specialized and transient adapter required to mediate IFT interaction with I1 dynein for entry and transport in the assembling cilium. IDA3 is the first example of an essential and selective IFT adapter that is regulated by ciliary length.

IDA3-mediated IFT Transport of the Ciliary Inner Dynein Arm I1

By

Emily L. Hunter
B.A. Biology, Connecticut College, 2012

Advisor: Dr. Winfield S. Sale

A dissertation submitted to the Faculty of the
James T. Laney School of Graduate Studies of Emory University
in partial fulfillment of the requirements for the degree of
Doctor of Philosophy
in the Graduate Division of Biological and Biomedical Science
Biochemistry, Cell and Developmental Biology
2018

Acknowledgements

I would first like to thank my mentor, Dr. Winfield S. Sale, for providing me the opportunity to complete my dissertation research in his laboratory. Win's mentorship helped me develop into a mature scientist and his presence brings curiosity and fun to the lab daily. Thank you to Dr. Lea M. Alford, for training and mentoring me throughout my graduate career, while simultaneously filling the days with laughter and exceptional stories. Thank you to Dr. Rasagnya Viswanadha for encouraging me daily as a young graduate student. I would like to thank Dr. Juyeon Hwang for always listening to my thoughts on new experiments and reassuring me each time I am skeptical of my results.

I would also like to acknowledge the scientists outside of the Sale Laboratory who have impacted my scientific training. Dr. Victor Faundez, Dr. James Zheng, Dr. Tamara Caspary, and Dr. Steven L'Hernault always provided lively discussion and innovative ideas at each committee meeting. Thank you to Dr. Susan Dutcher for providing me with the *IDA3* gene and numerous *Chlamydomonas* mutants and to Dr. Karl Lechtreck for imaging IDA3 and guiding our experimentation in novel directions. I would like to formally recognize the Kowalczyk Lab and the Faundez Lab for providing me with the liquid nitrogen for my matrix preps each time the departmental supply was depleted.

Finally, I would like to thank my friends and loved ones that have supported me through this journey. Thank you friends for evenings in the swimming pool, nights in Decatur, hikes through the Muir Woods, and the endless amounts of yoga in great company. Most importantly, thank you to my parents who have always supported me. Without my parents, I would not be the woman I am today.

TABLE OF CONTENTS

List of Figures and Tables

Chapter I

Chapter II

Chapter III

Chapter IV

Dissertation Overview

My dissertation focuses on the molecular mechanisms required to assemble the motile cilium, also referred to as the flagellum. I have divided my thesis into four main chapters. Chapter I introduces the motile cilium and includes concepts essential to my dissertation research of *IDA3*. Chapter II narrows the discussion to assembly of the inner dynein arm I1 dynein. Here, I introduce the I1 dynein complex in greater detail and provide a detailed introduction to my *Chlamydomonas* mutant of interest, *ida3*. The chapter is predominately focused around our 2014 publication (of which I am a co-author) that explores the mechanisms required to assemble I1 dynein in the axoneme and provides the first in-depth characterization of the *ida3* mutant. I will then transition in Chapter III to my dissertation research that examines the role of the novel gene *IDA3,* which encodes the IDA3 protein that is required to mediate IFT transport of I1 dynein. Finally, Chapter IV presents the future directions of my dissertation research and a discussion of what I think are the most pertinent questions that must be addressed in the future to further our understanding of ciliary assembly. Materials and methods for all research associated with this dissertation can be found in the materials and methods appendix at the end of this dissertation text.

Chapter I

General Mechanisms of Ciliary Assembly

Chapter I provides a general introduction to the study of the cilium including the importance of the cilium to human health, a general overview of the ultra-structure of the motile cilium, and an introduction to the model organism used throughout my dissertation, *Chlamydomonas reinhardtii*. In addition, I will provide an overview of the discovery and current understanding of Intraflagellar Transport (IFT). I will then narrow the scope of discussion to cargos dependent on IFT for assembly in the axoneme and the mechanisms required to efficiently load cargos onto IFT. The chapter will end with a discussion of the outer dynein arm adapter ODA16 that provided the original frame work for my study of the *Chlamydomonas* mutant *ida3* and shaped our original thinking on the role of adapters in IFT-mediated transport of axonemal cargos. Key methods discussed throughout the introduction that directly relate to my dissertation research include: *Chlamydomonas* dikaryon rescue (particularly dikaryon rescue taking advantage of the *fla10* mutant), generation of *Chlamydomonas* mutants, use of cryo-electron tomography to study the axoneme ultrastructure, flagellar fractionation, and live-cell total internal reflection fluorescence microcopy (TIRF) of IFT proteins and cargos of IFT.

Introduction to the Eukaryotic Cilium

Eukaryotic cilia, also termed flagella, are antenna-like structures that project from most cells in the human body. Cilia, which are either motile or immotile, play essential roles in development, organ function, and cell signaling (Reiter et al., 2017). For example, during development, both motile and immotile cilia are found on the embryonic

node and are essential for determining the left-right axis of the embryo (Grimes et al., 2017; Slough et al., 2008). Motile cilia are required to move mucus out of the lungs and are required in brain ventricles to move cerebral spinal fluids (Spassky et al., 2017). Defective ciliary assembly or motility results in numerous human diseases including Primary Cilia Dyskinesia (PCD), also known as immotile cilia syndrome (Knowles et al., 2016; Reiter et al., 2017). PCD patients exhibit a wide variety symptoms caused by defective ciliary function. These symptoms include, but are not limited to, chronic bronchitis, chronic sinusitis, male infertility, hydrocephalus, situs inversus, and malformation of the heart (harrisHorani et al., 2016).

A pioneering study by Cecilia Lo's Lab at the University of Pittsburgh explored the link between congenital heart defects and mutations in genes that encode ciliary proteins (Klena et al., 2017; Li et al., 2015). In this study, mice exposed to ethylnitrosourea were bred to recover mouse fetuses defective in heart development. By taking advantage of echocardiography, 100,000 mouse fetuses were screened for congenital heart defects, allowing the identification of mutants that normally die prior to term. Intriguingly, a very large number of the mutant mouse lines with heart defects contained mutations in genes that encode ciliary proteins (Li et al., 2015). The genes identified are essential for building and/or transporting essential ciliary complexes or for proper ciliary signaling, such as Wnt, hedgehog, and calcium signaling (Li et al., 2015). Given the vast number of disease-related symptoms and developmental defects that can arise due to defective ciliary assembly and/or motility (Braun et al., 2017; Brown et al., 2014), it is imperative that we expand our understanding of how the cilium is built.

Ultrastructure of the Motile Cilium

The motile cilium can be divided into three main compartments: the microtubule core of the cilium, termed the axoneme, the matrix fraction in which ciliary protein trafficking occurs, and the ciliary membrane which is continuous with the plasma membrane but is unique it it's protein and lipid composition (Fig. 1A (a-c) (Jensen et al., 2017; Pazour et al., 2005). The axoneme of motile cilia is a microtubule-based structure that extends out of the basal body and contains nine peripheral doublet microtubules and two central singlet microtubules that make up the central pair, typically described as the 9 +2 axoneme (Fig. 1B) (Ishikawa, 2013, 2017). The nine peripheral doublet microtubules contain a complete A-tubule made of 13 protofilaments and an incomplete B-tubule comprised of 10 protofilaments (Nicastro et al., 2011). The 9 + 2 microtubule structure provides the scaffold required to bind the axonemal complexes necessary for ciliary motility.

The best-studied axonemal complexes include the outer dynein arms (ODA), the inner dynein arms (IDA), the radial spokes (RS), and the nexin-dynein regulatory complex (N-DRC) (Fig. 1B-C). The outer dynein arm binds the periphery of the doublet microtubules once every 24 nm and is required to provide power and control beat frequency of the cilium (Brokaw et al., 1987; Goodenough et al., 1982; Ishikawa, 2018; King, 2018; King, 2016). While the outer dynein arm is fairly homogeneous in structure, the inner dynein arms are comprised of seven major inner arm dyneins (*a, b ,c ,d ,e ,f/I1,* and *g*) and three minor inner dynein arms that localize to the proximal region of the axoneme and contain unique heavy-chains (DHC3, DHC4, and DCH11) (Kamiya et al., 2014; Piperno et al., 1990; Viswanadha et al., 2017). The inner dynein arms are required

for the proper waveform of the motile cilium (Viswanadha et al., 2017). Together, the inner and the outer dynein arms drive microtubule bending to generate ciliary motility (Satir et al., 2014; Summers et al., 1971). Both the radial spoke and the nexin-dynein regulatory complex are responsible for the regulation of dynein-driven motility (Bower et al., 2013; Porter, 2018; Smith et al., 1992b; Yang et al., 2004). In addition, the nexin-dynein regulatory complex is essential to maintain microtubule integrity during ciliary bending (Alford et al., 2016; Awata et al., 2015; Kubo et al., 2017).

The axonemal components repeat every 96 nm along the length of the cilium (Fig. 1C). In the biflagellate algae *Chlamydomonas reinhardtii,* each 96 nm repeat contains four outer dynein arms, one of each major inner dynein arm, one nexin-dynein regulatory complex, and two radial spokes (Fig. 1C) (Ishikawa, 2013; Nicastro et al., 2006). The 96 nm repeat is defined, in part, by two coiled-coil proteins, FAP59 and FAP172 (Oda et al., 2014a). These proteins appear to positively regulate inner dynein arm and nexin-dynein regulatory complex assembly by providing definitive docking sites (Oda et al., 2014a). In contrast, FAP59 and FAP172 negatively regulate radial spoke binding by blocking radial spoke docking sites that should not be used (Oda et al., 2014a). In addition to these well-defined axonemal complexes, the axoneme also contains microtubule inner proteins (MIPs) of unknown function (Nicastro et al., 2011), docking components required to anchor the large axonemal components to the microtubules such as the outer dynein arm docking complex (ODA-DC) (Owa et al., 2014; Wakabayashi et al., 2001), and regulatory kinases and phosphatases required to regulate dynein activity and subsequent motility (Elam et al., 2011; Gokhale et al., 2009; Porter et al., 2000; Yang et al., 2000). To date, there are still numerous components of

the axoneme that remain uncharacterized. Interestingly, the axoneme alone is sufficient to propagate the bending required for ciliary motility (Gibbons et al., 1972). *In vitro* reactivation studies revealed that in the absence of the ciliary matrix and the membrane, the axoneme can still propagate bends in the presence of ATP (Gibbons et al., 1972). Thus, the axoneme contains all necessary machinery required for ciliary motility.

The matrix is the soluble fraction of the cilium in which directional transport of ciliary proteins such as the axonemal precursors and signaling molecules occurs (Cole, 2003). In order for these ciliary components to enter the cilium, they must pass through a selection barrier at the base of the cilium (Fig. 1A (d)) (Takao et al., 2016). The barrier structure, also termed the transition zone, spans the region between the basal body (Fig. 1A (e)) and the formation of the axoneme proper (Goncalves et al., 2017; Takao et al., 2017). This structure is defined by the presence of microtubules that span from the basal body region to the surrounding membrane, defined as Y-linkers, and a ciliary necklace of unknown function (Goncalves et al., 2017). The barrier structure is believed to regulate which soluble protein complexes enter the ciliary compartment and defects in the transition zone have been tightly linked to various ciliopathies (Garcia-Gonzalo et al., 2017; Shi et al., 2017). At this time, we believe the molecular composition and the mechanical properties of the ciliary barrier are similar to the nuclear pore (Takao et al., 2016). For instance, similar to the nuclear pore, active transport of ciliary proteins into the primary cilium relies on importin-like proteins, a RanGTP/GDP gradient, and ciliary localization signals (Takao et al., 2016). In addition, some nucleoporins (Nups) have been localized to the base of the cilium and may play a role in generating a hydrogel-based barrier (Takao et al., 2016).

We are just beginning to localize individual proteins within the transition zone by taking advantage of super-resolution imaging techniques such as stimulated emission depletion microscopy (STED) (Yang et al., 2015). For example, in the primary cilium CEP290 appears to localize distal to the basal body region while CEP164 localizes to the Y-linkers (Yang et al., 2015). The function of these individual proteins remains unclear. Given the complexity of the axoneme and the ciliary barrier, in addition to the dynamic composition of the ciliary membrane and matrix, we must ask how the cilium is properly assembled and maintained.

Chlamydomonas reinhardtii: A Model System for Study of Ciliary Assembly

For decades scientists have taken advantage of model organisms to understand the function of various cellular components, including individual organelles and proteins. The cilia field has benefited from study of numerous model organisms including *Chlamydomonas*, *Tetrahymena*, *C. elegans*, zebra fish, and mice. For instance, the fluorescent visualization of the Intraflagellar Transport motor kinesin-2 was first performed in *C.elegans* (Orozco et al., 1999).

In addition, human cilia derived from primary cell culture have been studied by immunofluorescence and electron microscopy to localize specific proteins to the cilium and to analyze the ultrastructure of human cilia respectively (Lin et al., 2014; Ostrowski et al., 2011). Still, study of human cilia is restricted by the small quantity of sample available to work with. Biochemical analyses of human cilia are difficult given the small sample size and lack of purity (Alford et al., 2016; Dougherty et al., 2016; Olcese et al., 2017; Wallmeier et al., 2016). In addition, while human patients with mutations that

affect ciliary proteins can be informative (Reiter et al., 2017), study of the function of individual ciliary proteins is challenging. Thus, in order to study the molecular mechanisms required for ciliary assembly, we take advantage of a bi-flagellate green algae *Chlamydomonas reinhardtii*.

The flagellar structure is highly conserved in all eukaryotes including *Chlamydomonas* (Nicastro et al., 2011; O'Toole et al., 2012). A cryo-electron tomography (cryo-ET) study out of Daniela Nicastro's lab in 2014 compared the evolutionary conservation of axonemal structures in *Chlamydomonas, Tetrahymena,* sea urchins, and human (Lin et al., 2014). While some minor differences in axonemal structure were noted, the relative positions of the axonemal components, including the complex arrangement of the inner dynein arms, are highly conserved (Lin et al., 2014). Therefore, study of assembly of *Chlamydomonas* flagella can provide great insight into the molecular mechanisms required to assemble human cilia.

Chlamydomonas is a haploid organism (Harris, 2009). Given *Chlamydomonas* only has a single copy of each gene, it is relatively easy to generate *Chlamydomonas* mutants that are defective in ciliary assembly and/or motility (Pazour et al., 2000b). These mutants can be used to discover conserved genes essential for ciliary assembly and motility in both *Chlamydomonas* and in humans (Ostrowski et al., 2011). Physicians can then use this information to diagnose the cause of patient ciliopathies (Braun et al., 2017; Brown et al., 2014; Reiter et al., 2017). For instance, an analysis of the *Chlamydomonas pf3* mutant revealed the mutant contained a nonsense mutation in the N-DRC protein DRC1 (Wirschell et al., 2013). Given the mutation in DRC1, the inner dynein arms and the nexin-dynein regulatory complex do not assemble, resulting in reduced swimming

speed and abnormal ciliary waveform (Wirschell et al., 2013). The human orthologue of DRC1 is CCDC164. Further analyses revealed a subset of PCD patients contain a mutation in CCDC164. Identical to the *Chlamydomonas pf3* mutant, human patients with mutations in CCDC164 showed defects in both the N-DRC linker and ciliary movement (Wirschell et al., 2013). Study of *pf3* provides one example of how study of *Chlamydomonas* mutants can result in the diagnosis of human ciliopathies. Similar links between *Chlamydomonas* mutants and human ciliopathies include study of *pf23* that is defective in DYX1C1 and results in loss of axonemal dyneins (Tarkar et al., 2013; Yamamoto et al., 2017). As will be discussed in greater detail in Chapter III and IV, IDA3 contains a domain similar to the human protein CCDC24. Analysis of IDA3 may reveal the function of CCDC24 in human tissues and provide insight into how defects in CCDC24 cause PCD.

Identification and characterization of individual *Chlamydomonas* genes is made possible by the versatile experimental techniques that can be applied to both wild-type and *Chlamydomonas* flagellar mutants. For example, whole-genome sequencing of flagellar mutants is used to identify individual genes required for proper ciliary assembly and motility (Lin et al., 2013b; Lin et al., 2015). To further understand the function of these individual genes, biochemical studies can be performed on isolated *Chlamydomonas* flagella. Given *Chlamydomonas* can be grown in large quantities, biochemical analyses of flagella are feasible (Craige et al., 2013). In addition to isolation of flagella, *Chlamydomonas* flagella can be fractionated into axonemes, matrix, and membrane that can then be further fractioned to study individual protein complexes or individual proteins (Kamiya et al., 2014; Pazour et al., 2005).

Through the use of cytoplasmic complementation, termed dikaryon rescue in *Chlamydomonas* studies, we can test whether individual ciliary proteins act in the same pathway to assemble essential ciliary components (Fig. 2 (A-B)) (Dutcher, 2014). While vegetative *Chlamydomonas* cells normally undergo mitotic divisions, *Chlamydomonas* cells can be forced to undergo sexual reproduction when starved of essential nutrients including nitrogen (Dutcher, 2014; Harris, 2009). When cells of the opposite mating type are suspended in nitrogen-free media, the lack of nutrients induces gametogenesis to generate gametes. Gametes of opposite mating type adhere to one another via their flagella and post-shedding of the cell wall, the two cells fuse to generate a single cell containing four flagella, termed a temporary dikaryon (Wilson, 2008). By taking advantage of *Chlamydomonas* flagellar mutants, we can test whether genes defective in ciliary assembly are involved in the same ciliary assembly pathway while also examining the rescue of individual ciliary components in the mutant axoneme. After roughly two hours, the dikaryon will become a diploid zygote that undergoes meiosis to generate a tetrad containing four haploid cells. Mating of cells also allows the isolation of progeny that contain multiple mutations within the same haploid cell. *Chlamydomonas* is also highly amenable to imaging techniques, including super-resolution microscopy studies, live-cell imaging studies, classic electron microscopy, and cryo-electron tomography studies. Specific examples of these techniques in use to study the cilium are both described and referenced throughout the introduction (Chapter I and II) and within my first author publication (Chapter III).

My dissertation research draws on each of the methods described above. Most important to my characterization of IDA3 is the use of live-cell total internal reflection

fluorescence microscopy (TIRF) (Fig. 3) (Engel et al., 2009a; Lechtreck, 2016; Wilson, 2008). By totally internally reflecting the light off the coverslip rather than transmitting the light through the coverslip, the range of fluorophore activation is limited to the first 200 nm of the cell (Lechtreck, 2016). In this way, I was able to visualize IFT transport of IDA3 and IC140 within the ciliary compartment. In addition, I was able to elucidate specific behaviors of IDA3, such as diffusion while in the cilium. As discussed in Chapter III, by combining live-cell TIRF microscopy with dikaryon rescue and analysis of double, triple, and quadruple mutants, I was able to test whether IDA3 requires the axonemal cargo I1 dynein for transport by IFT and whether IDA3 transport is regulated by changes in cilium length or by the need to assemble I1 dynein in the axoneme. Thus, *Chlamydomonas* has been, and continues to be, an important organism for understanding ciliary biology.

The Discovery of Intraflagellar Transport (IFT)

In the 1960s and 1970s Joel Rosenbaum and George Witman pioneered study of ciliary assembly in *Chlamydomonas* (Rosenbaum et al., 1967; Rosenbaum et al., 1969; Witman, 1975). In 1969, Rosenbaum began an examination of flagellar elongation and shorting in *Chlamydomonas* (Rosenbaum et al., 1969*)*. *Chlamydomonas* cells were deflagellated and allowed to regenerate to half-length prior to addition of radio-labeled protein precursors. Cilia then regenerated to full-length and light-microscopy audioradiography was used to determine the distribution of labeled proteins within the cilium. Approximately 70% of the labeled proteins were at the distal half of the cilium, providing the first clue that during assembly of the cilium new material is added at the

distal tip of the axoneme. These results were further confirmed in 1975 by George Witman in which he found 65 % of ^{3}H acetate incorporates into the distal segment of the axoneme during regeneration (Witman, 1975).

In 1992, studies of ciliary assembly in *Chlamydomonas* were refined to focus on the assembly of individual axonemal components (Johnson et al., 1992). A HA-tagged tubulin cell line was mated to wild-type cells containing half-length cilia to generate a dikaryon containing two full-length HA-tagged flagella and two regenerating cilia that could incorporate HA-tagged tubulin. The localization of HA-tagged tubulin was stained with an antibody against HA and was visualized by immunofluorescence. HA-tagged tubulin incorporated at the distal tip of the cilium, consistent with previous studies. In addition to tubulin, radial spoke assembly was also examined by mating wild-type cells to the *Chlamydomonas pf14* mutant which is defective in the assembly of the radial spoke in the axoneme. Radial spoke assembly in the *pf14* flagella of the temporary dikaryon was visualized by immunofluorescence using an antibody against RSP3. RSP3 incorporated into the radial-spoke deficient axonemes in a tip-down fashion, thus suggesting axonemal components are transported to the tip of the cilium prior to assembly in the axoneme. In related experiments using dikaryon rescue, we also determined that the radial spokes are transported to the tip of the cilium before assembly in the axoneme (Alford et al., 2013). As discussed in Chapter II and III, we also took advantage of dikaryon rescue to determine ciliary dyneins are transported to the tip of the cilium before docking in the axoneme (Viswanadha et al., 2014).

If axonemal components are transported to the tip of the cilium prior to assembly in the axoneme, there must be some type of transport machinery responsible for moving

axonemal complexes to the tip of the cilium. In 1992, Kozminski et al., first defined and characterized the machinery required for the transport of axonemal cargos to the distal tip of the cilium (Kozminski et al., 1995). Paralyzed *Chlamydomonas* flagellar mutants were examined by differential interference contrast microscopy (DIC) to visualize the bi-directional movement of particle-like structures within the cilium. The movement they observed was much faster than previously recorded speeds for gliding (0.6 +/- 0.2 μm/s) or for the movement of polystyrene beads along the membrane (1.1 +/- 0.5 μm/s) (Bloodgood, 1995) and the speed was dependent on the direction of movement (2.0 +/- 0.5 μm/s base to tip; 3.5 +/- 0.7 μm/s tip to base) (Kozminski et al., 1995). The authors speculated this newly identified movement, which they termed Intraflagellar Transport (IFT), was responsible for the movement of tubulin and large axonemal complexes to the tip of the cilium for assembly in the axoneme. In addition, given the differences in IFT speed depending on the directionality of the movement, the authors predicted two distinct motors would be involved in IFT transport and speculated kinesin would be a key motor to explore in the future.

Now, 25 years after the discovery of IFT, we have a detailed picture of the IFT machinery and the role IFT plays in assembling the cilium. The particles observed moving from base to tip of the cilium by DIC were Intraflagellar Transport complexes, also termed IFT trains. The IFT complexes are comprised of at least twenty-two individual proteins that can be broken into the IFT sub-complexes A, B1, and B2 (Fig. 4 A-B) (Cole et al., 1998; Taschner et al., 2012; Taschner et al., 2016b). The IFT A complex is comprised of six individual IFT proteins (IFT44, IFT40, IFT39, IFT22, IFT121, and IFT43) (Fig. 4A). The IFT B1 complex is comprised of nine IFT proteins

(IFT88, IFT81, IFT74, IFT70, IFT52, IFT46, IFT27, IFT25, and IFT22 (Lucker et al., 2005; Taschner et al., 2014). IFT172, IFT80, IFT57, IFT54, IFT20, and IFT38 comprise the IFT B2 complex (Fig. 4B) (Taschner et al., 2014). IFT components that are integral to the assembly of IFT trains are termed core IFT components, while IFT proteins that are not required for IFT complex assembly and overall function, and are more commonly involved in binding cargos of IFT, are termed peripheral IFT components (Behal et al., 2012; Lechtreck, 2015; Lechtreck et al., 2017; Lucker et al., 2005). IFT proteins are comprised of protein-protein interaction domains including WD, tetratricopeptide (TPR) repeats and coiled-coils (Behal et al., 2012; Taschner et al., 2014). Some of these domains are required for IFT proteins to interact with each other while some binding sites are used to bind the cargos of IFT such as the axonemal complexes (Taschner et al., 2014). While the 15-subunit IFT-B complex has been assembled *in vitro* from recombinant proteins, *in vivo* isolation of the IFT complexes has not been accomplished, likely due in part to the dynamic interactions between IFT particles (Taschner et al., 2016a). My study of IDA3 reveals that in addition to interactions found amongst IFT proteins, there are also transient IFT adapters that bind IFT under specific circumstances such as during ciliary growth. Given the transitory and dynamic nature of IFT protein interactions, it is highly unlikely that all IFT components have been identified at this time.

In place of biochemical analyses, scientists have turned to live-cell imagining of individual IFT proteins to better understand the mechanisms of IFT assembly and transport. Pioneering studies in *C. elegans* sensory cilia revealed the potential of live-cell imaging for study of IFT by imagining transport of Kinesin-2::GFP (Orozco et al., 1999).

By taking advantage of live-cell imagining, the Lechtreck lab at the University of Georgia has now shown that IFT proteins form into sub-complexes localized to precise territories of the basal body region for final assembly into a complete IFT train (Wingfield et al., 2017). The IFT A and IFT B-2 complexes are recruited first, followed by IFT B-1. Finally, kinesin-2, the motor responsible for anterograde IFT transport to the distal tip of the cilium (Cole et al., 1998; Walther et al., 1994), is attached to the IFT complex. Thus, IFT train formation in the cytoplasm is dependent upon a spatial and temporal organization of IFT proteins within the basal body pool (Wingfield et al., 2017).

Once assembled, the IFT train, transported by kinesin-2, enters and is transported to the distal tip of the cilium (termed anterograde IFT transport) (Fig. 5 (a)) (Engel et al., 2009a; Engel et al., 2009b). Individual IFT proteins tagged with GFP have now been visualized in transit using both time-lapse fluorescent microscopy and live-cell total internal reflection fluorescence microscopy (Engel et al., 2009a). Use of live-cell imagining to study IFT transport in *Chlamydomonas* began in 2005 when the bi-directional movement of GFP-tagged kinesin-associated protein (KAP), the non-motor subunit of the kinesin-2 motor, was visualized (Engel et al., 2009b; Mueller et al., 2005). Soon after, both GFP::IFT27 and GFP::IFT20 were visualized (Engel et al., 2009a; Qin et al., 2007). The rate of anterograde transport of GFP::KAP, GFP::IFT27, and GFP::IFT20 was consistent with the rate of IFT transport visualized by DIC (Engel et al., 2009a). While GFP::IFT27 and GFP::IFT20 use retrograde IFT to return to the cell body, fluorescent imagining of GFP::KAP revealed kinesin diffuses through the cilium rather than being transported by retrograde IFT (Chien et al., 2017; Engel et al., 2009a). Thus, live-cell imaging of IFT particles opened a new avenue to study the intricacies of IFT

behavior, allowing analysis of the behavior and function of individual IFT proteins. Numerous studies including my own, which will be discussed further in succeeding chapters, have taken advantage of live-cell imaging to show that IFT is essential to transport axonemal components to the distal tip of the cilium for incorporation in the axoneme (Craft et al., 2015; Wren et al., 2013). These studies will be discussed in greater detail below.

In the absence of anterograde IFT transport, the cilium cannot assemble (Brazelton et al., 2001; Jonassen et al., 2008; Pazour et al., 2000a). The *bld1* mutant in *Chlamydomonas* for instance is defective in IFT52 and thus does not assemble cilia since IFT cannot transport the necessary components to the tip of the cilium (Brazelton et al., 2001). In addition to playing an essential role in ciliary assembly, anterograde IFT is also required to transport ciliary signaling machinery, such as components of the Hedgehog and Wnt pathways (Bangs et al., 2017; He et al., 2017). Retrograde IFT, driven by the cytoplasmic dynein 1b/2 (Lechtreck et al., 2009; Lechtreck et al., 2013; Pazour et al., 1998; Pazour et al., 1999; Porter et al., 1999), transports ciliary components from the distal tip of the cilium back into the cell body (Fig. 5b). Not only does retrograde transport export ciliary proteins from the cilium in order to maintain protein homeostasis but retrograde IFT is also likely required to remove non-ciliary proteins that may have accidently diffused through the ciliary barrier (Lechtreck et al., 2009; Lechtreck et al., 2013; Pazour et al., 1999; Porter et al., 1999) and required for Hedgehog signaling (Wu et al., 2017).

Anterograde and retrograde trains are roughly the same length (233 nm and 209 nm respectively) but are distinct in their appearance by electron microscopy (Stepanek et

al., 2016). Anterograde trains appear as short electron dense trains whereas retrograde trains are less condensed and show a less regular architecture (Stepanek et al., 2016). Stalled trains, which for unknown reason have stopped mid-transit along the axoneme, are longer (650 nm in length) and resemble what had previously been defined as long trains (Stepanek et al., 2016). With anterograde, retrograde, and stalled trains transiting the axoneme at the same time, it is hard to imagine IFT train collisions do not occur. In 2016, Gaia Pigino's lab adapted an innovative technology known as the Correlative Light and EM Approach (CLEM) to further study IFT in *Chlamydomonas* cilia. For this method, GFP-tagged IFT trains in *Chlamydomonas* were first imaged by TIRF microscopy to determine the directionality of the train. Cells would then be immediately fixed with glutaraldehyde and imaged by 3D electron microscopy. Fixed trains could then be cross-referenced with TIRF kymograms to determine the directionality of the trains observed by EM (either anterograde, retrograde, or stalled). Based on this study, anterograde and retrograde trains avoid collision by using different microtubule tracks. Anterograde trains use the B-microtubule and retrograde trains use the A microtubule. While our understanding of IFT has advanced greatly over the past two decades, we still do not understand how IFT trains recognize and bind specific cargos of IFT or the precise role IFT plays in regulating cilium length.

Intraflagellar Transport and Length Regulation of the Cilium

How cilium length is determined remains an open-ended question. The original balance point model proposed by Marshall and Rosenbaum in 2001 predicted that the rate of flagellar assembly is length dependent (Marshall et al., 2001). Therefore, the

flagellum would be maintained at full-length when the rate of assembly of the cilium is equivalent to the rate of disassembly of the cilium. One way to regulate the rate of assembly and disassembly is to regulate the number of IFT trains in transit at any given time. The initial phase of flagellar regeneration is rapid and gradually slows as the cilium lengthens (Craft et al., 2015; Marshall et al., 2005). Therefore, based on this observation, we would predict a large number of IFT trains are present in the cilium early in regeneration and less IFT trains are present in the full-length cilium. In contrast to this prediction, the number of IFT trains present in the cilium at any given times remains constant, regardless of the length of the cilium (Dentler, 2005; Marshall et al., 2001; Marshall et al., 2005). Therefore, as the cilium lengthens, the number of IFT trains and the rate of IFT movement remains the same. In 2009, Engel and Marshall proposed a revised balance point model to take into account the observation that IFT train size appeared to vary (Engel et al., 2009b). Although the total amount of kinesin-2 and IFT remains relatively constant regardless of the cilium length, Engel and Marshall suspected the IFT proteins were redistributed into a greater number of small trains as the cilium lengthens, thereby reducing the rate at which the flagellum assembles.

As will be described in greater detail in the following section, our understanding of ciliary length regulation was drastically changed in 2013 when the Lechtreck lab determined ciliary length is in part regulated by the amount of cargo transported by IFT (Wren et al., 2013). Therefore, while IFT remains constant during ciliary growth, large quantities of IFT-cargo (i.e. axonemal components) are transported early on during ciliary growth (Craft et al., 2015; Wren et al., 2013). The quantity of cargo transported decreases linearly over time as the cilium lengthens (Craft et al., 2015; Wren et al., 2013).

Thus, a differential cargo-loading model of length regulation was proposed in which cells, by unknown mechanisms, sense the presence of truncated cilia. In response, the cells increase the quantity of cargo loaded onto IFT particles until the cilium reaches full length (Craft et al., 2015; Wren et al., 2013).

The Cargos of Intraflagellar Transport (IFT)

Given there are no ribosomes within the eukaryotic cilium, the axonemal components must be synthesized in the cytoplasm prior to IFT transport into and within the cilium for assembly at the distal tip of the axoneme (Fig. 5) (Pazour et al., 2005; Piperno et al., 1997; Rosenbaum et al., 1969). For example, the outer dynein arm assembles into a 2 mDa complex in the cytoplasm while the inner dynein arm I1 assembles into a 1.5 mDa complex (Fowkes et al., 1998; Viswanadha et al., 2014). The radial spoke assembles into 12S radial spoke complex in the cytoplasm prior to entry into the cilium where it matures into a 20S radial spoke complex (Diener et al., 2011; Qin et al., 2004). In the *Chlamydomonas* cilia field, cytoplasmic assembly of the large axonemal complexes is known as pre-assembly to distinguish it from axonemal assembly, also termed docking.

Prior to live-cell imagining, identification of axonemal cargos dependent on IFT for assembly in the axoneme was difficult and relied heavily on the temperature sensitive *Chlamydomonas* mutant *fla10* (Huang et al., 1977). The *FLA10* locus encodes the kinesin-homologue protein KHP1 (Kozminski et al., 1995; Walther et al., 1994). In the *fla10* mutant, a single base transversion results in a temperature sensitive kinesin motor domain. At 21°C, the *fla10* kinesin motor is functional whereas at 32°C the *fla10* kinesin

motor can no longer function and Intraflagellar Transport comes to a halt (Kozminski et al., 1995; Walther et al., 1994). In 1996, Piperno and colleagues took advantage of the *fla10* mutant in combination with dikaryon rescue to test whether the inner and outer dynein arms require the kinesin motor to assemble in the axoneme (Piperno et al., 1996). For this analysis, *ida4; fla10* and *oda2; fla10* double mutants were generated. The *ida4* mutant is null for the inner dynein arm light chain p28 while the *oda2* mutant is defective in the outer dynein arm heavy chains. Thus the *ida4; fla10* double does not assemble the inner dynein arms while the *oda2; fla10* double lacks the outer dynein arms along the length of the axoneme. Both cell types contained the temperature-sensitive *fla10* kinesin mutation. Each double was mated to the *fla10* mutant to generate temporary dikaryons. At the permissive temperature the *fla10* kinesin motor is functional and thus the inner and outer dynein arms assemble into the *ida4; fla10* and *oda2; fla10* flagella as expected. In contrast, when dikaryons were held at the restrictive temperature the inner dynein arms failed to assemble into the *ida4; fla10* flagella while the outer dynein arm still assembled on the *oda2; fla10* flagella in the absence of the kinesin motor. Using the requirement of the kinesin motor as an indicator of IFT transport, the authors concluded the inner dynein arms require IFT for transport and assembly in the axoneme while the outer dynein arm does not. Given we now know the outer dynein arm does require IFT for entry through the barrier into the cilium, it is likely the *fla10* mutant retained some residual activity at the restrictive temperature during experimentation (Wang et al., 2006).

The *fla10* mutant also proved useful for biochemical studies designed to define cargos of IFT. For instance, in order to determine whether the radial spoke relied on IFT to be transported to the distal tip of the cilium, the membrane-matrix from regenerating

wild-type *Chlamydomonas,* in addition to the membrane-matrix from *fla10* at permissive temperature and *fla10* at restrictive temperature, was isolated and fractionated on a 10-20% sucrose density gradient (Qin et al., 2004). In both wild-type membrane-matrix and *fla10* membrane-matrix isolated at the permissive temperature, the 12S radial spoke precursor was present. In comparison, the 12S radial spoke complex was not detected in the membrane-matrix isolated from *fla10* cilia at the restrictive temperature. Therefore, the radial spoke precursor is also reliant on the kinesin motor and IFT for entry into the ciliary compartment. Other IFT cargos in the wild-type membrane-matrix fraction were revealed by analyses that detected axonemal protein interactions with IFT components (Qin et al., 2004). In these analyses, kinesin, dynein heavy chain (DHC1B), various IFT subunits, RSP1, IC69, IC140, and acetylated tubulin were all detected by co-IP. Thus, the radial spoke, the outer dynein arm, the inner dynein arm I1, and acetylated tubulin interact with IFT in the matrix of the cilium, suggesting each component is an IFT cargo.

While the *fla10* mutant and immunoprecipitation analyses provided indirect evidence of the axonemal cargos transported by IFT, live-cell TIRF microscopy provided the methodology necessary to visualize the transport of individual IFT cargos in live cells. In 2013, the Lechtreck lab visualized IFT transport of the nexin-dynein regulatory complex protein DRC4 (Wren et al., 2013). GFP-tagged DRC4 and mCherry-tagged IFT20 were expressed in *pf2,* a DRC4 null mutant. Using live-cell TIRF microscopy coincident transport of DRC4::GFP and IFT20::mCherry was visualized moving towards the tip of the cilium at 1.9 μm/s. Once transported to the tip of the cilium by anterograde IFT, DRC4::GFP typically lingers at the tip for roughly 1.7 seconds before diffusing throughout the cilium and eventually docking to the axoneme. The dwell time at the tip of

the cilium is likely due to IFT-train remodeling that permits the detachment of DRC4 from the IFT train (Wren et al., 2013). At times, DRC4::GFP could be visualized returning to the cell body along with IFT-mCherry at 3 μm/s but in general, turnover of DRC4::GFP within the axoneme is rare indicating the axoneme is a highly stable structure with little turnover. In addition to analyzing IFT-mediated transport of DRC4::GFP within the cilium, the authors also examined DRC4 entry into the ciliary compartment. Soluble non-ciliary proteins up to roughly 40 kD in size can enter the cilium by diffusion (Kee et al., 2012). For instance the ciliary membrane proteins phospholipase D, roughly 25 kD in size, and SAG1, which is 65 kD in size, are not dependent on IFT-mediated entry into the cilium (Belzile et al., 2013; Lechtreck et al., 2013). Surprisingly, proteins up to 650 kD have been observed diffusing into the cilium at a slow rate (Lin et al., 2013c). DRC4::GFP is dependent on IFT-mediated transport to efficiently enter the cilium. While DRC4::GFP could be observed diffusing through the cilium in the absence of IFT, eighteen times less DRC4::GFP enters the cilium in comparison to IFT-mediated entry of the DRC4::GFP. Thus, efficient entry of DRC4::GFP and transport to the distal tip of the cilium for assembly in the axoneme depends on IFT. DRC2::GFP and PF16::GFP, which is a central pair protein, were also visualized and are also dependent on IFT-mediated transport for assembly in the axoneme (Wren et al., 2013).

As described previously, the number of IFT trains transported at any given times remains constant regardless of cilium length (Dentler, 2005; Marshall et al., 2001; Marshall et al., 2005). The live-cell imagining of DRC4::GFP provided new insight into the regulation of IFT cargo loading in full-length and regenerating cilia. The data

described below is crucial to our understanding of IDA3 behavior in steady-state versus regenerating cilia. In steady-state cilia, 0.65 DRC4::GFP particles were imaged per minute while approximately 60 particles of IFT20::mCherry were imaged per minute in the steady-state cilia. Thus, less than one percent of IFT trains carry DRC4::GFP as a cargo. Retrograde transport of DRC4::GFP cargo in full-length cilia is also rare with less than 0.1 particles per minute carrying DRC4::GFP. In contrast, DRC4::GFP is transported in much higher quantities in regenerating cilia with on average 8.4 particles of DRC4::GFP being transported per minute. In the early phase of regeneration when the cilium less than approximately 5 μm in length, fifteen DRC4::GFP particles are transported per minute. As the cilium lengthens the quantity of DRC4::GFP decreases linearly with flagellar length. Given these observations, the differential cargo-loading model was proposed. By unknown mechanisms, a cell can sense a truncated cilium and respond by loading increased quantities of ciliary cargos onto IFT for transport into the cilium. As the cilium lengthens, less cargo is required resulting in the linear decrease in cargo quantity over time until the cilium reaches full-length (Wren et al., 2013).

In a subsequent paper, the Lechtreck lab showed tubulin is also a cargo of IFT and that the quantity of tubulin transported is regulated by ciliary length (Craft et al., 2015). In addition, transport of tubulin by IFT is regulated independently in each of the two cilia. For example, GFP-tagged tubulin expressing cells were mechanically sheared to generate a subset of cells that contained one full-length cilium and one short regenerating cilium. These long-short cells were then visualized by TIRF microscopy to determine if the increase in tubulin transport by IFT occurred in both cilia or solely in the cilium that was in the process of regenerating. Within the short cilium, 20.5 particles of tubulin were

transported per minute while IFT only transported 3.3 particles of tubulin per minute in the full-length cilium. This difference in particle transport per minute decreases as the short cilium elongates until the short and long cilium each transport equivalent quantities of tubulin. Thus, cargo loading onto IFT is regulated in a cilium-autonomous manner. As will be discussed in Chapter III, IDA3 transport is also regulated in a cilium-autonomous manner, though IDA3 is not an axonemal component.

At this time little is known in regard to how the cell is able to distinguish the short and long cilium and selectively increase cargo loading on trains destined to enter the growing cilium. Likely regulatory kinases and phosphatases play a key role in transmitting feedback to the cell body regarding cilium length (Hilton et al., 2013; Nguyen et al., 2005; Tam et al., 2003; Tam et al., 2013). How does the cell increase the quantity of cargo loaded onto IFT? Does each IFT train carry a single cargo or does each train carry a number of axonemal complexes at one time? How can a complex of roughly 22 proteins bind a vast array of unique cargos in varying quantities? While the answers to these questions remain largely unknown, study of IDA3 provides insight into how IFT binds specific cargos. This concept will be further developed in Chapters III and IV.

Cargo Interaction with IFT: Direct Binding to IFT and the Use of IFT Adapters

Over the past decade, numerous cargos of IFT have been identified including the outer and inner dynein arm, the radial spoke, the central pair protein PF16, tubulin and the N-DRC (Lechtreck, 2015). In addition to axonemal cargos of IFT, transmembrane proteins such as the TRP calcium channel transmembrane protein PKD2-like and numerous signaling factors including the Shh signaling proteins GliA and GliR have been

shown to also be dependent on IFT transport (Haycraft et al., 2005; Huangfu et al., 2003; Lechtreck, 2015; Liu et al., 2005). Given the large number of distinct IFT cargos that are required to bind IFT, we must ask how the IFT complex is able to bind such a vast array of protein complexes. Cargos that must be transported in great abundance likely have direct binding sites to the IFT proteins (Lechtreck, 2015). For instance, tubulin has been shown to bind directly to IFT through both IFT81 and the N-terminal region of IFT74 (Fig. 6 (a)) (Bhogaraju et al., 2013; Kubo et al., 2016).

Less abundant protein complexes appear to require specialized adapter proteins to effectively bind IFT. Ciliary adapter proteins define a class of proteins that are essential to mediate interaction between specific cargos and IFT but may not be integral to the assembly of the IFT complex or to the overall function of IFT in terms of building the cilium (Lechtreck et al., 2009). The concept of cargo adapters is not unique to the cilium. For example, cytoplasmic dynein is essential for transport of endosomes, peroxisomes, lipid droplets, RNA, and mitochondria (Cianfrocco et al., 2015). In order to transport this vast array of cargos, the dynein motor relies on cargo adapters to link the various cargos to the dynein motor (Cianfrocco et al., 2015; Fu et al., 2014; Huynh et al., 2017; McKenney et al., 2014; Schroeder et al., 2016). Cargo adapter proteins include BICD2, Hook3, Snapin, and RILP (Cianfrocco et al., 2015; Fu et al., 2014) and typically these proteins contain long coiled-coil domains that likely permit both the dynein motor and the cargo to interact. Adapter proteins are also required for vesicle transport in neurons. For instance, axonal transport of Syntaxin 1 is mediated by a kinesin-1 adapter known as FEZ1 (Chua et al., 2012). Interestingly, FEZ1 binding to kinesin is mediated by phosphorylation (Chua et al., 2012). As will be discussed in Chapter IV, phosphorylation

of IDA3 may be critical for IDA3 attachment to IFT. Thus, the use of adapters to permit and regulate cargo binding to molecular motors is highly conserved throughout the cell.

One of the first defined ciliary cargo adapters was the BBSome (Eguether et al., 2014; Klink et al., 2017; Lechtreck et al., 2009; Lechtreck et al., 2013; Liew et al., 2014; Liu et al., 2018). Defects in the BBSome proteins can result in Bardet-Biedl Syndrome (BBS) that results in blindness, kidney abnormalities, and obesity (Sheffield, 2004). While the BBSome proteins had been linked to IFT transport in *C.elegans,* loss of the BBSome protein BBS4 in *Chlamydomonas* does not influence IFT train assembly or assembly of the cilium (Lechtreck et al., 2009). Coincident transport of IFT20::mCherry and BBS4::GFP was visualized by live-cell TIRF microscopy confirming the BBSome is transported by IFT (Lechtreck et al., 2009). Taken together with the fact the *bbs4-1 Chlamydomonas* mutant shows no defect in IFT train assembly or overall function, the BBSome is not an integral IFT component. Notably, the BBS4 protein, indicative of the BBSome complex, is only transported on a subset of IFT trains (Lechtreck et al., 2009). In addition, we now know the BBSome is required for the retrograde transport of the signaling proteins phospholipase D type c (PLD), single-domain hemoglobin (THB1), and serine/threonine protein kinase (STPK) (Lechtreck et al., 2009; Lechtreck et al., 2013). Thus given the BBSome is not integral to overall IFT train assembly and is sporadically transported on IFT trains to remove specific signaling proteins from cilium, the BBSome is defined as an IFT-adapter (Fig. 6(b)) (Lechtreck et al., 2009).

In contrast to the BBSome that is required for the retrograde transport of a number of cargos, the ODA16 adapter is specifically required for IFT transport of the outer dynein arm (Fig. 6(c)) (Desai et al., 2018). ODA16, a WD-repeat protein of 449 amino

acids, shares homology with the zebrafish protein Wdr69 (Gao et al., 2010). In the absence of ODA16, roughly 10-20 % of the outer dynein arms are randomly assembled along the length of the axoneme (Ahmed et al., 2005; Ahmed et al., 2008). In addition, immunofluorescence analyses of the *oda16 Chlamydomonas* mutant revealed there is a higher quantity of outer dynein arms present in the cytoplasm of the *oda16* mutant than in the cytoplasm of wild-type cells (Ahmed et al., 2008). This result was further confirmed through immunoblot analyses (Ahmed et al., 2008). The authors hypothesized the increase in outer dynein arm protein in the cytoplasm is due to the lack of outer dynein arm transport and assembly in the *oda16* axoneme. What role does the ODA16 protein play in assembling the outer dynein arm in the axoneme?

In order to elucidate the role ODA16 plays in outer dynein arm assembly, the Mitchell lab first asked whether the *oda16* axoneme was competent to bind to the outer dynein arm. To test this idea, the outer dynein arms were purified from wild-type axonemes under high salt conditions and incubated with *oda16* axonemes (Ahmed et al., 2008). Wild-type outer dynein arms successfully bound the *oda16* axonemes in this *in vitro* reconstitution analysis, thus removing the possibly there is an outer dynein arm docking defect in the *oda16* mutant.

Alternatively, the outer dynein arm could be defective in cytoplasmic pre-assembly in *oda16* mutants. As previously mentioned, many of the axonemal components, including the outer dynein arm and radial spoke, have been shown to assemble into megadalton-sized complexes in the cytoplasm prior to transport into the cilium by IFT (Fowkes et al., 1998; Qin et al., 2004). If the outer dynein arm were not fully assembled in the *oda16* cytoplasm, the outer dynein arm would be unable to

assemble in the axoneme. To test this hypothesis, the outer dynein arm heavy chain (ODA-HCβ) was immunoprecipitated from *oda16* cytoplasmic extract using an anti-ODA-HCβ monoclonal antibody (Ahmed et al., 2008). Within the *oda16* cytoplasm, the outer dynein arm complex contained all major subunits and was presumed to be fully assembled.

While fully assembled, it is also possible the pre-assembled outer dynein arm must be modified in some way to dock the axoneme. Surprisingly, the pre-assembled *oda16* outer dynein arm is fully capable of binding outer-dynein arm deficient axonemes *in vitro* (Ahmed et al., 2008). Therefore, the outer dynein arm is fully assembled in the cytoplasm of *oda16* and can dock the axoneme. Thus, the protein defective in the *oda16* mutant must be extrinsic to the outer dynein arm complex, is not required for ODA pre-assembly in the cytoplasm, and is not an outer dynein arm docking component (Ahmed et al., 2008).

By immunofluorescence microscopy, ODA16 predominately localizes to the basal body region at the base of the cilium and sporadically along the length of the cilium (Ahmed et al., 2008). Biochemical fractionation of the cilium also shows that ODA16 is present within the matrix of the full-length cilia (Ahmed et al., 2005). The localization of ODA16 is reminiscent of IFT proteins and the kinesin motor and does not appear to co-localize with the outer dynein arm in the cytoplasm or the axoneme (Ahmed et al., 2008). Thus, the authors predicted ODA16 was associated with IFT machinery.

To test this hypothesis, full-length flagella were isolated from both wild-type and the *fla10*^{ts} mutant grown at the restrictive temperature. If ODA16 were a component of IFT, a decrease in ODA16 protein should be detectable in the flagella of the *fla10*^{ts} mutant

grown at the restrictive temperature. Indeed, while the quantity of the ODA detected in the *fla10* flagella was consistent with the quantity in wild-type flagella, the quantity of ODA16 detected within the flagellum decreased in the *fla10*^{ts} mutant at restrictive temperature (Ahmed et al., 2008). ODA16 therefore depends on IFT transport to enter the cilium. In addition, immunoprecipitation analyses revealed a direct or indirect interaction of ODA16 with IFT proteins. However, though required for outer dynein arm assembly, ODA16 does not co-IP with the outer dynein arm. Instead, based on a yeast-2-hybrid analysis, the ODA16 protein interacts with IFT46 of the IFT B1 complex (Ahmed et al., 2008). In addition, a separate study examining the function of individual IFT proteins found IFT46 is required for the assembly of the outer dynein arms (Hou et al., 2007). Recent studies show that ODA16 binds directly to the N-terminal 147 residues of the IFT46 protein and that the IFT46-ODA16 interaction is very strong (Fig. 6(c)) (Taschner et al., 2017). In addition, IFT46 is required for ODA16 transport (Hou et al., 2017). These data suggest that ODA16 is an IFT adapter required to efficiently transport the outer dynein arm through the transition zone into the cilium (Ahmed et al., 2008). These results are in contrast to the results of Piperno et al. in which the outer dynein arm did not required the kinesin motor to enter the cilium and assemble in outer dynein arm-deficient axonemes of *oda2fla10*^{ts} x *fla10*^{ts} temporary dikaryons (Piperno et al., 1996). It is now predicted that a minor amount of residual IFT transport continues at the restricted temperature (Wang et al., 2006). Given the outer dynein arm is not reliant on transport to the tip of the cilium for assembly in the axoneme, the minor amount of IFT activity could account for the outer dynein arm assembly in the *fla10*^{ts} at restrictive temperature (Ahmed et al., 2008; Wang et al., 2006). Notably, in contrast to other adapters including IDA3

(see Chapter III), ODA16 remains associated with IFT in all conditions in wild-type cells (Ahmed et al., 2005; Ahmed et al., 2008). Thus, ODA16 may be a component of IFT rather than an IFT adapter. This distinction will be discussed further in Chapter IV.

Addressing Novel Questions: IDA3 and I1 Dynein Assembly

The discovery of IFT was critical to the study of ciliary assembly. In 25 years of study, our understanding of IFT and the assembly of the cilium has been greatly enhanced by live-cell and super resolution microscopy in addition to cryo-electron tomography. Though we have a general understanding of IFT and the critical role this transport plays in ciliary assembly, many unanswered questions remain. For example, we have a limited understanding of how cargo is loaded onto IFT. Is there a mechanism that generally regulates cargo-IFT interaction? Alternatively, is each cargo of IFT regulated independently to allow precise loading and transport of specific IFT cargos? If the ability of a cargo to bind IFT is regulated independently of other cargos, how does this regulation occur and does this mechanism play a role in cilium length regulation?

To further our understanding of cargo-IFT interactions, I have focused my study on the transport and assembly of the highly conserved inner dynein arm I1/f dynein. As will be described in the following chapters, I have determined the I1 dynein complex requires a highly-specialized and transient adapter, IDA3, to bind IFT, enter the ciliary compartment and be transported to the tip of the cilium for assembly in the axoneme (Fig. 6(d)). IDA3 differs from the previously defined IFT adapters in that IFT-mediated transport of IDA3 is regulated by cilium length. We now propose that each axonemal

complex likely requires a highly specialized and transient adapter to bind IFT for entry and transport within the cilium.

Figures Chapter I

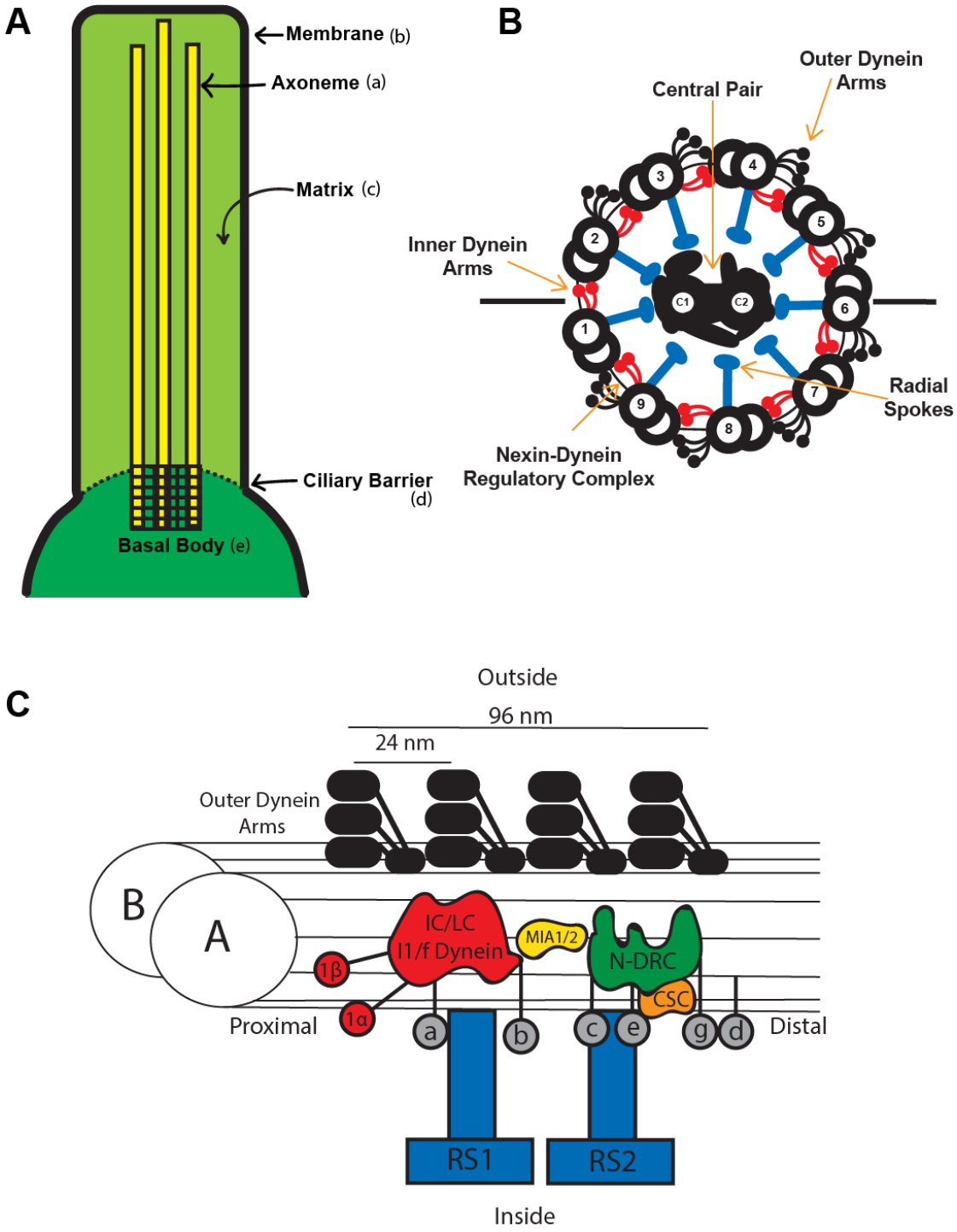

Figure 1. Ultrastructure of the motile cilium.

(A) General components of the motile cilium. The cilium is comprised of three main compartments. **(a)** The axoneme, represented in yellow **(b)** The outer membrane. This membrane is continuous with the cell membrane but is unique in protein and lipid composition. **(c)** The matrix defines the soluble compartment of the cilium in which trafficking of ciliary proteins occurs. The ciliary barrier **(d)** restricts the proteins permitted into the cilium and is located just above the basal body region **(e)**. **(B)** The 9+2 cross-section of the motile cilium defined by nine outer doublet microtubules and two central pair microtubules. Axonemal components represented include the central pair, outer dynein arms, radial spokes, the nexin-dynein regulatory complex, and the inner dynein arms (orange arrows). **(C)** Schematic of the axonemal complexes organized in the 96 nm repeat. Key to this dissertation, I1/ f dynein binds in the proximal most position of the 96 nm repeat (red).

A

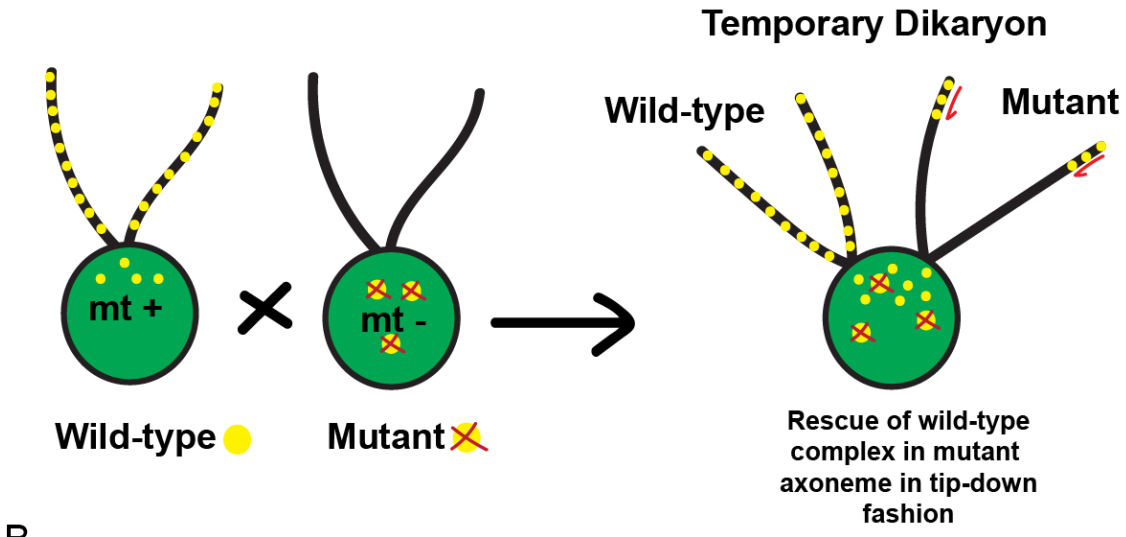
Temporary Dikaryon
Wild-type
Mutant
mt +
mt -
Wild-type
Mutant
Rescue of wild-type complex in mutant axoneme in tip-down fashion

B

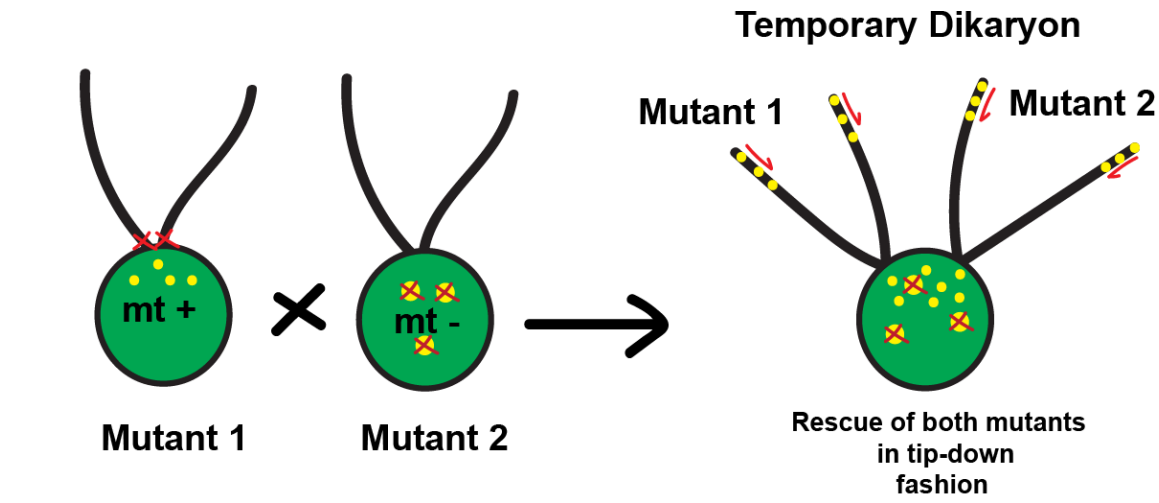
Temporary Dikaryon
Mutant 1
Mutant 2
mt +
mt -
Mutant 1
Mutant 2
Rescue of both mutants in tip-down fashion

Figure 2. Dikaryon rescue in *Chlamydomonas reinhardtii*

(A) In *Chlamydomonas reinhardtii,* cytoplasmic complementation studies are termed dikaryon rescue. In terms of ciliary assembly, dikaryon rescue can be used to determine if *Chlamydomonas* mutants contains mutations in independent pathways. In this example, wild-type *Chlamydomonas* assembles an axonemal component (yellow dots). The *Chlamydomonas* mutant cannot assemble this component (yellow dots and red X). When mated, cells fuse to create a single cell with shared cytoplasm and four flagella. The wild-type axonemal component will be transported into the mutant flagella and assemble into the axoneme in a tip down fashion (indicated by red arrows beginning at the distal tip of the cilium and moving towards the cell body). **(B)** Example of dikaryon rescue with two *Chlamydomonas* mutants. Both Mutant 1 and Mutant 2 are defective in the assembly of the same axonemal complex (yellow). Upon formation of dikaryons, the axonemal complex assembles in all four flagella indicating the mutations in each mutant act in independent assembly steps. If the mutants were unable to complement, the mutants would likely be defective in the same axonemal assembly step.

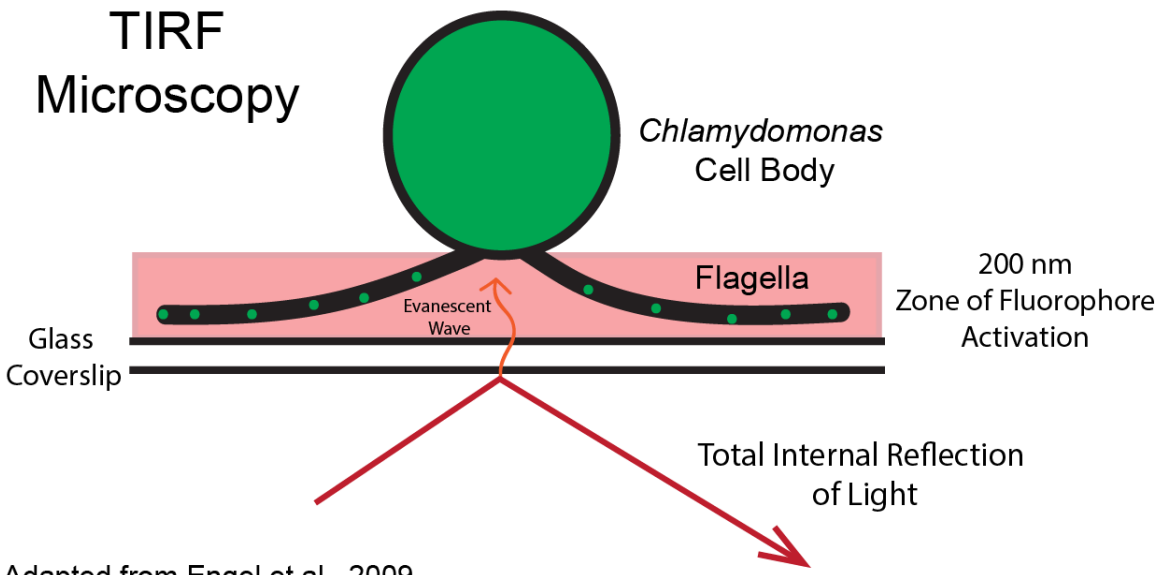

Adapted from Engel et al., 2009

Figure 3. TIRF Microscopy using *Chlamydomonas*

Total Internal Reflection Fluorescence Microscopy is used to activate and visualize fluorescently tagged proteins that appear at the surface of cells. To perform TIRF, light is totally internally reflected off of a glass coverslip, generating an evanescent wave that decays exponentially as it travels into the sample. This permits the activations of fluorophores within a restricted region of the cell (~ 200 nm in depth). Because *Chlamydomonas* flagella naturally lay flat again glass coverslips, fluorescent proteins within the flagella will be activated by the evanescent wave, while fluorescent proteins in the cytoplasm will remain inactivated. Additionally, this method prevents *Chlamydomonas* auto-fluorescence, allowing the visualization of IFT transport of IFT proteins and cargos of IFT.

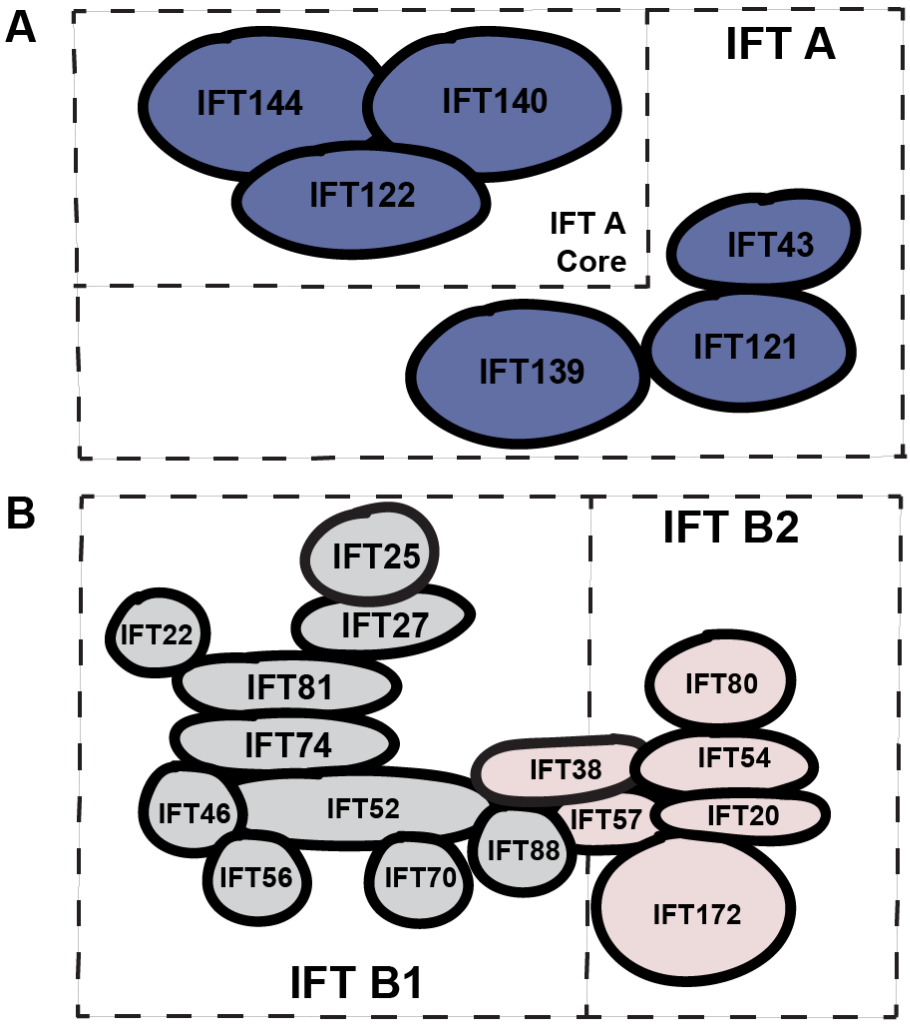

Adapted from Mourão et al., 2016

Figure 4. Composition of the IFT complex

(A) IFT A composition (purple IFT proteins). The IFT A core is comprised of IFT144, IFT40, and IFT122. The remainder of IFT A included IFT139, IFT121, and IFT43. **(B)** IFT B composition. IFT B is divided into sub-groups IFT B1 (gray) and IFT B2 (pink). Determining which IFT proteins interact directly continues to be difficult and most models remain speculative.

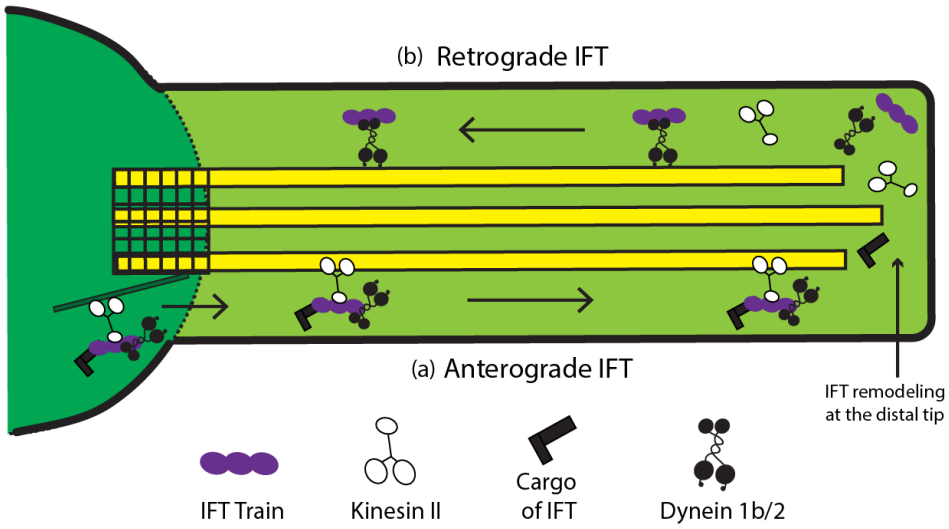
(b) Retrograde IFT
(a) Anterograde IFT
IFT remodeling
at the distal tip
IFT Train
Kinesin II
Cargo
of IFT
Dynein 1b/2

Figure 5. Intraflagellar Transport in *Chlamydomonas reinhardtii*.

(a) Anterograde IFT moves ciliary components from the cytoplasm to the distal tip of the cilium. Anterograde IFT is driven by the kinesin-2 motor. Anterograde IFT particles carry numerous IFT cargos including axonemal components and the retrograde IFT motor Dynein 1b/2. **(b)** IFT complexes are re-organized at the distal tip of the cilium where IFT cargos are released. IFT particles bind the activated Dynein 1b/2 motor, and return to the cell by retrograde IFT. The kinesin-2 motor diffuses throughout the cilium and eventually re-enters the cell body.

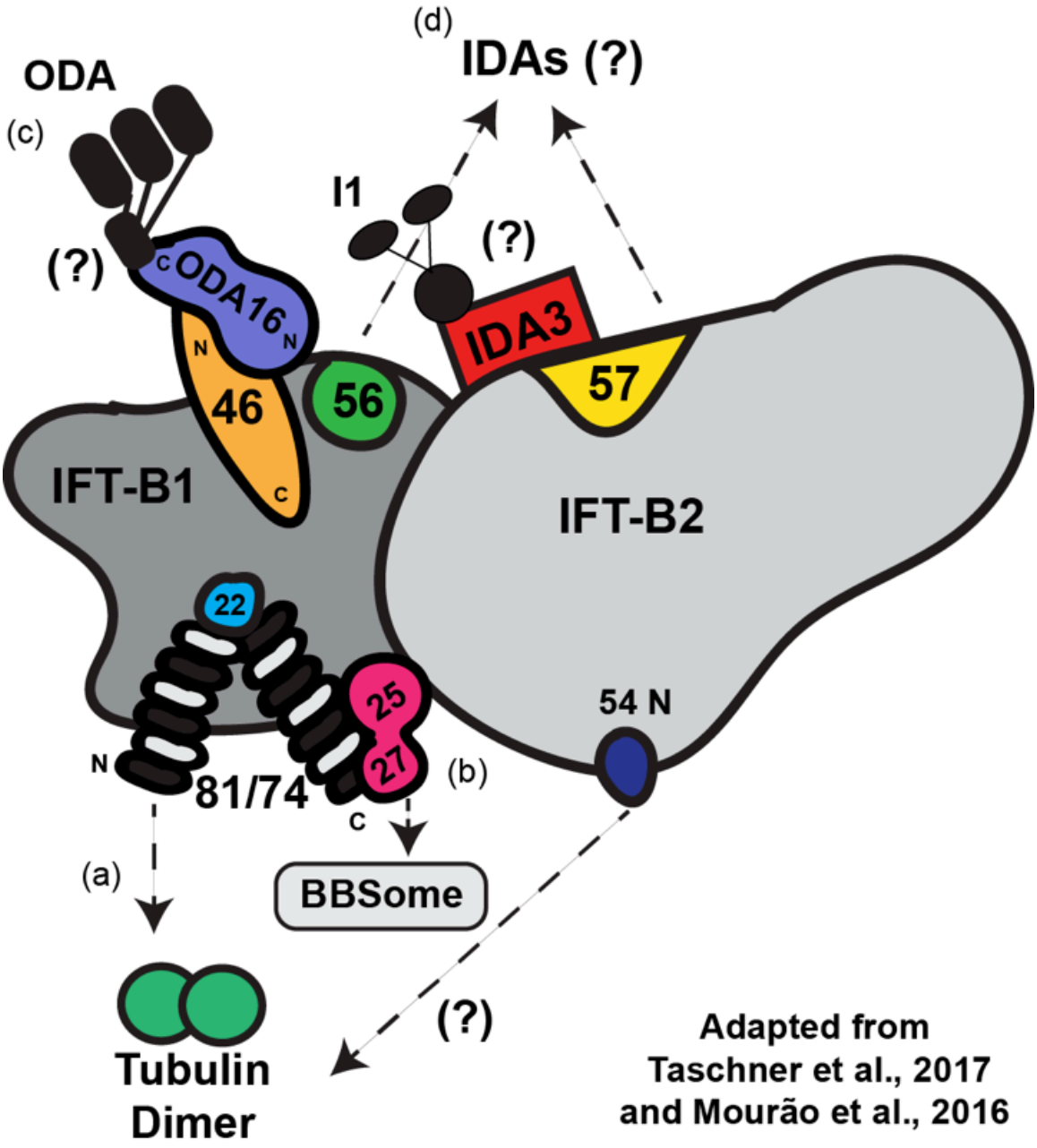
(d)
IDAs (?)
ODA
(c)
I1
(?)
(?)
C ODA16 N
IDA3
N
46
56
57
IFT-B1
C
IFT-B2
22
25
54 N
N
81/74
27
(b)
C
(a)
BBSome
(?)
Tubulin
Dimer
Adapted from
Taschner et al., 2017
and Mourão et al., 2016

Figure 6. Model of known and potential IFT cargo binding sites
(a) Tubulin has been shown to bind directly to IFT81 and IFT74. Tubulin may also bind IFT54. **(b)** The BBSome is believed to bind through IFT25 and IFT27. **(c)** The outer dynein arm binds the IFT adapter ODA16 that in turn binds IFT46. **(d)** The inner dynein arms are predicted to bind IFT through IFT57 and IFT56. We predict IDA3 may interact with IFT57 to transport the I1 dynein complex

Chapter II

Study of inner dynein arm assembly

In this chapter, I will first provide an overview of the I1 dynein complex. My discussion will then shift to focus on the assembly of I1 in the cytoplasm and in the axoneme. The bulk of the chapter stems from a study on I1 dynein assembly performed by Dr. Rasagnya Viswanadha, a previous graduate student in the lab, and myself. Only the figures most crucial to my study of IDA3 are included in this chapter. Additional data described in this chapter can be found in Viswanadha et al., 2014.

Here, we discover I1 dynein assembles into a 1.5 mDA complex in the cytoplasm that is transported by IFT to the distal tip of the cilium for assembly in the axoneme. In the *Chlamydomonas* mutant *ida3*, I1 dynein cannot enter the cilium preventing assembly in the axoneme. Complementation studies amongst various I1 dynein *Chlamydomonas* mutants suggest IC140, one of the I1 dynein light chains, and the protein defective in *ida3* interact. Overall, Chapter II sets the stage for my study of the *Chlamydomonas ida3* mutant and discovery of the function of IDA3 in I1 dynein assembly.

The I1/f Dynein Complex

As described in Chapter I, defective assembly of axonemal components including the ciliary dyneins, results in primary cilia dyskinesia (PCD) (Knowles et al., 2013; Kurkowiak et al., 2015; Zariwala et al., 2011). My dissertation focuses specifically on the transport and assembly of the inner dynein arm I1/f dynein. I1 dynein is a highly conserved inner dynein arm required for normal control of bending (Bayly et al., 2010; Brokaw et al., 1987; VanderWaal et al., 2011; Wickstead et al., 2007). *Chlamydomonas*

mutants defective in I1 dynein assembly in the axoneme, such as *ida7, ida1,* and *ida3,* swim slowly due to abnormal ciliary waveforms and also exhibit defects in the ability to phototax (Wirschell et al., 2007).

I1 dynein is the only two-headed inner arm dynein (Piperno et al., 1990). I1 localizes to the proximal most region of the 96 nm repeat just adjacent to radial spoke 1 (one of the two radial spoke species found in *Chlamydomonas*) (Fig. 1C) (Heuser et al., 2012; Nicastro et al., 2006; Porter et al., 1992; Smith et al., 1992a; Yamamoto et al., 2013) and this localization is conserved through humans (Lin et al., 2014). Once docked in the axoneme, I1 makes contact with the outer dynein arm, the neighboring inner dynein arms, the A-tubule, the N-DRC, and the uncharacterized tether structure (Fig. 1C) (Bui et al., 2009; Bui et al., 2012; Heuser et al., 2012; Nicastro et al., 2006). In the *Chlamydomonas* I1 dynein mutants, loss of I1 in the axoneme results in a periodic gap once every 96 nm along the length of the axoneme (Kamiya et al., 1991). The specific loss of the I1 dynein complex from the axoneme in the I1 mutants suggests I1 is targeted independently of other axonemal components including the other single-headed inner dynein arms (Kamiya et al., 1991; Piperno et al., 1990; Smith et al., 1992a). I1 dynein, like other large axonemal complexes such as the outer dynein arms and radial spokes, is assembled in the cytoplasm prior to transport within the cilium (Piperno et al., 1990; Smith et al., 1991; Viswanadha et al., 2014). The 20S I1 dynein complex is comprised of 2 heavy chains (1α and 1β), three intermediate chains (IC140, IC138, IC97), and six light chains (Tctex1, Tctex2b, LC7a, LC7b LC8, FAP120) organized in a stable two-headed complex (Fig. 7) (Kotani et al., 2007; Smith et al., 1992a; Toba et al., 2011; Wirschell et al., 2007).

When we began our study of I1 dynein assembly, very little was known. Aside from the observation that IC140 co-immunoprecipitated with IFT172 from the matrix of growing cilia (Qin et al., 2004), evidence of the location of I1 dynein assembly or transport did not exist. As discussed further below, a founding observation was discovery that I1 dynein preassembles in the cytoplasm as a 20S complex with the same composition as I1 dynein isolated from the axoneme (Viswanadha et al., 2014). Thus, we suspected the 20S I1 dynein complex requires IFT to enter the cilium and be transported to the distal tip of the cilium. To test this hypothesis, we first took advantage of dikaryon rescue to determine if I1 dynein is transported to the tip of the cilium prior to assembly in the axoneme (Viswanadha et al., 2014). The dikaryons were generated by mating wild-type cells to either *ida3* or *ida7* I1 dynein mutants. The *ida7* mutant is defective in IC140 and this defect prevents assembly of the 20S I1 dynein complex in the cytoplasm. The *ida3* mutant, the focal point of my dissertation, does not assemble I1 in the axoneme due to a loss of the IDA3 adapter required for I1 dynein transport. (The nature of the IDA3 adapter will be explored further in Chapter III and IV.) Temporary dikaryons were fixed for immunofluorescence at 30, 60, and 90 minutes post-formation. The fixed dikaryons were stained for both IC140 to mark I1 dynein incorporation in the axoneme and the outer dynein arm intermediate chain IC69 (now termed IC2) used to visualize the length of all four cilia of the dikaryons. Based on our analyses, I1 dynein is transported to the tip of the cilium and assembles in a tip down fashion over the course of 90 minutes (Fig. 8) (Viswanadha et al., 2014).

Further taking advantage of dikaryon rescue, we mated various I1 dynein mutants to determine if the genes defective in each I1 dynein mutant were in the same I1 dynein

assembly pathway. When we mated the *ida3* x *ida1*, (*ida1* is a mutant containing a mutation in DHC1 (Kamiya et al., 1991; King et al., 1997; Myster et al., 1997)), rescue of I1 dynein assembly in the axoneme occurred at the same rate as I1 dynein assembly in wild-type x *ida3* (Fig. 9A). Thus, the defects in *ida3* and *ida1* are independent and therefore able to compliment when the cytoplasm of each cell type fuse. In contrast, when we mated *ida3* to *ida7*, (*ida7* is a null mutation in IDA7 that encodes IC140) rescue of I1 assembly in the axoneme occurred at a slower rate (Fig. 9A) (Viswanadha et al., 2014). Furthermore, protein translation is not required for rescue of I1 dynein assembly in wild-type x *ida3*, wild-type x *ida7*, or wild-type x *ida1* dikaryons but is required to rescue I1 dynein assembly in the *ida3* x *ida7* dikaryon (Fig. 9B). To date, it is unclear why the *ida3* x *ida7* dikaryon requires translation to rescue I1 dynein assembly. Initially we believed the IDA3 protein was unstable in the absence of IC140 and therefore must be translated in order for the two cell types to complement. As will be discussed in Chapters III and IV, we now know IDA3 is stable in the absence of IC140. Therefore, an additional, unidentified protein must be unstable in both the *ida7* and *ida3* mutants, suggesting both IC140 and IDA3 are required to stabilize this unidentified protein. In addition, this unidentified protein must be required to transport and assembly I1 dynein in the axoneme. Pull-down analyses of IDA3 and IC140 from regenerating matrix followed by mass spectrometry will be critical to identifying this unknown player in I1 dynein transport and assembly.

We next predicted IDA3 is transported by IFT to reach the distal tip of the cilium. Originally, we aimed to use live-cell TIRF imagining to visualize IC140::GFP movement towards the distal tip of *ida7; IC140::GFP* cilia. Unfortunately, our *ida7; IC140::GFP*

transformants isolated at the time expressed low levels of IC140::GFP making it difficult to imaging I1 dynein transport. As an alternative approach, we examined whether I1 dynein undergoes tip-down assembly in the absence of the anterograde IFT kinesin motor by taking advantage of the *fla10*^{ts} mutant. As described previously, at restrictive temperature the *fla10* kinesin motor ceases to function, halting anterograde IFT (Kozminski et al., 1995; Walther et al., 1994). Therefore, for this experiment we generated an *ida3; fla10*^{ts} double mutant. This mutant was mated to *fla10*^{ts} to give rise to temporary dikaryons at both the *fla10*^{ts} permissive and restrictive temperatures. In this way, we could ask whether I1 dynein tip-down assembly continues to occur in the absence of anterograde IFT.

As expected, I1 dynein assembly was rescued in the *ida3; fla10*^{ts} axonemes of *ida3; fla10*^{ts} x *fla10*^{ts} dikaryons held at 21°C (Viswanadha et al., 2014) (Fig. 10A-B). In contrast, *ida3; fla10*^{ts} x *fla10*^{ts} dikaryons held at the restrictive temperature did not rescue I1 dynein in the *ida3; fla10*^{ts} axonemes (Fig. 10A-B). To control for any secondary effects caused by the temperature variation, we generated *fla10 x ida3* and *ida3* x wild-type dikaryons that were held at both the permissive and restrictive temperatures. Thus, *ida3* contributes a wild-type copy of the anterograde kinesin motor and therefore at restrictive temperature, I1 dynein should continue to assemble in a tip-down fashion. Consistent with our prediction, I1 dynein assembles in the *ida3* axonemes at both the permissive and restrictive temperature as expected and rescue occurs at a rate consistent with I1 dynein rescue under normal conditions (Fig. 10B). Thus, temperature variation alone does not inhibit I1 dynein assembly in the *ida3* axonemes. As a further control, *ida3* x *ida3; fla10*^{ts} dikaryons were generated. As predicted, rescue of I1 dynein did not

occur at either the permissive or restrictive temperature (Fig 10B). This is because the *ida3* mutation is present in either cell types, preventing cytoplasmic complementation and rescue of I1 dynein assembly in the axoneme, as expected. All together, these results suggest I1 is transported by IFT to the distal tip of the cilium for assembly in the axoneme.

We eventually were able to isolate a *ida7; IC140::GFP* rescued transformant that efficiently expressed IC140::GFP. At the same time, we received an additional *ida7; IC140::GFP* strain from T. Oda (Department of Anatomy and Structural Biology, Graduate School of Medical Science, University of Yamanashi). Live-cell TIRF imagining of *ida7::IC140::GFP* confirmed IC140::GFP, indicative of I1 dynein, is transported by IFT for entry into and transport within the cilium (Fig. 11). Notably, like DRC4 and tubulin, IC140::GFP exhibits increased anterograde transport during regeneration. The significance of this observation is discussed below. In addition, I1 diffuses throughout the cilium until the complex docks the axoneme (Fig. 11). In summary, the 20S I1 dynein complex is pre-assembled in the cytoplasm prior to attachment to IFT for transport to the distal tip of the cilium. Once at the tip of the cilium, I1 is released from IFT and diffuses through the cilium until I1 docks the axoneme. To further understand the mechanisms required to assemble I1 dynein, we turned to the *ida3* mutant.

Introduction to *ida3*

Ritsu Kamiya originally isolated the *ida3* mutant in 1991. This classic paper aimed to distinguish the role of the inner and outer dynein arms by isolating

Chlamydomonas mutants defective in inner dynein arm assembly (Kamiya et al., 1991). The outer dynein arm mutant *oda1* was mutagenized through exposure to N-methyl-N'-nitro-N-nitrosoguanidine. Cells that contained both inner and outer dynein arm mutations are paralyzed (Kamiya et al., 1991). Therefore, cells that had acquired inner and outer dynein arm mutations would sink to the bottom of liquid media test tubes and could be isolated. The paralyzed mutants isolated were then back-crossed to remove the outer dynein arm mutation. Once back-crossed, the inner dynein arm mutants were characterized for motility defects. Not only did this screen isolate mutants defective in the assembly of inner dynein arm subunits, but also additional surprising mutants. For instance, this screen also revealed genes required for tubulin polyglutamylation on the B-microtubule required for inner dynein arm function (Kubo et al., 2010; Kubo et al., 2012). One additional mutant revealed in this screen is *ida3*. This mutant exhibited a slow swimming phenotype and a defect in phototaxis due to the loss of the inner dynein arm (Bayly et al., 2010; Bayly et al., 2011; Kamiya et al., 1991; King et al., 1997). Conventional electron microscopy of the *ida3* mutant revealed the I1 dynein does not assemble in the axoneme of the *ida3* mutant (Kamiya et al., 1991; Viswanadha et al., 2014).

Why is the I1 dynein complex unable to assemble in the *ida3* axoneme? One possibility is the I1 dynein complex is unable to assemble in the cytoplasm of *ida3*. Assembly of the large axonemal complexes is a highly complex multi-step process dependent not only on the synthesis of the individual subunits of the complex but also dependent on cytoplasmic assembly factors required to fold individual proteins, stabilize the pre-assembled complexes in the cytoplasm, and transport the preassembled complex

to the basal body region of the cilium (Desai et al., 2018; Kobayashi et al., 2012). For example, pre-assembly of the outer dynein arm requires the synthesis of individual outer dynein arm subunits, followed by the dimerization of the intermediate chains and folding of the heavy chains (Desai et al., 2018). Once complete, the heavy-chains must co-assemble with the intermediate chains (Desai et al., 2018). This step is dependent on the cytoplasmic assembly factors ODA7 and PF13 (Duquesnoy et al., 2009; Omran et al., 2008). In addition, the pre- assembled outer dynein arm is unstable in the cytoplasm prior to modification by ODA8 (Desai et al., 2015). Modification of the outer dynein arm by ODA8 stabilizes the pre-assembled outer dynein arm which then permits the complex to interact with both ODA16 and IFT machinery for transport into the cilium (Desai et al., 2015). Thus, the assembly of the outer dynein arm, like other axonemal complexes, depends on a large number of proteins and protein complex, most of which remain undiscovered at this time (Desai et al., 2018). Defects in any of the assembly steps would prevent proper assembly of the outer dynein arm and subsequent assembly in the axoneme. The complexity of outer dynein arm assembly is representative of the overall complexity of assembling axonemal components. I1 dynein likely requires numerous cytoplasmic assembly factors to build the 20S I1 dynein complex. One factor required for assembly of I1 dynein is DYX1C1/PF23 (Yamamoto et al., 2017), however both *PF23* and *IDA3* do not map together. Overall, our grasp of mechanisms required for pre-assembly of I1 dynein is not well understood.

If the protein defective in in the *ida3* mutant were a cytoplasmic assembly factor or a necessary subunit of the I1 dynein complex, I1 would not assemble in the cytoplasm. To test this hypothesis, we fractionated cytoplasmic extracts from wild-type and various

I1 dynein mutants including *ida7, ida1*, and *ida3* by velocity sedimentation of sucrose gradients (Viswanadha et al., 2014). Our analysis of wild-type cytoplasmic extract confirmed I1 dynein sediments into a 20S I1 dynein complex. We confirmed the 20S complex identified in the cytoplasm was not recycled from the axoneme by fractionating cytoplasmic extracts from the *Chlamydomonas bld1* mutant, which is unable to assemble cilia. The 20S I1 dynein complex is still present within the cytoplasm of the *bld1* mutant confirming the 20S I1 dynein complex is present in the cytoplasm prior to transport into the cilium. In comparison, the 20S I1 dynein did not assemble in cytoplasm from *ida1* (an I1 dynein heavy-chain 1α null), *ida2-6* (an I1 dynein heavy-chain 1β null), and *ida7* (a null in IC140) (Myster et al., 1997; Myster et al., 1999; Perrone et al., 1998; Perrone et al., 2000; Viswanadha et al., 2014). As predicted, in these mutants the 20S I1 dynein complex does not assemble in the cytoplasm. In contrast, fractionation of cytoplasmic extract isolated from the *ida3* mutant revealed the 20S I1 dynein complex does properly assemble in the cytoplasm. In addition, the 20S I1 dynein complex has the same heavy and intermediate chain composition as wild-type. From this data we determined the 20S I1 dynein complex does properly assemble in the *ida3* cytoplasm. Given all known subunits of I1 dynein are present in the pre-assembled I1 dynein complex in *ida3,* the protein defective in the *ida3* mutant must be extrinsic to I1 dynein but is not a cytoplasmic assembly factor.

We next tested the hypothesis that *ida3* is defective in I1 dynein docking in the axoneme by taking advantage of an *in vitro* reconstitution assay. As mentioned previously, I1 dynein binds in the proximal most region of the 96nm repeat. Isolated I1 dynein is capable of precisely binding I1-dynein deficient axonemes *in vitro* (Smith et al.,

1992b). Both *ida3* and *ida7* axonemes were isolated in the presence of ATP (Yamamoto et al., 2006). The I1-deficient axonemes were then mixed with varying quantities of high salt extract containing I1 dynein from *oda2* axonemes. The axonemes and supernatant were separated through high-speed centrifugation and analyzed by immunoblot to determine if wild-type I1 docked in the axoneme. IC140, indicative of the I1 dynein complex, was bound to both *ida7* and *ida3* isolated axonemes. Thus, the *ida3* axoneme is competent to bind I1 dynein and therefore is not a docking protein. However, intriguingly, the pre-assembled cytoplasmic I1 dynein isolated from *oda2* cytoplasmic extract was unable to dock both the *ida3* and *ida7* axonemes. This result indicates the pre-assembled I1 dynein complex is not competent to dock the axoneme. At this time, it remains unclear why I1 dynein derived from the cytoplasm fails to bind the axoneme *in vitro*. One possibility is the pre-assembled I1 dynein is held in an inactive state both in the cytoplasm and during transit by IFT. I suspect the I1 dynein complex is modified at the tip of the cilium, post-IFT transport and during release of I1 from IFT, to activate the dynein motor, and allow docking in the axoneme. Recent biochemical and structural studies have revealed mechanisms of auto-inhibition of cytoplasmic dynein and the IFT retrograde motor dynein 2 (Torisawa et al., 2014; Toropova et al., 2017).

Our analyses of the *ida3* mutant thus far revealed *ida3* is neither defective in preassembly of the 20S I1 dynein complex nor is the *ida3* axoneme incapable of docking I1. If the I1 dynein complex is fully assembled in the cytoplasm and the mechanisms required to dock the axoneme are functional in the *ida3* mutant, there may be a defect in the transport of I1 dynein from the cytoplasm into the ciliary compartment. We tested whether I1 was capable of entering the ciliary compartment by examining both matrix

and membrane-matrix of full-length and regenerating cilia by immunoblot (Viswanadha et al., 2014). Importantly, though I1 is properly assembled in the cytoplasm, I1 dynein does not enter the ciliary compartment in the *ida3* mutant (Fig. 12). Thus, IDA3 appeared to play a role in transport.

What Role Does IDA3 Play in I1 Dynein Assembly: Potential Hypotheses

Our characterization of *ida3* revealed that I1 dynein complex properly assembles in the *ida3* cytoplasm but the dynein is unable to enter the ciliary compartment. The most probable explanation is that I1 dynein is unable to undergo IFT-mediated transport thereby preventing entry into and transport along the cilium for ultimate incorporation in the axoneme. We thus proposed two potential hypotheses for the role of IDA3 in I1 dynein transport and assembly (Fig. 13). First, the protein defective in the *ida3* mutant could be a cytoplasmic modifier of the I1 dynein complex (Fig. 13A). In this way, cytoplasmic I1 may be modified in a way that would allow I1 dynein to load onto IFT for entry and transport in the cilium. Alternatively, *IDA3* may encode an IFT adapter required to allow attachment of I1 dynein to IFT for entry and transport (Fig. 13B). Less likely, but still possible, IDA3 could encode an unknown subunit of I1 dynein. In addition, while IDA3 may have encoded a modifier required to generate a dynein complex competent to dock in the axoneme, or a protein required to allow release of I1 dynein from IFT machinery, these possibilities would not be consistent with the fact I1 dynein does not enter the ciliary compartment rendering these hypotheses much less likely.

In the following chapter we discover IDA3 encodes an adapter required to load I1 dynein onto IFT for entry and transport in the cilium. IDA3 is unique as compared to previously described IFT adapters such as ODA16 and the BBSome in that IDA3 transport is regulated by ciliary length. We propose other axonemal complexes require highly specialized and transient adapters to bind and be transported by IFT.

Chapter II Figures

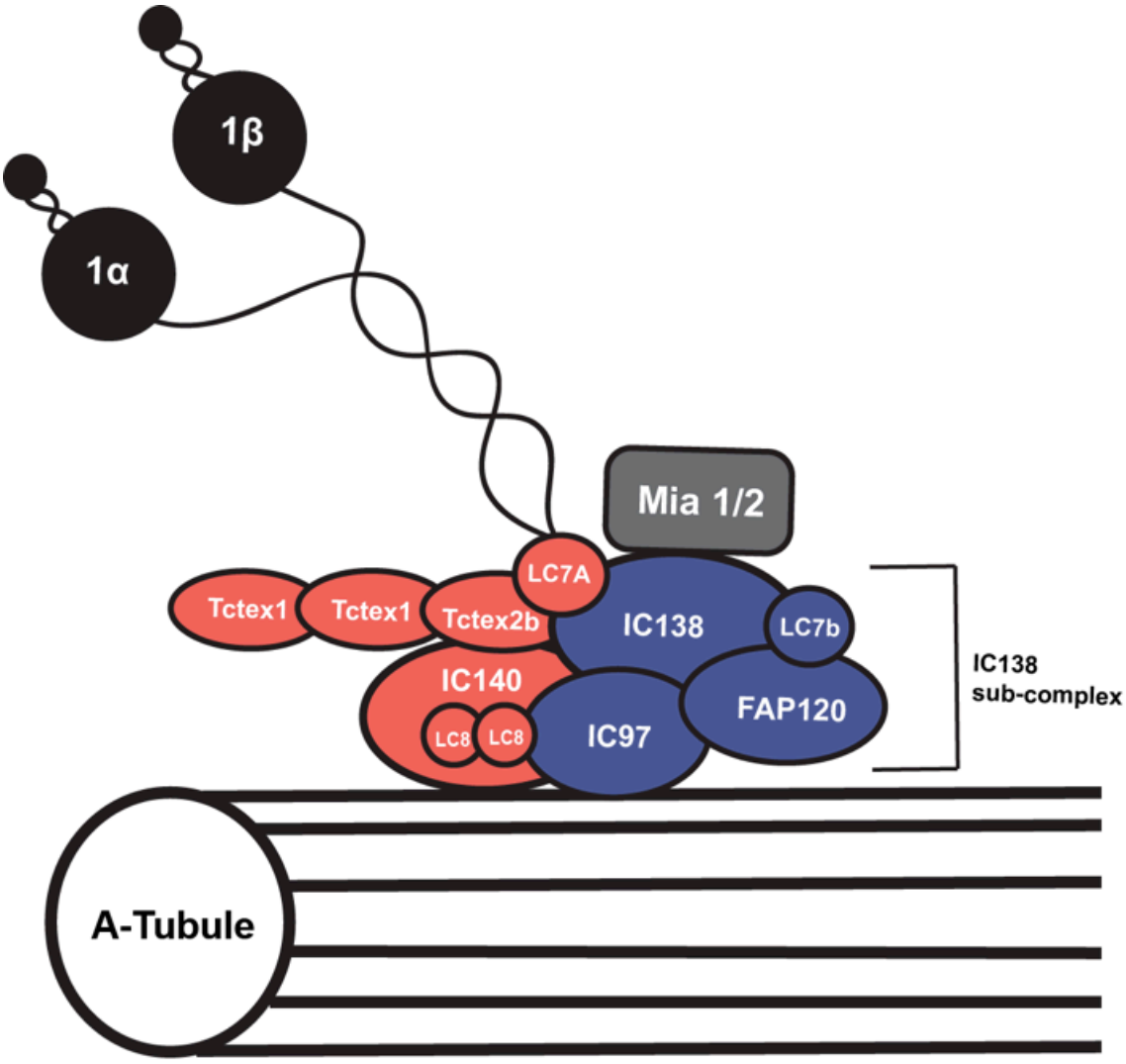

Figure 7. I1/f Dynein Subunit Composition

I1/f dynein is comprised of 14 known subunits. Antibodies to IC140 and IC138 are used through the dissertation study to detect the I1 dynein complex. IC140 is also tagged with GFP to visualize I1 dynein transport in live-cells. As will be discussed in later chapters, we believe IC140 interacts with IDA3, making this intermediate chain critical in our study of IDA3.

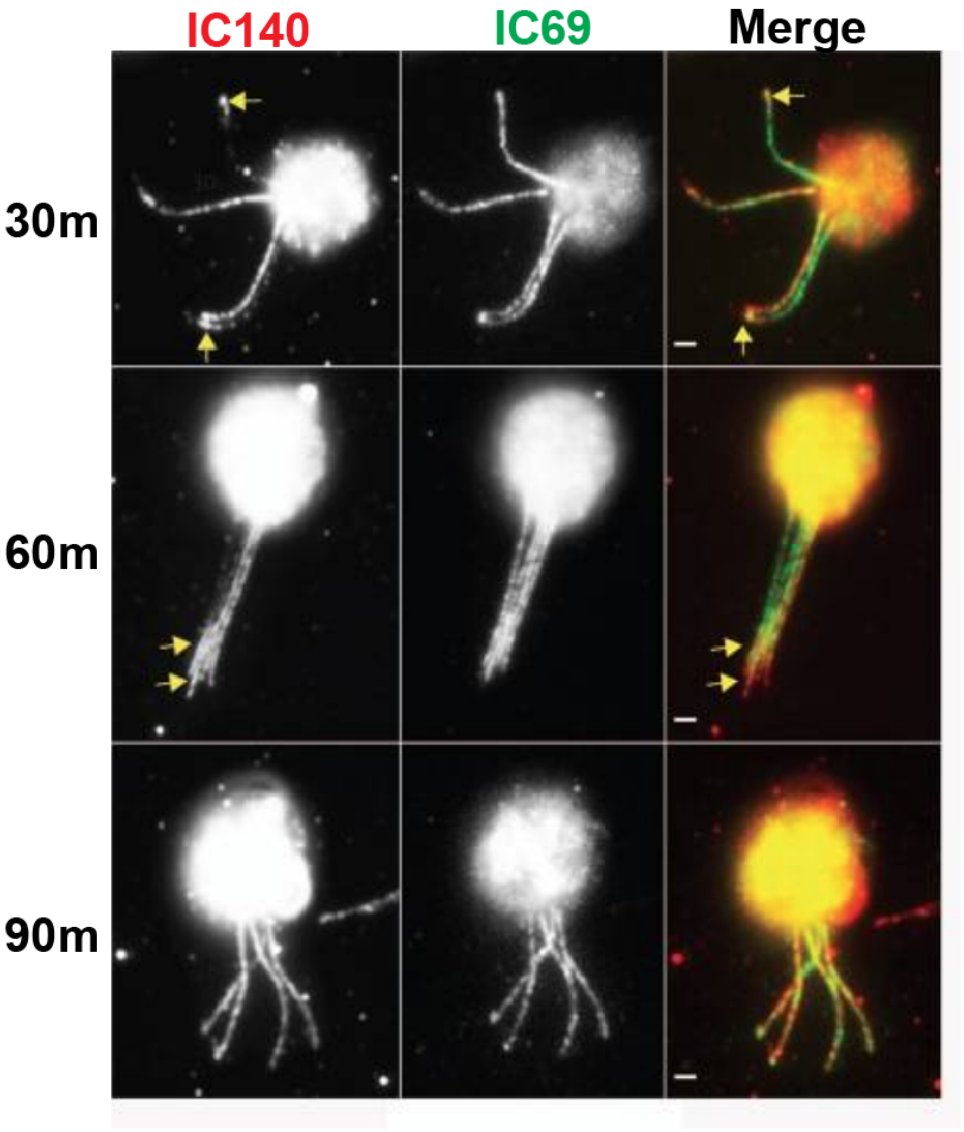
IC140
IC69
Merge
30m
60m
90m

Figure 8. Dikaryon rescue of I1 dynein assembly occurs from the distal tip

Immunofluorescence of IC140 in *ida7* x wild-type (WT) dikaryons. Cytoplasmic complementation in WT and I1-deficient dikaryons results in the rescue of I1 dynein assembly (arrows) from the distal tip to base in the *ida7* mutant cilia. Scale bar = 2μm. (From Viswanadha et al., 2014)

A

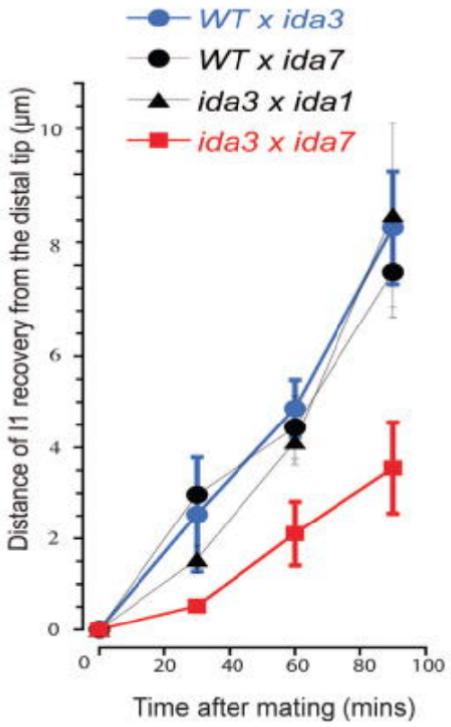
WT x ida3
WT x ida7
ida3 x ida1
ida3 x ida7
Distance of I1 recovery from the distal tip (µm)
0
2
4
6
8
10
0
20
40
60
80
100
Time after mating (mins)

B

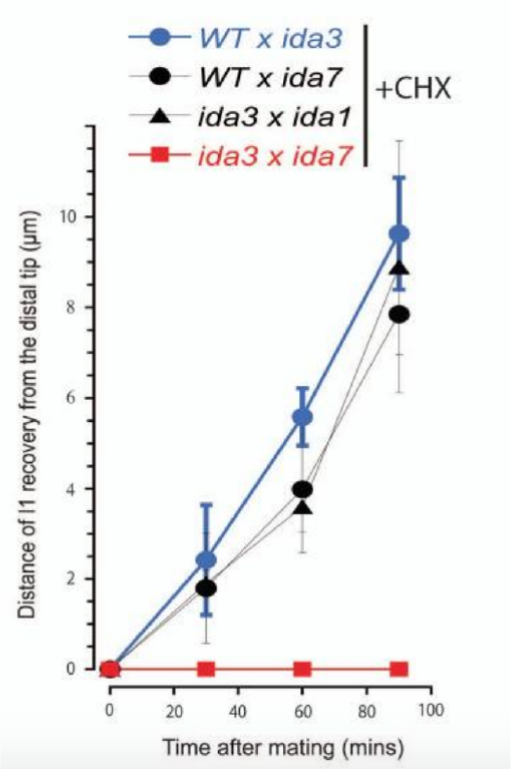
WT x ida3
WT x ida7
ida3 x ida1
ida3 x ida7
+CHX
Distance of I1 recovery from the distal tip (µm)
0
2
4
6
8
10
0
20
40
60
80
100
Time after mating (mins)

Figure 9. Dikaryon rescue of axonemal I1 assembly requires protein synthesis

(A) Comparison of dikaryon rescue rates of I1 assembly in various mutant combinations. The length of IC140 staining at the distal end of the cilium is plotted versus time. WT x *ida3* (blue circles, n = 83) and WT x *ida7* (black circles, n = 29) dikaryons demonstrate progressive rescue of axonemal I1 dynein assembly with complete recovery at 90m. Dikaryons between *ida3* and *ida1* show this same pattern of rescue along all four cilia (black triangles, n = 59). Rescue of axonemal I1 dynein assembly is delayed in *ida3* x *ida7* dikaryons (red squares, n = 30), but occurs from the distal tip like other dikaryon combinations. (Viswanadha et al., 2014) **(B)** Immunofluorescence of IC140 in *ida3* x *ida7* dikaryons 60 minutes after mixing gametes was performed (data not shown in dissertation; See Viswanadha et al., 2014). Shown here is the quantification of IC140 staining from the distal tip of I1-deficient cilia in the presence of CHX. Axonemal I1 dynein assembly occurs progressively from the distal tip to base in WT x *ida3* (blue circles, n = 25), wild-type x *ida7* (black circles, n = 25) and *ida3* x *ida1* (black triangles, n = 22) dikaryons. In contrast I1 dynein is not assembled on the axoneme in *ida3* x *ida7* dikaryons (red squares, n = 29) (From Viswanadha et al., 2014).

A

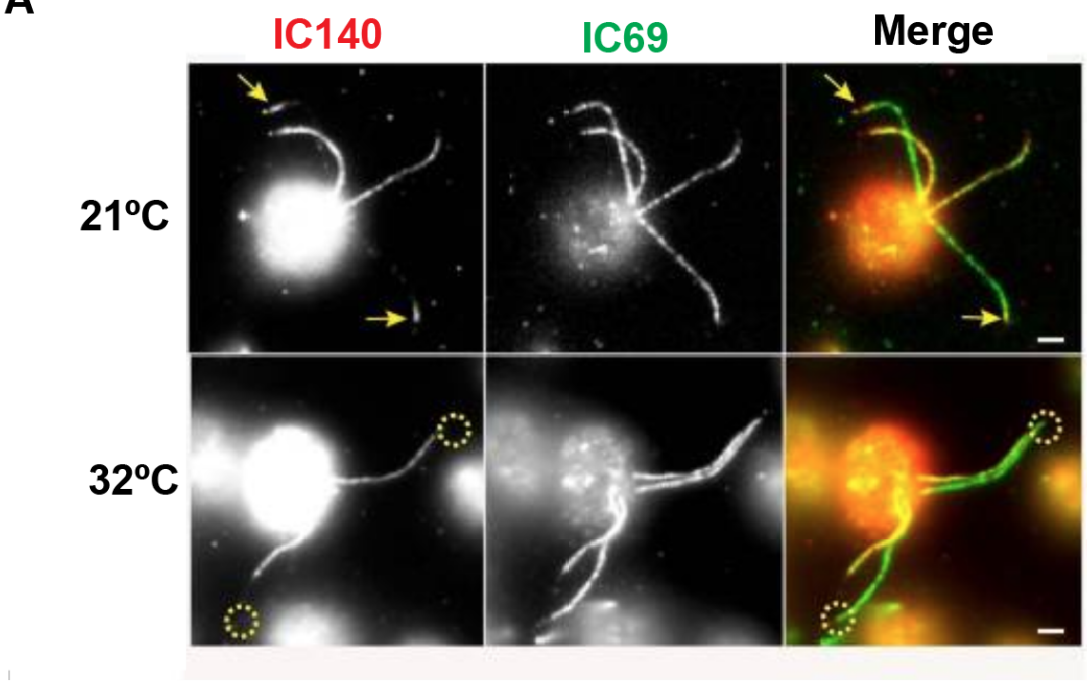
IC140
IC69
Merge
21ºC
32ºC

B

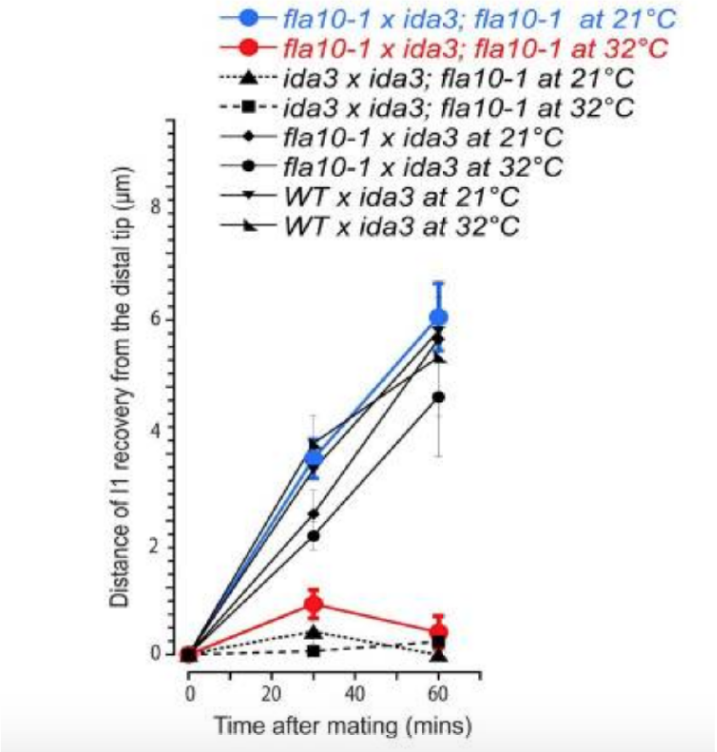
fla10-1 x ida3; fla10-1 at 21°C
fla10-1 x ida3; fla10-1 at 32°C
ida3 x ida3; fla10-1 at 21°C
ida3 x ida3; fla10-1 at 32°C
fla10-1 x ida3 at 21°C
fla10-1 x ida3 at 32°C
WT x ida3 at 21°C
WT x ida3 at 32°C
Distance of I1 recovery from the distal tip (µm)
0
2
4
6
8
0
20
40
60
Time after mating (mins)

Figure 10. Transport of I1 to the tip of the cilium requires kinesin-2

(A) Immunofluorescence of IC140 in *fla10-1* x *ida3; fla10-1* dikaryons 60 minutes after mixing gametes. At the permissive temperature (21°C), recovery of axonemal I1 dynein assembly occurs from the distal end of *ida3* cilia (arrows). At the restrictive temperature (32°C), I1 dynein assembly on the axoneme is not seen in *ida3; fla10-1* cilia (dotted circles). Scale bar = 2μm. **(B)** Quantification of IC140 staining at the distal end of I1-deficient cilia at permissive (21°C) and restrictive (32°C) temperatures. Axonemal I1 dynein assembly occurs progressively from the distal tip to base in wild-type x *ida3* (n = 19) and *fla10-1* x *ida3* (black diamonds and black circles, n = 39) dikaryons at both permissive and restrictive temperatures. While I1 assembly at the distal tip is seen at the permissive temperature in *fla10-1* x *ida3; fla10-1* dikaryons (blue circles, n = 52), I1 assembly at the tip does not occur at restrictive temperature (red circles, n = 19). As a control, *ida3; fla10-1* x *ida3* dikaryons were tested for a lack of I1 axonemal assembly at both temperatures (black dotted triangles and squares, n = 46). (From Viswanadha et al., 2014).

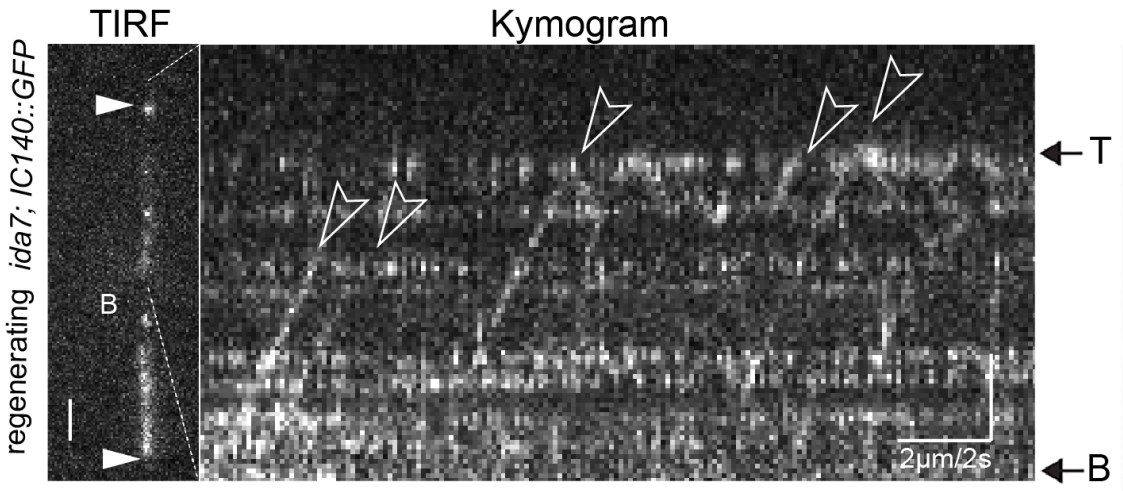
TIRF
Kymogram
regenerating ida7; IC140::GFP
B
T
B
2µm/2s

Figure 11. IC140::GFP is transported by anterograde IFT

Kymogram of *ida7; IC140::GFP* transport in regenerating cilium. IC140::GFP is transported by anterograde IFT to the tip of the cilium. Bars = 2 s and 2 μm.

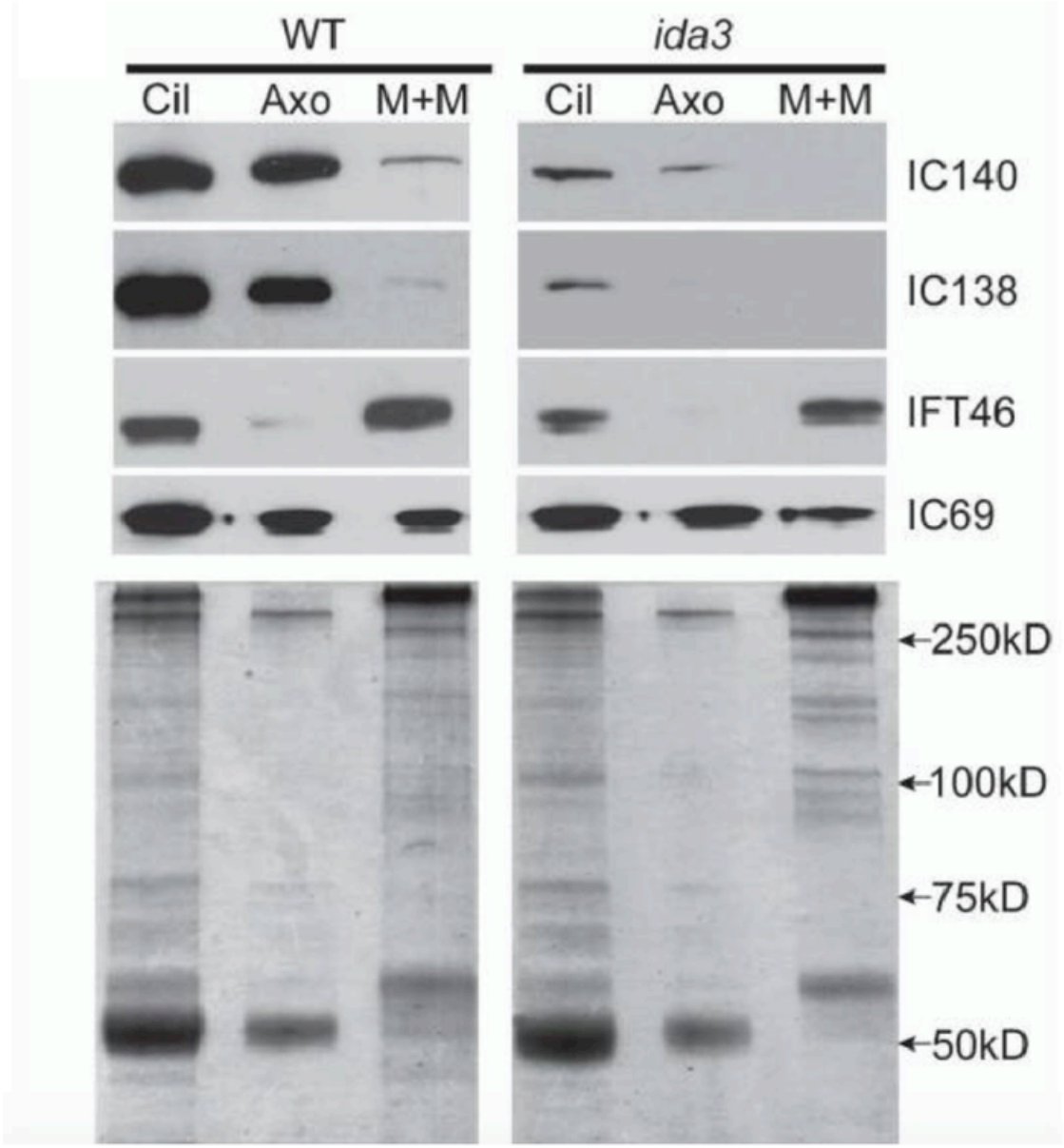
WT
ida3
Cil
Axo
M+M
Cil
Axo
M+M
IC140
IC138
IFT46
IC69
←250kD
←100kD
←75kD
←50kD

Figure 12. The *ida3* mutant is defective in I1 dynein entry into the ciliary compartment

Immunoblots of ciliary (Cil), axonemal (Axo) and membrane + matrix (M+M) fractions were analyzed using antibodies to the IC138 and IC140 subunits of I1 dynein. For detection of axonemal subunits (IC69, IC140, IC138), the M+M was loaded at five times the relative amount of cilia and axonemes. Analysis showed a significant reduction in ciliary and axonemal I1 dynein in *ida3* compared to wild-type. In addition, M+M fractions show that I1 dynein is absent in *ida3* compared to wild-type indicating inefficient entry into the ciliary compartment. The M+M samples from WT and *ida3* were also examined by immunoblots at twice the protein load (data not shown), and I1 dynein subunits were never present in *ida3*. The outer arm component, IC69, is present in equivalent amounts in WT and *ida3* M+M and serves as a control for IFT cargo. The IC69 immunoblot also validates that the defect in *ida3* is specific to I1 dynein. IFT46 serves as a positive control for M+M fractionation. CBB = Coomassie Brilliant Blue loading control. (From Viswanadha et al., 2014).

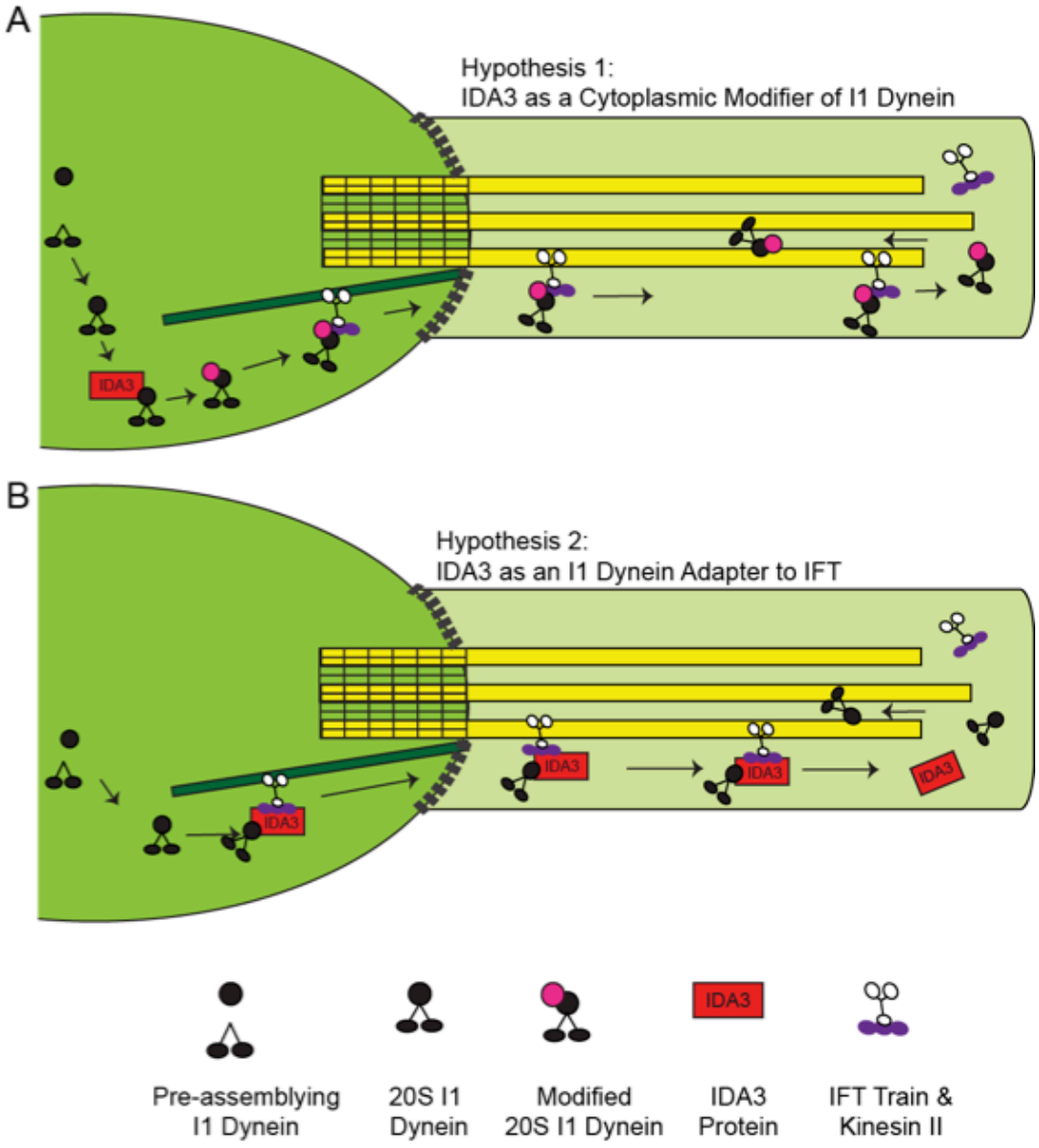
A
Hypothesis 1:
IDA3 as a Cytoplasmic Modifier of I1 Dynein
IDA3
B
Hypothesis 2:
IDA3 as an I1 Dynein Adapter to IFT
IDA3
IDA3
IDA3
IDA3
Pre-assemblying I1 Dynein
20S I1 Dynein
Modified 20S I1 Dynein
IDA3 Protein
IFT Train & Kinesin II

Figure 13. Potential hypotheses for the role of IDA3 in I1 dynein assembly

(A) Hypothesis 1: IDA3 acts as a cytoplasmic modifier of I1 dynein, rending I1 dynein competent to bind IFT for transport to the distal tip of the cilium. **(B)** Hypothesis 2: IDA3 acts as an I1 dynein/ IFT adapter mediating interaction of I1 dynein with IFT for transport to the tip of the cilium.

Chapter III

Identification and Characterization of IDA3

In this section, I will discuss my work characterizing the gene defective in the *ida3* mutant, termed *IDA3*. I begin this chapter with a brief discussion of our cryo-ET and EM analyses of the *ida3* mutant. I will then discuss the identification of the *IDA3* gene, rescue of the *ida3* mutant, and localization of the IDA3 protein. The bulk of this chapter will focus on live-cell imagining of IDA3 tagged with NeonGreen (NG) and the relationship between ciliary assembly and IDA3 transport by IFT. The live-cell imagining has been an outstanding collaboration with Dr. Karl Lechtreck in Cellular Biology at the University of Georgia. I will conclude by showing IDA3 interacts biochemically with the I1 dynein complex and that IDA3 transport by IFT is less processive in the absence of I1 dynein. Most content and text in Chapter III has been pulled from my first author publication but in some cases content has been altered to allow expansion of specific ideas and to incorporate unpublished but essential IDA3 data.

Inner Dynein Arm I1 is Specifically Missing in *ida3* Mutant Axonemes

As mentioned in Chapter II, I1 dynein does not enter the cilium in the *ida3* mutant, preventing I1 dynein incorporation in the axoneme (Kamiya et al., 1991; Viswanadha et al., 2014). While the loss of I1 dynein in the axoneme of the *ida3* mutant was clear, we wanted to confirm the *ida3* mutant defect was specific to the I1 dynein complex and to ensure all other axonemal components were assembled properly in the axoneme. For this reason, we examined the structure of the *ida3* axoneme by cryo-electron tomography and subtomogram averaging. This was a collaboration with Drs.

Gang Fu and Dany Nicastro in the Departments of Cell Biology and Biophysics at the University of Texas Southwestern Medical Center. Tomographic slices (Fig. 14A a-f) and isosurface renderings (Fig. 14A g-j) reveal I1 dynein is missing in *ida3* axonemes. Only on rare and isolated occasions was I1 observed in the axoneme (Fig 14B a-e). Notably, all other axonemal structures assemble properly in the *ida3* axoneme, as seen by both the cryo-ET and by thin-section electron microscopy (Figure 15). Thus, like other I1 dynein mutants that include *ida1, ida2, ida7,* and *bop5* (Heuser et al., 2012; Kamiya et al., 2014; King, 2016; Wirschell et al., 2007), only I1 dynein fails to assemble in *ida3* axonemes. In contrast to other I1 mutants, all known I1 dynein subunits of the 20S I1 dynein complex assemble in the *ida3* cytoplasm (Viswanadha et al., 2014). As mentioned above, we postulated *IDA3* encodes a protein extrinsic to I1 dynein that is specifically required for ciliary entry and/or transport of I1 dynein by IFT.

A Nonsense Mutation in *IDA3* Results in Loss of I1 Dynein in the Axoneme

Once we confirmed the defect in *ida3* is specific to the I1 dynein complex, we then were ready to address what role the protein defective in the *ida3* mutant plays in I1 dynein assembly. In order to address this question, we first needed to identify the gene defective in the *ida3* mutant. Using both tetrad mapping and whole-genome sequencing (Lin et al., 2015), the *ida3* mutant was mapped to a small region on Chromosome 3 between markers 953 and 120055 (Table I). This 369 KB region contains the centromere and better resolution could not be obtained with additional markers. With 40x coverage of the *ida3* genome, we identified only one SNP in the mapped region after filtering. This change is in Cre03.g205000 and there is a G to A transition that changes a

tryptophan codon (TGG) to a stop codon (TAG) at amino acid 22 (Fig. 16A). Using tetrad analysis, we determined this mutation cosegregates with the slow swimming phenotype in 75 meiotic progeny, suggesting the premature stop codon is linked to the loss of I1 dynein in the axoneme and subsequent slow swimming phenotype. The *IDA3* gene is approximately 4.2 KB in length when including upstream and downstream regulatory elements and is composed of four exons and three introns (Fig. 16B).

We confirmed *IDA3* is the gene defective in the *ida3* mutant through both transformation-rescue of *ida3* with a wild-type copy of *IDA3* and reversion/suppressor analysis. Transformation of *ida3* with an untagged *IDA3* or *IDA3* fused to 3xHA or NeonGreen (NG) rescued I1 assembly in the axoneme and the slow-swimming phenotype (Table II, Fig. 17 (A-C)). This result is strong evidence that *IDA3* is the gene defective in the *ida3* mutant. It is important to note that while most tagged IDA3 constructs (i.e. untagged IDA3 or IDA3 tagged N-terminally, C-terminally, and embedded in the second exon with 3xHA or NG) rescued I1 dynein assembly, *ida3* was not rescued when the 3xHA tag was inserted within the first exon of *IDA3* (Table II).

As a secondary method of confirmation, we took advantage of reversion analyses (Lin et al., 2015). Briefly, *ida3; oda2* cells (defective in both I1 and outer dynein arm assembly) were mutagenized using UV light. Cells were screened for rescue of paralysis and assembly of I1 dynein in the axoneme. Revertants isolated either contained a mutation within the *IDA3* gene that allowed expression of the IDA3 protein (intragenic reversion) or revertants contained a suppressor mutation that alters a gene other than IDA3 and allows I1 dynein assembly to occur (extragenic suppressor). Intragenic reversion of *ida3* rescues assembly of I1 dynein and paralysis of *ida3; oda2* (Fig. 18A-

B). In addition to the isolation of numerous independent revertants, two potential extragenic suppressors, Z1 and Z3, were also isolated and remain largely uncharacterized at this time. These cells isolated by Dr. Susan Dutcher at Washington University St. Louis, are believed to be extragenic suppressors as the cells, originally *ida3; oda2* mutants, continue to contain the *ida3* point mutation but are now able to assemble I1 dynein in the axoneme. Analysis of Z1 and Z3 axonemes revealed IC140 migration is altered when analyzed by immunoblot (Fig. 19). IC140 in Z1 axonemes appears as a doublet with about half the IC140 protein running at the wild-type molecular weight and the remainder running slightly lower (Fig. 19). IC140 in the Z3 axonemes is predominately comprised of the lower IC140 band with very little IC140 running at the wild-type molecular weight (Fig. 19). Why IC140 appears to be altered in the two extragenic revertants remains unanswered. The simplest explanation is that the change in IC140 migration is due to a truncation of the IC140 protein or an alteration in IC140 post-translational modification in the extragenic suppressors and this change bypasses the need for IDA3 in assembly of I1 dynein. This result is potentially very important and further analyses are required to confirm Z1 and Z3 are in fact true extragenic suppressors of the *IDA3* gene. The extragenic suppressors provide an independent means of addressing IDA3 protein interactions, in particular interactions between IDA3 and IC140.

IDA3 is Transported by Anterograde IFT within the Regenerating Cilium

The *IDA3* gene encodes a ~115kD coiled-coil protein that contains a CCDC24 domain in the N-terminal half of the protein (Pfam domain PF15669) (Fig. 20A-B). At this time, very little is known regarding the human CCDC24 protein. Examination of

CCDC24 RNA expression in human tissues has been explored. In 2014, one study analyzed the human tissue-specific expression of numerous transcripts and found that *CCDC24* RNA is found in highest quantity in the testis, thyroid, prostate, kidney, gallbladder, and lung (Fagerberg et al., 2014). In another tissue- specific RNA expression analysis performed by The Human Protein Atlas found that *IDA3* RNA was most highly expressed in the male and female reproductive tissues, endocrine tissue, liver, and gallbladder. No protein expression data is available at this time. The RNA expression data can be found at: (https://www.proteinatlas.org/ENSG00000159214-CCDC24/tissue).

While CCDC24 has not been linked to the cilium at this time, *CCDC24* RNA expression appears to be expressed in tissues containing motile cilia. In terms of the CCDC24 protein structure, the human CCDC24 protein is 307 amino acids (33.8 kD) in length and consists of coiled-coils (Fig. 20A). Though CCDC24 is noticeably shorter than IDA3, we believe the N-terminal half of IDA3 is essential for IDA3 function (see below). It is possible throughout evolution the remainder of the IDA3 protein was lost resulting in the shorter CCDC24 protein. A *CCDC24* knockout mouse has been generated by the Knockout Mouse Project (KOMP) at UC Davis. This mouse exhibits no noticeable phenotypes at this time. I predict, if CCDC24 does act similarly to IDA3, the knockout mouse will exhibit subtle signs of ciliopathies such as a reduction in fertility and minor malformation of the heart. These defects could be easily overlooked in the preliminary mouse screen. At this time, our analysis of IDA3 function likely provides the best framework for study of CCDC24.

Immunoblot analysis of cytoplasmic extract from *ida3; IDA3::HA* revealed that IDA3::HA is present in the cytoplasm of ciliated cells but is not present in the axoneme (Fig. 21A-B). Though not included in our publication, immunofluorescence analysis of *ida3;IDA3::HA* cells confirmed IDA3::HA was present in the cytoplasm and was not present in the axoneme (Fig. 22, 23). We noted in our immunofluorescence images that IDA3::HA appears to localize near the basal body region similar to the localization of IFT components, the kinesin subunit FLA10, and axonemal cargos of IFT (Fig. 22(a-b)). (Brown et al., 2015; Deane et al., 2001; Qin et al., 2004; Vashishtha et al., 1996; Wingfield et al., 2017). In addition to localization of IDA3::HA near the basal body region, I also observed, at times, a small quantity of tiny circular puncta clustered within the cytoplasm (Fig. 23). At the time of first observation I thought these puncta resembled processing bodies, also known as P-bodies. Intriguingly, at the 2017 FASEB Cilia Conference, Dr. John Wallingford from the University of Texas at Austin presented unpublished work defining dynein assembly particles (DynAps). Generally, these particles contained a number of dynein assembly factors clustered together in distinct granules within the cytoplasm. These particles likely contain necessary factors required to build the inner and outer dynein arms and act as hubs for dynein motor assembly. It is possible that IDA3::HA localized to puncta within the cytoplasm could also be present within the dynein assembly particles and interact with I1 dynein soon after pre-assembly into the 20S I1 dynein complex. As will be discussed below, my analysis of IDA3 has focused primarily on IDA3 behavior within the ciliary compartment. Thus, we did not further pursue study of the IDA3::HA particles observed in the cytoplasm. Future studies

may require super-resolution imagining techniques to better characterize these IDA3::HA granular-like structures.

Given that the 20S I1 dynein does not enter the cilium in *ida3* (Viswanadha et al., 2014), and given IDA3 does not assemble in the axoneme, we predicted IDA3 function would be tightly linked to I1 dynein transport into the cilium. To test this prediction, we took advantage of the freeze-thaw method to analyze matrix (Cole et al., 1998; Craige et al., 2013) from full-length and regenerating *ida3; IDA3::HA* cilia. For reference, the regenerating cilia isolated were on average two-thirds of full-length cilia (~ 6 μm in length) (Fig. 24, Table IV). It is important to note the regeneration was performed in a manner in which the cilia regenerated in an asynchronous manner. Therefore, while on average the cilia were two-thirds of full-length, individual cilia in each sample varied between one-half to three-quarters of full-length.

IDA3::HA, though absent in the matrix of full-length cilia, is present in the matrix of regenerating cilia, as are the intermediate chains IC140 and IC138 of I1 dynein (Fig. 25 A-B). Thus, I1 dynein only enters the cilium when IDA3 is present. To our surprise, the results also revealed, IDA3, though not an axonemal component, selectively enters cilia during regeneration and is essential for I1 entry into the cilium. IDA3 appears to be modified in the matrix of regenerating cilia as indicated by the presence of two distinct IDA3 bands (arrowheads, Fig. 25B). The nature of this modification remains unknown and implications of the IDA3 modification will be discussed in greater detail in Chapter IV.

In addition to the analysis of the matrix compartment of the cilium, I also analyzed the membrane + matrix compartment of regenerating *ida3;IDA3::HA* cilia using

a nonidet P-40 detergent procedure (Craige et al., 2013). My unpublished data confirmed our finding that IDA3::HA is present within the regenerating cilium (Fig. 25C). In addition to the HA antibody used to probe for IDA3::HA on immunoblot, I also probed the immunoblot with an antibody designed against the endogenous IDA3 protein. Briefly, (described in detail in Methods Appendix) the IDA3 antibody was designed against the first ~139 amino acids of the IDA3 protein. Purified His-tagged IDA3 proteins were used to inject a rabbit to produce antibodies against IDA3. The final bleed was affinity-purified using HisTALON Gravity Columns (Clontech) with antigens attached to the resin. This antibody was used to probe the matrix blot and detected IDA3 in both wild-type and *ida3; IDA3::HA* samples (Fig. 25C). (Detailed information regarding the generation of the IDA3 fusion protein and characterization of the antibody can be found in Appendix I. Information on the generation of the IDA3 peptide antibody can also be found in Appendix I, though to date the IDA3 peptide antibody has not been found to be useful.) For unknown reason, unlike in the regenerating matrix samples, IDA3 does not appear as a doublet in the membrane + matrix fractions. It is possible isolation of the membrane + matrix with detergent releases phosphatases, or other enzymes, from the membrane that alter the IDA3 modification-see below. Regardless, this data indicates both IDA3::HA and endogenous IDA3 enter the cilium during regeneration. Though preliminary, immunofluorescence of regenerating *ida3* and *ida3; IDA3::HA* cells revealed diffuse IDA3 staining in the flagellar compartment (Fig. 26). We now know this diffuse staining is IDA3 in transit to the distal tip of the cilium.

As discussed briefly in Chapter II, I1 dynein, marked by IC140::GFP, is transported by anterograde IFT (Fig. 11). Given that IDA3 is essential for I1 dynein

assembly in the axoneme, we asked if IDA3 is also a cargo of IFT inside of the cilium. Using live-cell total internal reflection fluorescence microscopy (TIRF) (Lechtreck et al., 2013), we imaged *ida3; IDA3::NG* cells with either full-length or regenerating cilia. Similar to *bona fide* axonemal proteins (Lechtreck et al., 2017), IFT transport of IDA3::NG in regenerating cilia is robust whereas IDA3 transport in full-length cilia is rare (Fig. 27A-B). Approximately 90% of individual IDA3::NG particles are transported processively to the distal tip of the cilium at a velocity of 1.98 +/- 0.37 μm/s, consistent with the speed of anterograde IFT in *Chlamydomonas* (Fig. 28 A(a), B, C, Fig. 29, Fig. 30A) Occasionally, we observed stationary IDA3::NG (Fig. 28A(d)). This could result from stalling of IFT trains along the length of the axoneme as recently described by Stepanek and Pigino (2016) and discussed briefly in Chapter I of this dissertation (Stepanek et al., 2016). Alternatively, IDA3 may transiently associate with the axoneme. At the tip, multiple IDA3 proteins linger before diffusion begins (Fig. 28A (b, c), Fig. 29. Fig 30A). IDA3::NG then diffuses within the cilium approximately 88% of the time (Fig.28D, Fig 30A). Occasionally, retrograde IFT transports IDA3::NG at a velocity of 2.66 +/1 1.2 μm/s (Fig. 28 A(b), B, D, Fig. 30B). One possibility is diffusion of IDA3 through the cilium into the cell body controls the pool of IDA3 available for I1 transport (Chien et al., 2017; Wingfield et al., 2017). Regulation of IDA3 quantity in the cytoplasm by diffusion and the implications of regulating IDA3 quantity will be further discussed in Chapter IV.

IDA3 Transport by Anterograde IFT is Dependent on Ciliary Length

To further explore the link between IDA3 and ciliary growth, we quantified the number of IDA3::NG particles that enter the cilium as the cilium lengthens. Similar to axonemal cargos of IFT (Craft et al., 2015; Wren et al., 2013), the number of IDA3 particles transported per minute decreases as the cilium lengthens (Fig. 31A). Thus, IDA3 is the first identified non-axonemal cargo of IFT whose transport frequency is regulated by ciliary length. It is possible the transport of IDA3, in addition to axonemal cargos of IFT, may be regulated by mechanisms that control cilium length (Chien et al., 2017; Ishikawa et al., 2017). The quantity of cargo transported by IFT at any given time may also be regulated by ciliary length.

We next asked whether IDA3 would selectively enter the growing cilium in a cell that had one growing and one full-length cilium. *ida3; IDA3::NG* cells with one regenerating (short) cilium and one full-length (long) cilium were imaged by TIRF. Anterograde IFT transport, dwell at the tip of the cilium, and diffusion of IDA3::NG were only observed in the regenerating cilium (Fig. 31B-C). These data confirm IDA3 selectively enters the growing cilium and indicate transport of IDA3 is regulated independently within each of the two cilia in a single *Chlamydomonas* cell. This behavior is reminiscent of the regulation of tubulin-IFT interaction (Craft et al., 2015). How the cell selectively targets IDA3 into the growing cilium remains unknown.

Given the specificity of IDA3 for I1 dynein, we predicted the need to assemble I1 dynein in the axoneme prompts IDA3 entry/transport in the growing cilium. To test this, we mated *ida3 x ida3; IDA3::NG* to generate dikaryons with four cilia; two full-length cilia with I1 docked in the axoneme and two full-length cilia lacking I1 dynein (Fig.

32A). TIRF imagining revealed IDA3::NG rarely enters any of the four cilia, consistent with the infrequent transport of IDA3 in full-length cilia (Fig. 32B (a-f)). Hence, it is changes in ciliary length, and not the need to assemble I1 dynein in the axoneme, that cues increased IDA3 transport. However, infrequent transport of IDA3 and I1 is eventually sufficient to rescue I1 dynein assembly and motility in the full-length axoneme (Viswanadha et al., 2014).

IDA3 Interacts Biochemically with IC140 in the Matrix of Regenerating Cilia

Considering IDA3 permits entry/transport of I1 dynein in the cilium, we predicted IDA3 and I1 dynein interact while in transit to the ciliary tip. Immunoprecipitation of IDA3::HA from the matrix of regenerating *ida3;IDA3::HA* cilia revealed the presence of both IDA3::HA and IC140 in pull-downs (Fig. 33A). IDA3::HA was also detected in complementary pull-downs of IC140::SNAP from the regenerating matrix of the quadruple mutant *ida7;IC140::SNAP; ida3; IDA3::HA* cilia (Fig. 33B). Together these data strongly indicate that IDA3 and I1 dynein interact in the matrix and are co-transported to the tip of the growing cilium. While a modified form of IDA3::HA exists in the matrix of regenerating cilia, only one of the two bands is pulled down in our interaction studies from isolated matrix. Whether the IDA3 modification regulates IDA3-I1 dynein interaction remains to be determined.

My unpublished data suggest IDA3 interacts with IC140 in both steady-state and regenerating cytoplasm (Fig. 34 A-B). These results bring to question whether IDA3 interacts specifically with IC140 in both the steady–state and regenerating cytoplasm or whether IDA3 is bound to the 20S I1 dynein complex at all times. Further pull-down

analyses and alternative live-cell imagining and biochemical fractionation approaches will be required to determine how IDA3 and I1 dynein interact in the cytoplasm under both steady-state and regenerating conditions. Future experimentation in regard to IDA3 behavior in the cytoplasm will be expanded upon in Chapter IV.

Stable Binding of IDA3 to IFT Requires I1 Dynein

Thus far, our analysis of IDA3 reveals IDA3 is an essential and selective adapter required to mediate the entry and transport of I1 dynein to the distal tip of the cilium. Since IDA3 is essential to mediate the interaction between I1 and IFT, we asked how I1 dynein acts as an adapter to mediate the I1 dynein/IFT interaction (Fig. 35). I hypothesized IDA3 links I1 to IFT. Alternatively, IDA3 may bind I1 dynein rendering I1 component to bind IFT or both I1 and IDA3 may bind IFT to create a stable interaction. In order to distinguish between these hypothesizes, we isolated the triple mutant *ida7;ida3;IDA3::NG* that has a mutation in the *IC140* gene (Perrone et al., 1998) that prevents cytoplasmic assembly of the 20S I1 dynein (Viswanadha et al., 2014), but carries wild-type IDA3::NG. In this way, we could image IDA3::NG transport in the absence of the I1 dynein cargo and begin to eliminate potential hypotheses as to how IDA3 acts as an I1 dynein/ IFT adapter. TIRF imaging revealed IDA3::NG is transported by IFT in growing cilia, even in the absence of I1 dynein (Fig. 36 A-C). This result eliminated the possibility that IDA3 binds solely to I1 dynein and, instead, IDA3 must bind IFT. However, in wild-type, IDA3 is typically transported without interruption from the base to the ciliary tip, whereas in the absence of I1, IDA3::NG transport is less processive (Fig. 36D). For instance, in wild-type cilia 74% of IDA3 transports are

processive from base to tip, whereas, in the *ida7* background, only 30% of IDA3 transport is continuous from base to tip (n=80 and 61 transports, respectively). As a consequence of increased dissociation of IDA3 from IFT, IDA3::NG diffusion is prominent in growing *ida7; ida3;IDA3::NG* cilia (Fig. 36 A, B). Thus, IDA3 is transported by IFT in the absence of I1 dynein, however the IDA3-IFT interaction appears to be more transient, suggesting I1 dynein stabilizes the IDA3-IFT interaction. Given these data, it is unlikely IDA3 links I1 to IFT and instead supports the adapter model in which both I1 and IDA3 bind IFT to create a stable interaction. Since I1 dynein does not bind IFT in the absence of IDA3, we suggest IDA3 bound to IFT renders IFT competent to bind and transport I1 dynein. In turn, I1 dynein possibly stabilizes IDA3 interaction with IFT.

An alternative interpretation of these results does exist. As mentioned in Chapter II, *ida7* x *ida3* dikaryons require translation to rescue I1 dynein assembly in the axoneme. Here we visualized IDA3::NG transport in an *ida7* background. This result reveals the IDA3 protein is in fact stable in the absence of the IC140 protein. Therefore, *ida7* x *ida3* rescue requires the translation of an unknown protein or proteins, which I will term protein X to simplify further discussion. Given the lack of immediate complementation, we presume protein X is unstable in both the *ida7* and the *ida3* mutants. In addition, because I1 dynein rescue is dependent upon translation of protein X in the *ida7* x *ida3* dikaryon, protein X must play a critical role in I1 dynein transport and assembly. While we have a wild-type copy of *IDA3,* IC140 is absent in *ida7; ida3; IDA3::NG* mutant and therefore we presume protein X is also absent. It is possible, protein X is required to stabilize IDA3 interaction with IFT. Therefore, lack of processive IDA3 transport in the

ida7 background may not be due to the loss of the I1 dynein cargo but instead is due to the absence of protein X in the *ida7* background. Structure-function analyses will be required to determine how IDA3 binds both IFT and I1 dynein and mass-spectrometry analysis of IDA3 and IC140 pull-down fractions from regenerating matrix will be critical to identify protein X. Also, predictably a mutation in the gene expressing protein X would result in an I1 dynein assembly phenotype.

Taking advantage of numerous biochemical, genetic, and live-cell imaging approaches, I have determined IDA3 is a highly specialized and transient adapter that is required to mediate interaction between I1 dynein and IFT for entry and transport of I1 dynein within the growing cilium. From this analysis, we now understand IDA3 function within the growing cilium and, as will be discussed below, can use IDA3 as a tool to address some of the most pertinent questions pertaining to ciliary assembly at this time.

Chapter III Figures

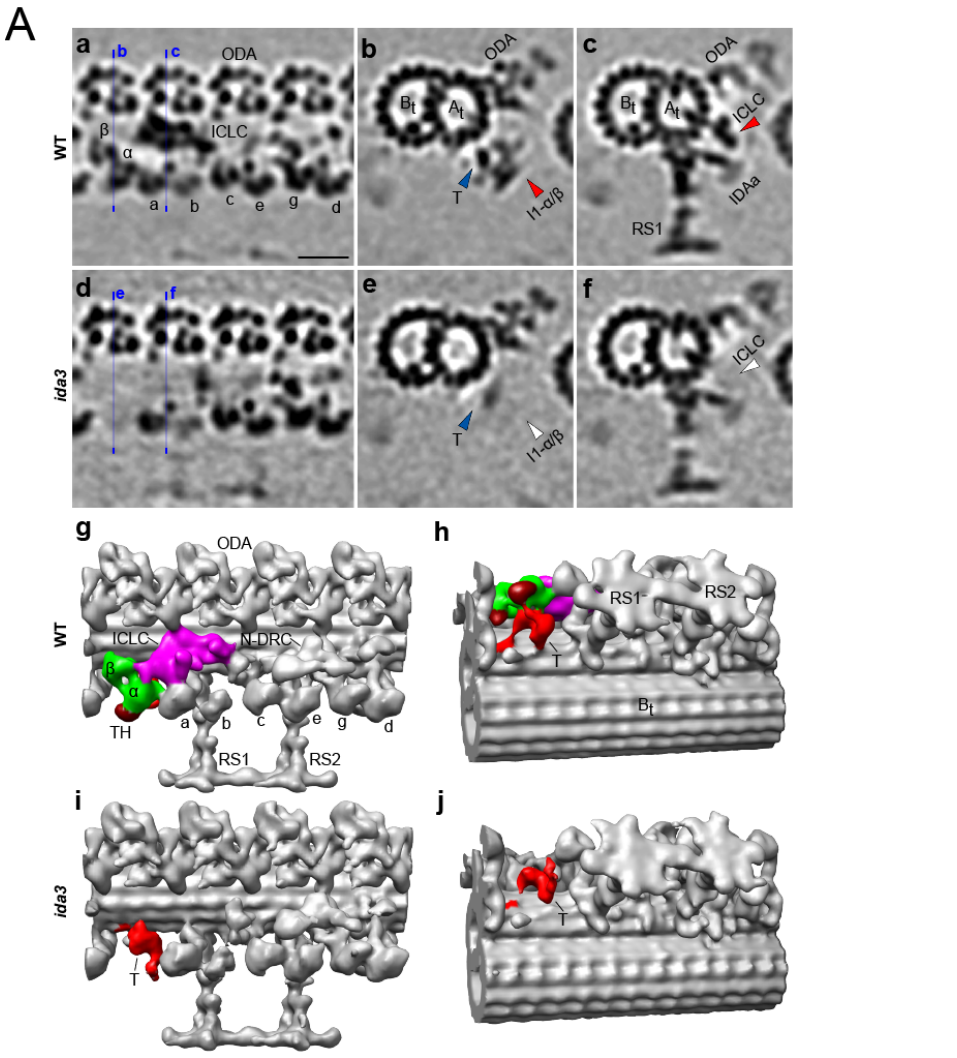

Tomogram	Number of repeats
TOM1	**26**
TOM2	**16**
TOM3	3
TOM4~8	2
TOM9~11	1
TOM12~16	0

Figure 14. I1 dynein is specifically missing in *ida3* axonemes

(A) Cryo-EM images of tomographic slices show the averaged axonemal 96 nm repeats from WT (a-c) and *ida3* mutant (d-f) in longitudinal (a and d) and cross-sectional (b, c, e, f) views. The localization of cross-sectional slices at I1 dynein heads (red arrowhead in b and white arrowhead in e) or intermediate chain/light chain complex (ICLC) (red arrowhead in c and white arrowhead in f) is indicated by the blue lines in a and d. 3D isosurface renderings show the front (g and i) and rotated bottom (h and j) views. The I1-tether structure (T) (blue arrowheads in b and e and red-colored structures in g-j is still visible in *ida3* (i and j), but the position and morphology differ somewhat from WT, likely due to the absence of the tether binding partners, the I1 dynein heads. The WT data have previously been published (Awata et al., 2015). Scale bar: 20 nm. **(B)** Cryo-ET and classification analysis of *ida3* axonemes reveals that I1 dynein is not completely missing in a subset of axonemes. (a – c) EM images of tomographic slices show the averaged 96 nm repeats from *ida3*_Class-1 (a), *ida3*_Class-2 (b) and WT (c). Class-1 consists of 2074 axonemal repeats (97%) that show a complete lack of I1 dynein, whereas Class-2 consists of 58 repeats (3%) that seem to possess intact I1 complex (I1α,β heads and ICLC). (d) Number of I1-possessing repeats among the 16 tomograms. Note that two tomograms (TOM1 and TOM2) have significantly more repeats with I1 dynein. (e) Distribution pattern of I1-possessing repeats in the two tomograms emphasized in (d). Each grid represents an axonemal repeat and the colors indicate whether I1 dynein is present (red) or absent (gray) in the repeat. The WT data have previously been published (Awata et al., 2015). Scale bar: 20 nm.

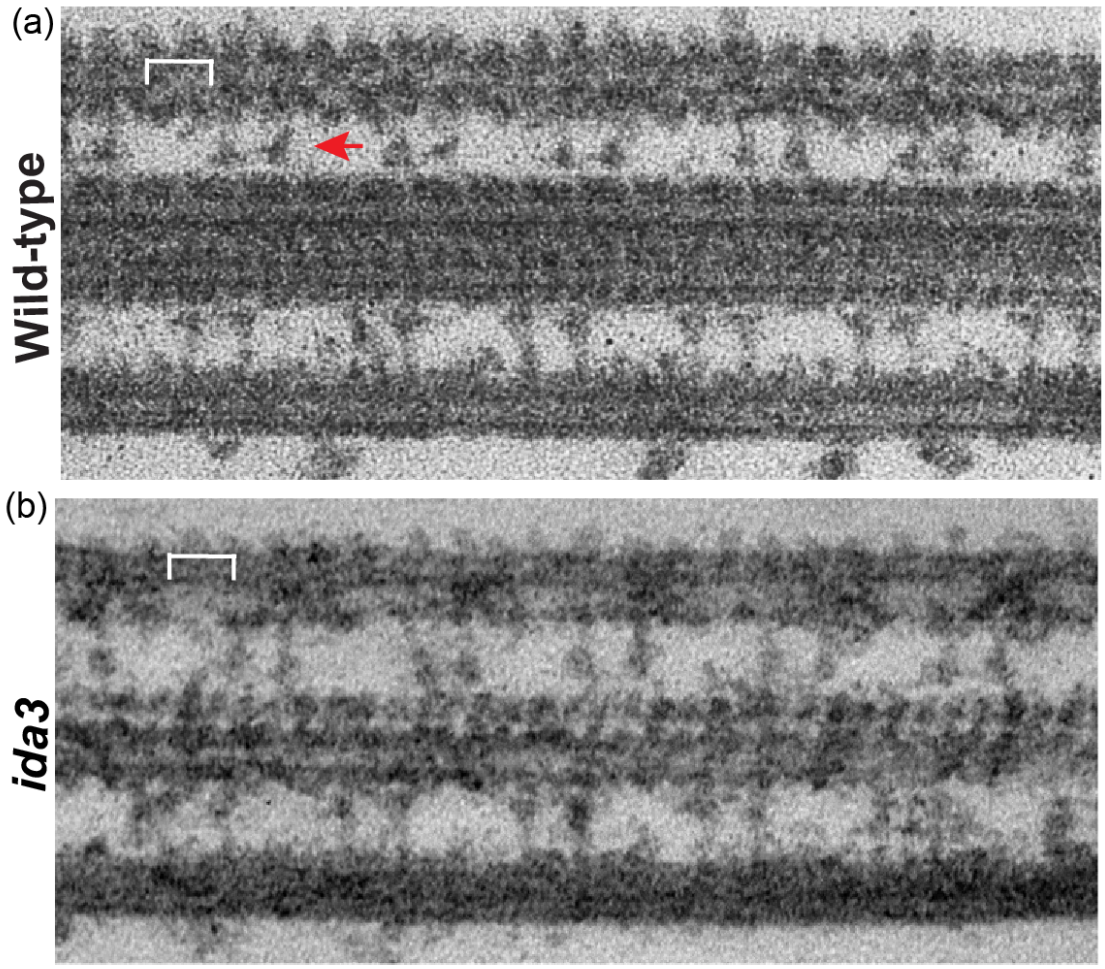
(a)
Wild-type
(b)
ida3

Figure 15. I1 dynein is absent in *ida3* axonemes when examined by electron microscopy

Comparison of longitudinal sections of wild-type and *ida3* axonemes. Conventional electron microscopy thin sections (~60 nm) were prepared as described in Materials and Methods. Longitudinal sections are oriented with the proximal end to the left and radial spoke 2 illustrated with a red arrow. I1 dynein is assembled in the axoneme of wild-type (see density under white bracket). The I1 dynein complex is absent in the *ida3* mutant (see loss of density under white bracket). Scale bar is 100 nm.

Markers/Chromosomal Position	Primers		Map Distance
DMAT 3734575-3734876	GGA CAT TCG TGT GGA GTG AA	GGG CAC GTC TGA CAG TAA CA	(52/200) 26
TUA1 6017824-6018236	GGC CAT GAG TTG CTT CTT TC	AGG AAA CGC AGT CAA GGG TA	(25/180) 14
120019 7212051-7212507	GCA CAT GCC ATC ATA TCA GC	AGC GCT ACA CCA GAA CGA GT	(18/220) 8
953 7414224-7414441	GTG TGC GTG TCA GTA TGA GCT GG	CGC AGG ACA GTG TAC CTA CCG TTT	(6/210) 3
Cre03.g205000 *ida3* cuts w/ *Sfc*I 7558888-7558973 W22X at 7558765	ATT TGG ACG GAG CCT TGA C	TGT TTC GCA CGC CTT CA	(0/75) 0
120055 7983109-7983437	GTG ATG GGC TAC CAG ACG TT	GCT GTC CAG GTT CTT CAG GA	(7/221) 3
PHOT 8321757-8322182	TGC AGT TTT GCA GTT TGG AG	CTG CCG TCC ATG TTC CTT AT	(36/200) 18

*Further information in Dutcher et al., 2012.

Table I. Primers used to map the *ida3* mutant to Cre03.g205000

Whole genome sequencing was used to identify Cre03.g205000 as the gene defective in the *ida3* mutant (Lin and Dutcher, 2013).

A

Cre03.g205000 *(IDA3)*

Wild-type

M D A Q P N T S F N A H Q L R V V Q Q L L W N V L

ATGGATGCGCAGCCAAACACCTCATTCAATGCGCACCAACTGCGCGTGGTCCAGCAGCTGCTATGGAATGTCCTC

ida3

M D A Q P N T S F N A H Q L R V V Q Q L L X

ATGGATGCGCAGCCAAACACCTCATTCAATGCGCACCAACTGCGCGTGGTCCAGCAGCTGCTA**TAG**AATGTCCTC

B

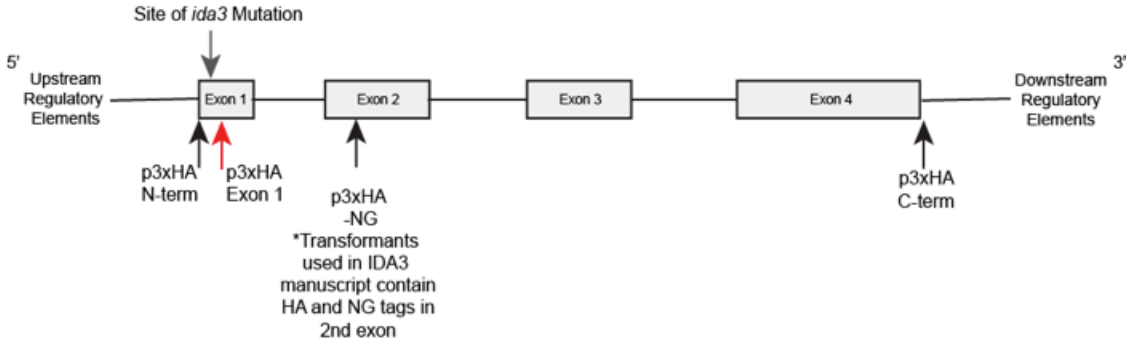

*Tags in Exon 1 and Exon 2 inserted into predicted disordered loops in the IDA3 protein

Figure 16. The *ida3* mutant contains a single base transversion that results in a premature stop codon.

(A) In the *ida3* mutant, Cre03.g205000 contains a nonsense mutation. IDA3 contains a CCDC24 domain in the N-terminal half. **(B)** Schematic of Cre03.g205000 *(IDA3)* gene. *IDA3* consists of four exons and is ~4.2kb when including upstream and downstream regulatory elements. The sequence encoding HA and NG were inserted in exon 2 for the published IDA3 studies. Other tagged locations in additional IDA3 constructs are also indicated. The red arrow indicates insertion of HA in the first exon of *IDA3* that prevents rescue of I1 dynein assembly. The site of mutation in *ida3* is also indicated.

Transformation

Cell Type	*IDA3* Construct	Rescue Swimming Defect	Restore IC140	Restore IC138
ida3;oda2	No Tag	Yes	Yes	Yes
ida3+	p3xHA N-term	Yes	Yes	Yes
ida3+	p3xHA C-term	Yes	Yes	Yes
ida3+	p3xHA Exon 1	No	No	No
ida3+	p3xHA Exon 2	Yes	Yes	Yes
ida3+	NeonGreen N-term	Yes	Yes	Yes
ida3+	NeonGreen Second Exon	Yes	Yes	Yes

Table II. *IDA3* constructs used for *ida3* transformation

IDA3 constructs used to rescue *ida3* mutants. *ida3* mutants were successfully rescued using *IDA3*, N-terminally and C-terminally tagged *IDA3* constructs, or with the tag embedded within the second exon of the *IDA3* gene. We were unable to isolate *ida3* rescued transformants when the HA tag was embedded within the first exon of the *IDA3* gene.

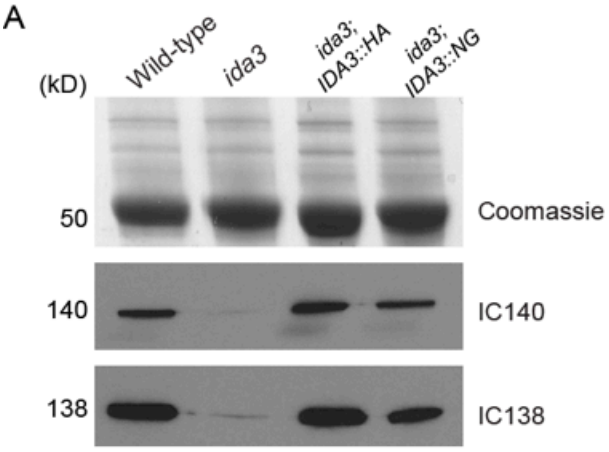
A
Wild-type
ida3
ida3; IDA3::HA
ida3; IDA3::NG
(kD)
50
Coomassie
140
IC140
138
IC138

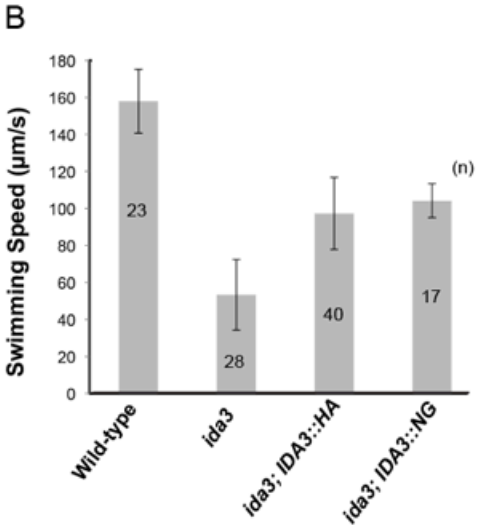
B
Swimming Speed (μm/s)
180
160
140
120
100
80
60
40
20
0
(n)
23
28
40
17
Wild-type
ida3
ida3; IDA3::HA
ida3; IDA3::NG

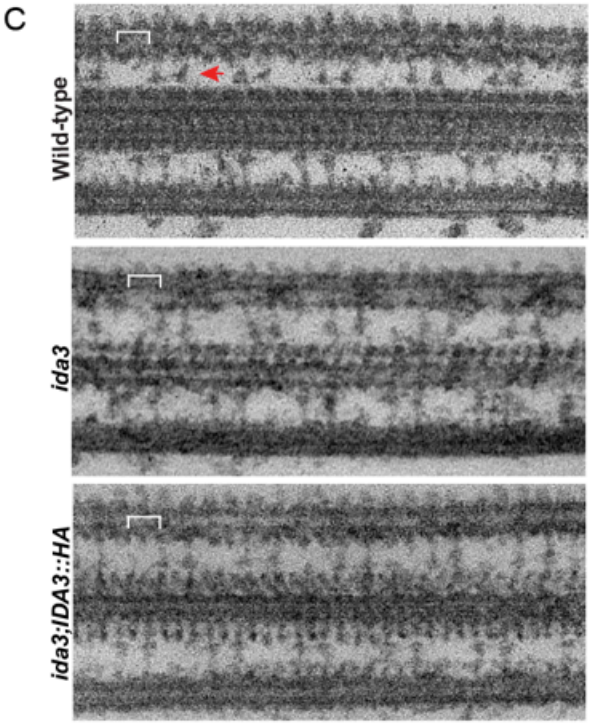
C
Wild-type
ida3
ida3;IDA3::HA

Figure 17. Transformation of *ida3* with *IDA3*-tagged constructs rescues I1 dynein assembly in the axoneme

(A) Immunoblot of isolated axonemes from WT, *ida3*, *ida3;IDA3::HA,* and *::NG* cells probed with antibodies to IC140 and IC138. (B) Swimming speed analysis for wild-type, *ida3*, *ida3; IDA3::HA*, and *::NG*. *ida3* slow swimming phenotype is rescued in *ida3* transformants. Error bars = SD. (C) Comparison of longitudinal sections of wild-type, *ida3* and *ida3; IDA3::HA* rescued transformant axonemes. Conventional electron microscopy thin sections (~60 nm) were prepared as described in Materials and Methods. Longitudinal sections are oriented with the proximal end to the left and radial spoke 2 illustrated with a red arrow. I1 dynein is assembled in the axoneme of both the wild-type and the *ida3; IDA3::HA* (see density under white bracket). The I1 dynein complex is absent in the *ida3* mutant (see loss of density under white bracket) (Fig. 14). Thus, the expression of the *IDA3* gene within the *ida3* mutant rescues the assembly of I1 dynein in the axoneme. Scale bar is 100 nm.

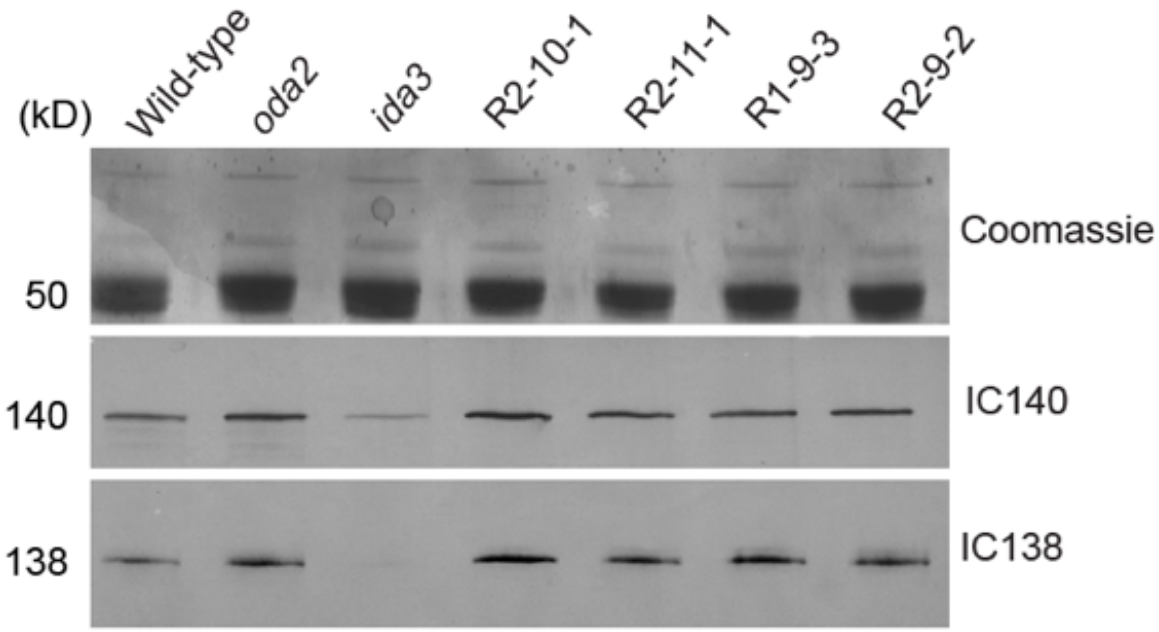
(kD)
Wild-type
oda2
ida3
R2-10-1
R2-11-1
R1-9-3
R2-9-2
50
Coomassie
140
IC140
138
IC138

Figure 18. I1 dynein assembly is rescued in the axoneme of intragenic revertants of *ida3; oda2* cells.

(A) Immunoblot of axonemes from *ida3; oda2* intragenic revertants. IC140 and IC138 assemble in axonemes from the intragenic revertants.

Table III

Cell Type	Single Base Transversion
Wild-type	CTGCTATGGAATGT W
ida3;oda2	CTGCTATAGAATGT
R1-9-3	CTGCTATATAATGT Y
R2-9-2	CTGCTATATAATGT Y
R2-10-1	CTGCTAAAGAATGT K
R2-11-1	CTGCTAAAGAATGT K
R2-13-1	CTGCTATATAATGT Y

Table III. Sequencing analysis of *ida3; oda2* intragenic revertants.

Single base changes observed within the *ida3; oda2* intragenic revertants removed the premature stop codon in *ida3* and allow rescue of I1 dynein assembly in the axoneme.

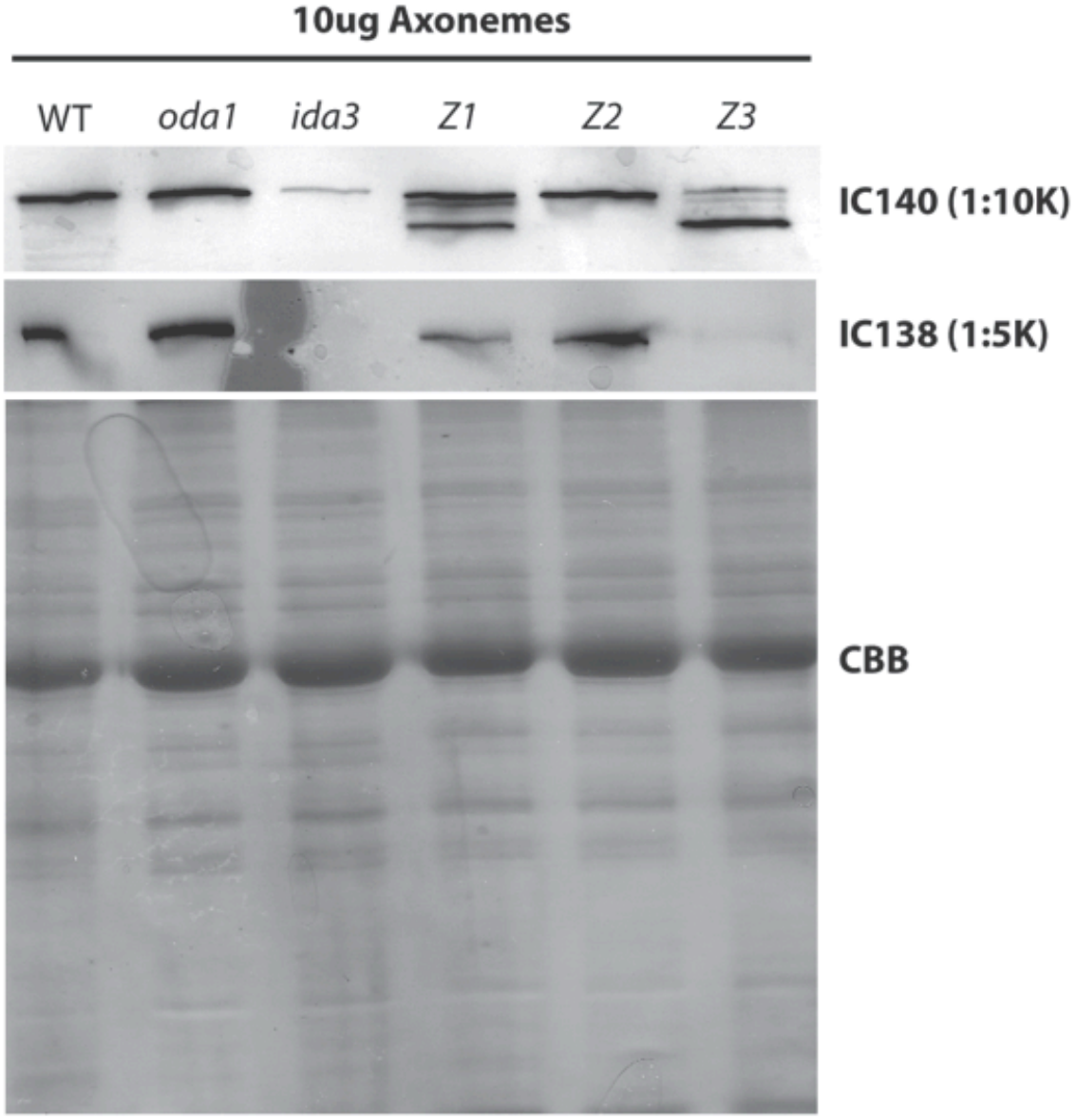
10ug Axonemes
WT
oda1
ida3
Z1
Z2
Z3
IC140 (1:10K)
IC138 (1:5K)
CBB

Figure 19. Extragenic reversion of *ida3; oda2* results in the assembly of truncated IC140 in the axoneme.

Immunoblot analyses of isolated axonemes from wild-type, *oda1, ida3, Z1, Z2,* and *Z3* cells. *Z1* and *Z3* are extragenic revertants. *Z2* is an intragenic revertant. *Z1* and *Z3* assemble truncated IC140 in the axoneme. IC138 does not assemble in *Z3* and is reduced in the *Z1* extragenic revertant. Coomassie Brilliant Blue (CBB) staining acts a load control.

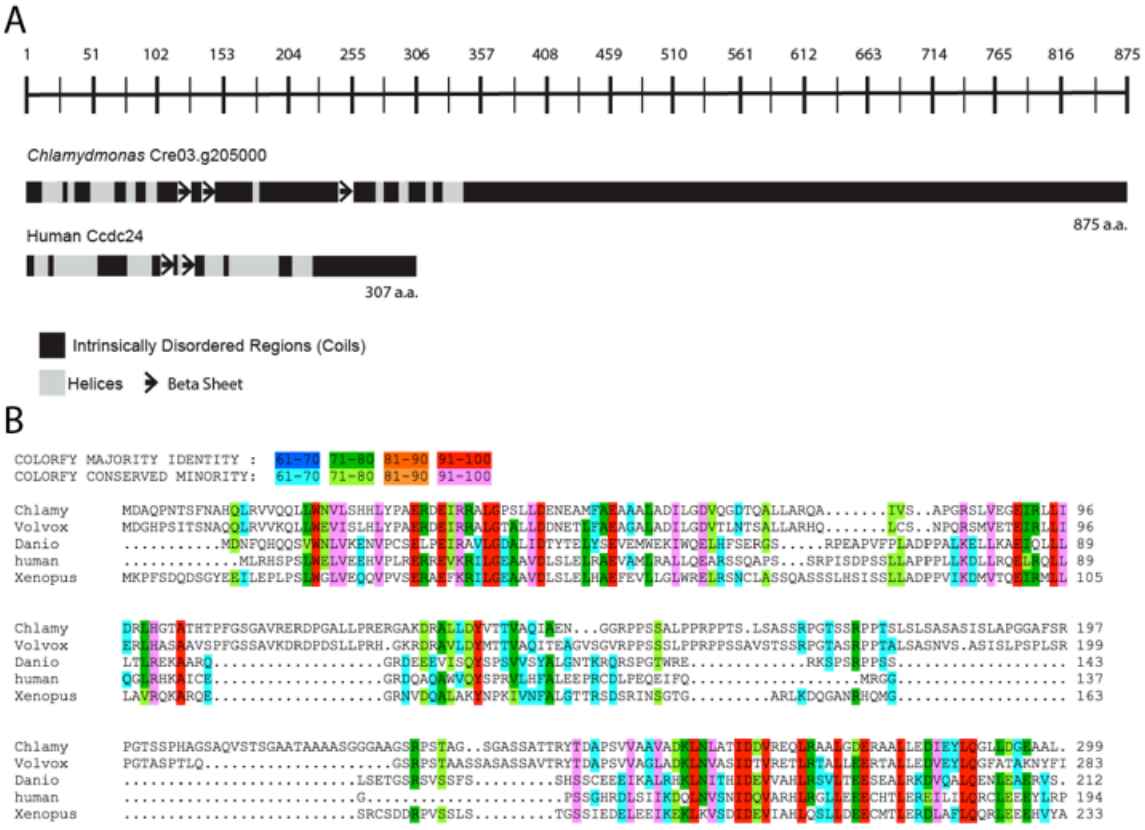
A
1
51
102
153
204
255
306
357
408
459
510
561
612
663
714
765
816
875
Chlamydmonas Cre03.g205000
875 a.a.
Human Ccdc24
307 a.a.
Intrinsically Disordered Regions (Coils)
Helices
Beta Sheet
B
COLORFY MAJORITY IDENTITY : 61-70 71-80 81-90 91-100
COLORFY CONSERVED MINORITY: 61-70 71-80 81-90 91-100
Chlamy MDAQPNTSFNAHQLRVVQQLLWNVLSHHLYPAERDEIRAALGPSLLDENEAMFALAAALADILGDVQGDTQALLARQA.....IVS..APGRSLVEGEIRLLI 96
Volvox MDGHPSITSNAQQLRVVKQLLWEVISLHLYPAERDEIRAALGTKLLDDNETLFAEAGALADILGDVTLNTSALLARHQ.....LCS..NPQRSMVETEIRLLI 96
Danio .....MDNFQHQQSVWNLVKENVPCSELPEIRAVLGDKLIDTYTELYSEVEMWEKIWQELHFSERGS.....RPEAPVFPLADPPALKELLKAEIQLLL 89
human .....MLRHSPSLWELVEEHVPLRERREVKRILGEAAVDLSLELRAEVAMLRALLQEARSSQAPS...SRPISDPSSLLAPPPLLKDLLRQELHQLL 89
Xenopus MKPFSDQDSGYEEILEPLPSLWGLVEQQVPVSERAEFKRILGEAAVDLSLELHAEFEVLLGLWRELRSNCLASSQASSSLHSISSLLADPPVIKDMVTQEIRMLL 105
Chlamy DRLHGTATHTPFGSGAVRERDPGALLPRERGAKDRALLDYVTTVAQIMEN...GGRPPSSALPPRPPTS.LSASSRPGTSSRPPTSLSLSASASISLAPGGAFSR 197
Volvox ERLHASAAVSPFGSSAVKDRDPDSLLPRH.GKRDRAVLDYMTTVAQITEAGVSGVRPPSSSLPPRPPSSAVSTSSRPGTASRPPTALSASNVS.ASISLPSPLSR 199
Danio LTLREKAARQ.....GRDEEEVISQYSPSVVSYALGNTKRQRSPGTWRE.....RKSPSRPPSS..... 143
human QQLRHKAICE.....GRDQAQAWVQYSPRVLHFALEEPRCDLPEQEIFQ.....MRGG..... 137
Xenopus LAVRQKARQE.....GRNVDQALAKYNPKIVNFALGTTRSDSRINSGTG.....ARLKDQGANRHQMG..... 163
Chlamy PGTSSPHAGSAQVSTSGAATAAAASGGGAAGSHPSTAG..SGASSATTRYTDAPSVVAAVADKLNLATIDDVREQLHAALGDERAALLEDIEYLQGLIDGEAAL. 299
Volvox PGTASPTLQ.....GSHPSTAASSASASSAVTRYTDAPSVVAGLADKLNVASIDTVRETLRTALLERRTALLEDVEYLQGFATAKNYFI 283
Danio .....LSETGSHSVSSFS.....SHSSCEEEIKALRHKLNITHIDEVVAHLRSVLTEESEALRKDVQALCENIEAERVS. 212
human .....G.....PSSGHRDLSIIKDQLNVSNIDQVARHLRGLEEECHTLEREILLLQRCLEEEYLRP 194
Xenopus .....SRCSDDMPVSSLS.....TGSSIEDELEEIKEKLKVSDIDEVIAHLQSLIDEECMTLERDLAFLQQRIEEEHVYA 233

Figure 20. Analysis of IDA3 protein structure and conservation

(A) IDA3 contains a CCDC24 domain in the N-terminal half. **(B)** Colorfly analysis of IDA3 protein as compared to *Volvox*, zebrafish, human, and *Xenopus* protein CCDC24. The N-terminal region of IDA3 (~ 250 amino acids) contains a CCDC24 domain.

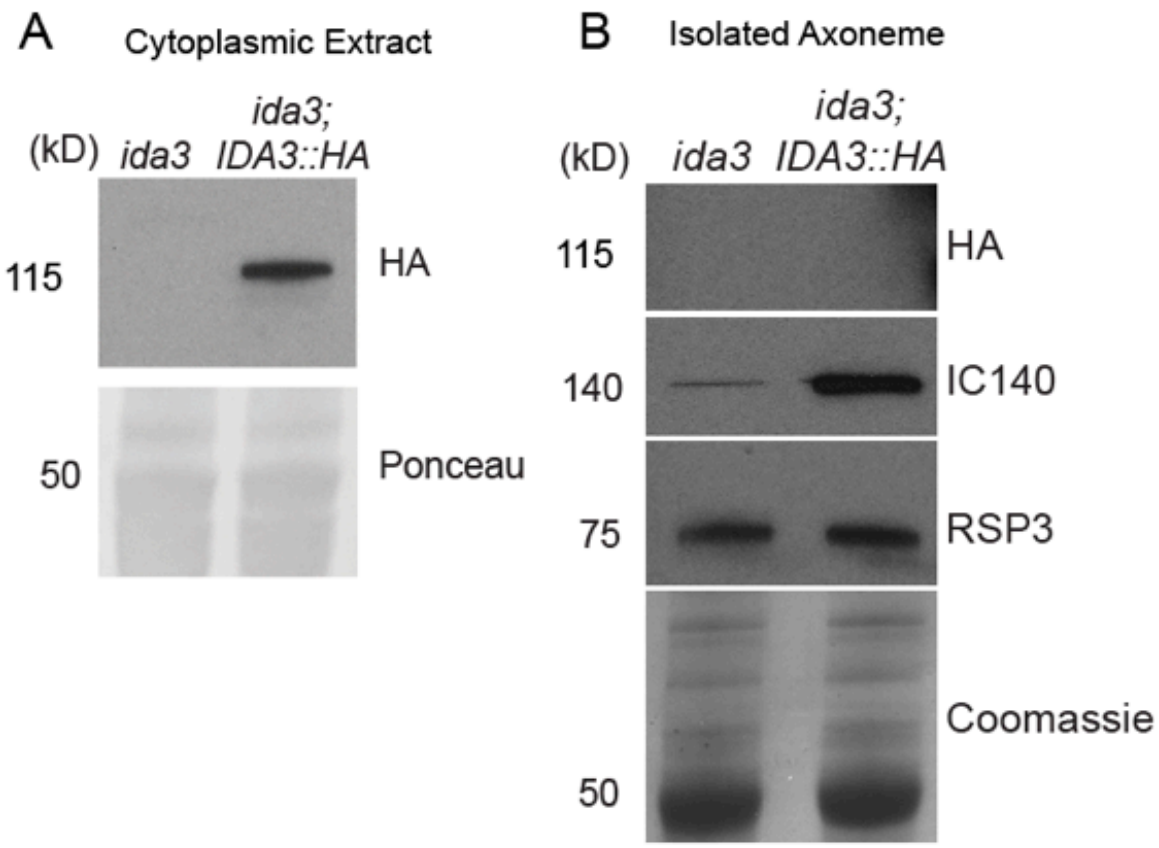
A
Cytoplasmic Extract
(kD)
ida3
ida3; IDA3::HA
115
HA
50
Ponceau
B
Isolated Axoneme
(kD)
ida3
ida3; IDA3::HA
115
HA
140
IC140
75
RSP3
50
Coomassie

Figure 21. IDA3 is present in the cytoplasm but does not assemble in the axoneme

(A) Immunoblot of cytoplasmic extract isolated from fully-ciliated *ida3* and *ida3; IDA3::HA* cells. IDA3::HA is detected in the cytoplasm. **(B)** Immunoblot of axonemes from *ida3* and *ida3; IDA3::HA* full-length cilia. IDA3::HA is not present in the axonemes but IC140 assembles as expected.

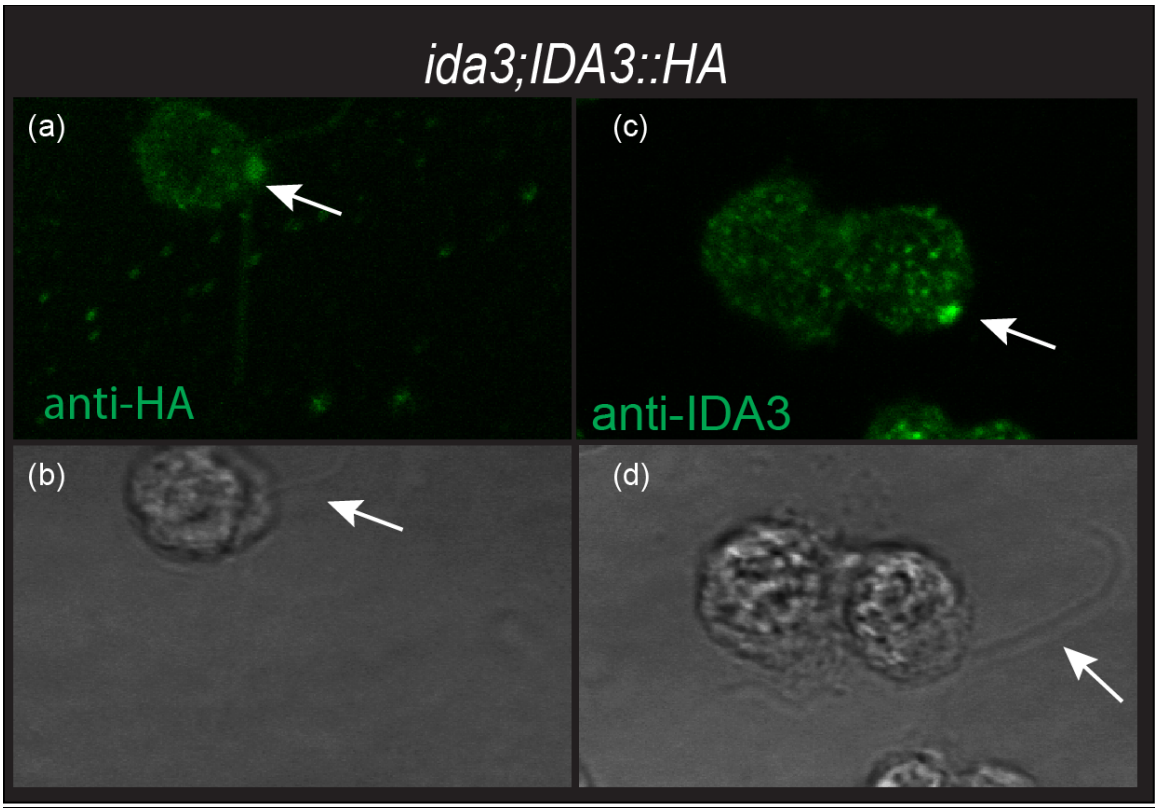
ida3;IDA3::HA
(a)
anti-HA
(c)
anti-IDA3
(b)
(d)

Figure 22. IDA3 localizes to the basal bodies

(a) *ida3;IDA3::HA* cells stained with HA (3f10) antibody and imaged by confocal microscopy. White arrow indicates IDA3::HA localization at the basal body. **(b)** Phase-contrast image of *ida3; IDA3::HA* cell imaged in (a). White arrow indicates location of cilia off cell body. **(c)** *ida3;IDA3::HA* cells stained with affinity purified IDA3 antibody and imaged by confocal microscopy. IDA3::HA is localized at the basal body (white arrow). **(d)** Phase-contrast of *ida3; IDA3::HA* cells imaged in (c). White arrow indicates location of cilium.

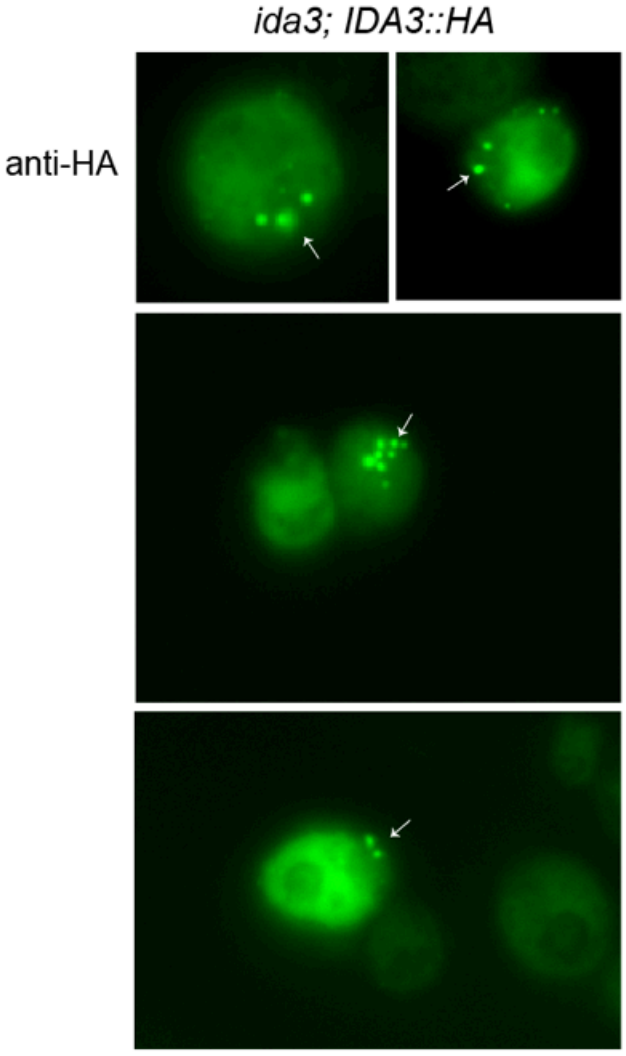
ida3; IDA3::HA
anti-HA

Figure 23. IDA3 localizes to distinct puncta in the cytoplasm

ida3;IDA3::HA cells stained with HA (3f10) antibody and imaged using conventional epifluorescence microscopy. Distinct green puncta are observed in the cytoplasm of numerous *ida3;IDA3::HA* cells. White arrows indicate distinct puncta.

A

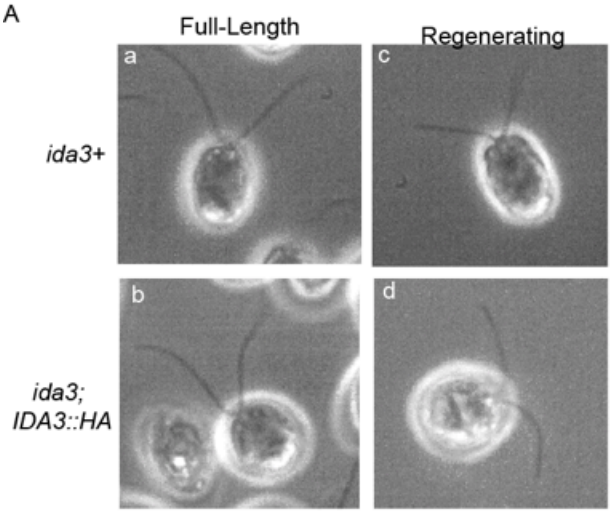

Table IV

Cell Type	Number of Cilia	Average Length of Cilia	Standard Deviation	Standard Error
ida3 Full-Length	n = 84	10.17 µm	+/- 1.33	+/- 0.15
ida3 Regenerating	n = 84	6.35 µm (62% of Full-Length)	+/- 1.63	+/- 0.17
ida3;IDA3::HA Full-Length	n = 84	10.70 µm	+/- 1.21	+/- 0.13
ida3; IDA3::HA Regenerating	n = 99	6.42 µm (60% of Full-Length)	+/- 1.3	+/- 0.13
Compiled Full-Length	n = 168	10.44 µm	+/- 1.30	+/- 0.1
Compiled Regenerating	n = 183	6.13 µm (59% of Full-Length)	+/- 1.49	+/- 0.11

Figure 24. Analysis of cilia length during regeneration

Bright-field microscopy was used to image full-length and regenerating *ida3* and *ida3; IDA3::HA* cells. **(a)** Full-length *ida3+* cilia. **(b)** Full-length *ida3; IDA3::HA* cilia. **(c)** Regenerating *ida3+* cilia. **(d)** Regenerating *ida3;IDA3::HA* cilia.

(Table IV) Quantification of cilia length during regeneration

The length of full-length and regenerating *ida3* and *ida3;IDA3::HA* cilia was measured. On average, cilia are roughly two-thirds the length of full-length cilia. Lengths range from one-half to three-quarters full-length cilia

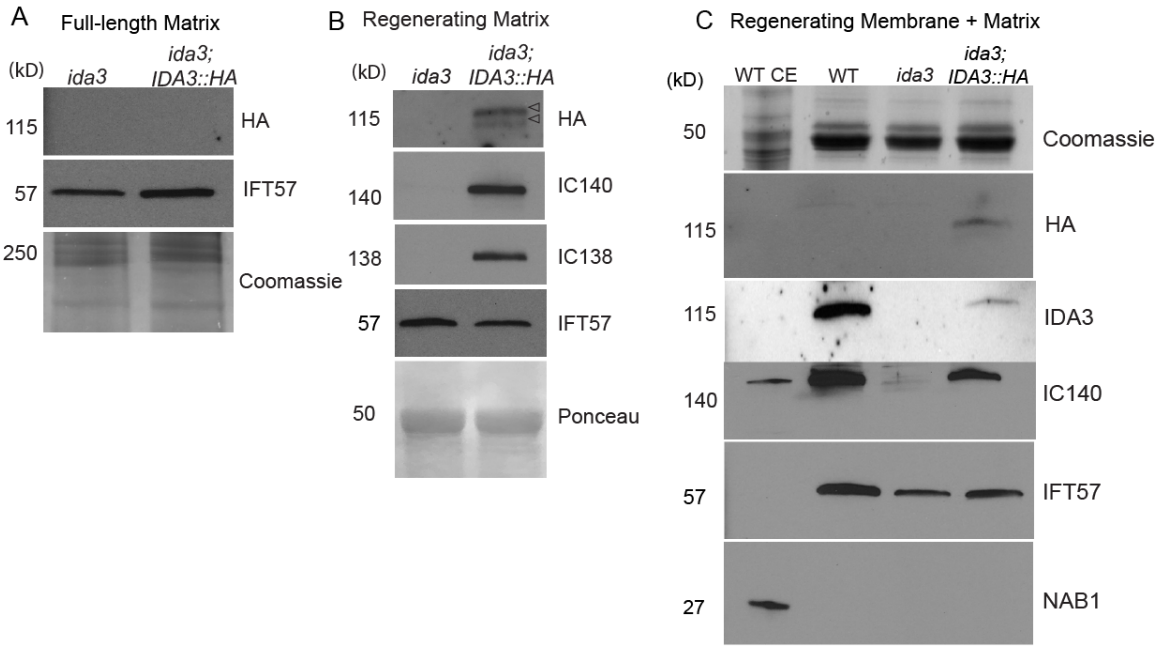
A
Full-length Matrix
(kD)
ida3
ida3; IDA3::HA
115
HA
57
IFT57
250
Coomassie
B
Regenerating Matrix
(kD)
ida3
ida3; IDA3::HA
115
HA
140
IC140
138
IC138
57
IFT57
50
Ponceau
C
Regenerating Membrane + Matrix
(kD)
WT CE
WT
ida3
ida3; IDA3::HA
50
Coomassie
115
HA
115
IDA3
140
IC140
57
IFT57
27
NAB1

Figure 25. IDA3 selectively enters the cilium during regeneration

(A) Immunoblot of matrix from *ida3* and *ida3; IDA3::HA* full-length cilia. Immunoblots were probed with antibodies to HA, and as a loading control, IFT57. IDA3::HA was not detectable in matrix of full-length *ida3; IDA3::HA* cilia. **(B)** Immunoblot of matrix isolated from *ida3* and *ida3; IDA3::HA* regenerating cilia. Immunoblots were probed with antibodies to HA, IC140, IC138, and, as a loading control, IFT57. IDA3::HA, IC140, and IC138 are present in the regenerating matrix of *ida3; IDA3::HA*. **(C)** Immunoblot of regenerating membrane + matrix from wild-type, *ida3,* and *ida3;IDA3::HA* cells. Wild-type cytoplasmic extract is also present on immunoblot as a control. The immunoblot was probed with HA and IDA3 antibodies. IDA3 is detected in the regenerating matrix of wild-type and *ida3;IDA3::HA* membrane + matrix. IC140 is present in wild-type and *ida3;IDA3::HA* membrane + matrix and absent in *ida3* as expected. IFT57 and Coomassie staining serves as a load control. NAB1 is specific to *Chlamydomonas* cytoplasm and serves as a control to ensure cytoplasmic contamination is not present in membrane + matrix samples.

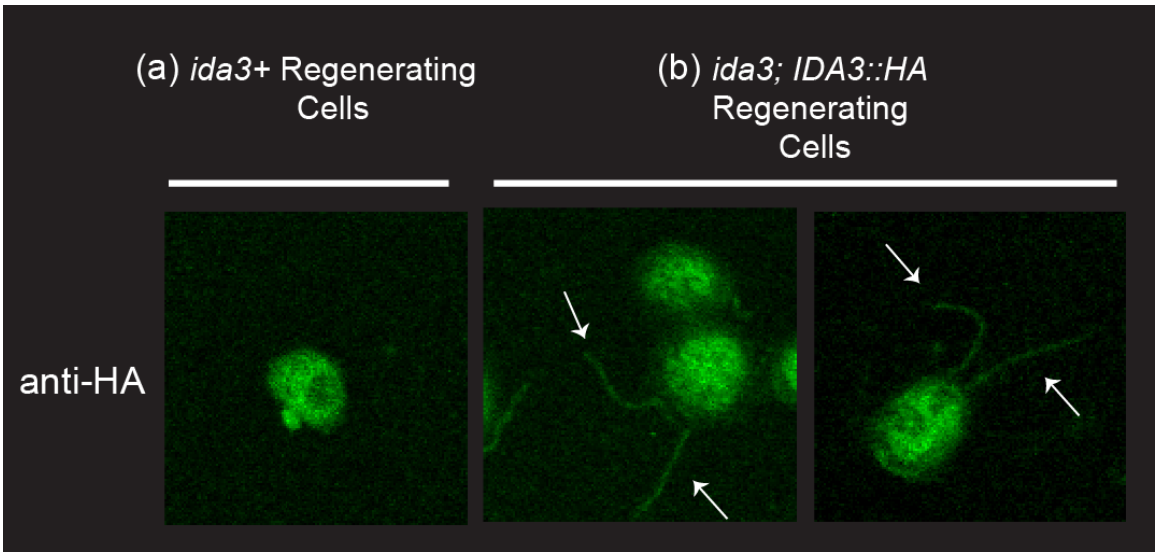
(a) ida3+ Regenerating Cells
(b) ida3; IDA3::HA Regenerating Cells
anti-HA

Figure 26. Immunofluorescence analysis detects IDA3::HA in the matrix compartment of the regenerating cilium

ida3 and *ida3; IDA3::HA* regenerating cells were fixed and stained with HA antibody for epifluorescence microscopy. **(a)** HA staining is not detected in *ida3* regenerating flagella. **(b)** Diffuse HA staining in detected in the *ida3;IDA3::HA* regenerating cilia. White arrows indicate cilia with diffuse HA staining.

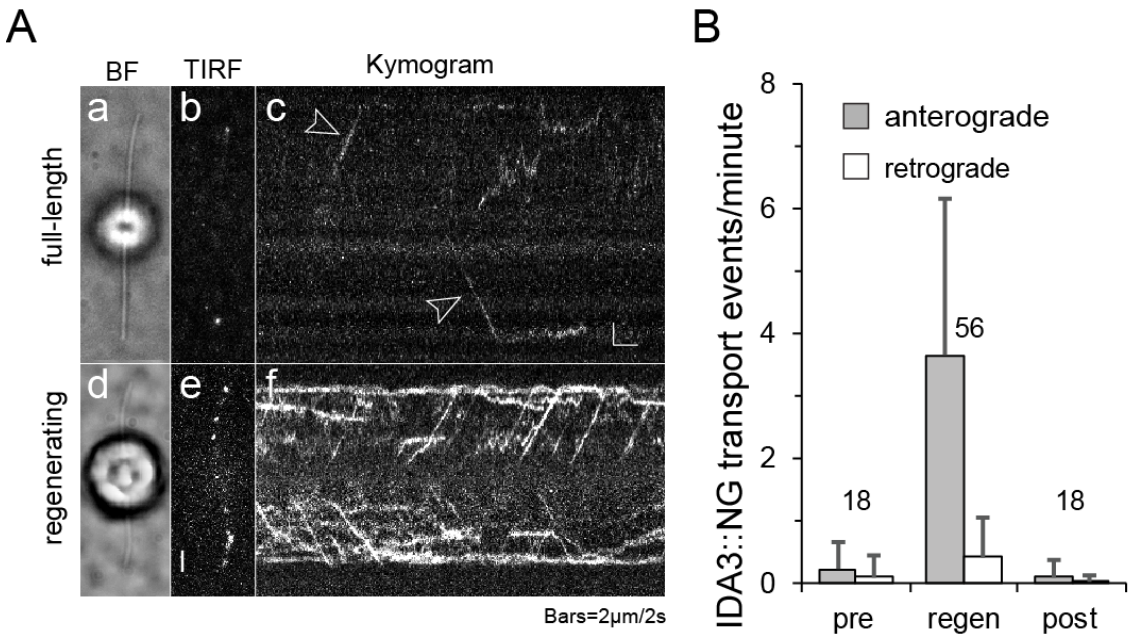
A
BF
TIRF
Kymogram
a
b
c
full-length
d
e
f
regenerating
Bars=2µm/2s
B
IDA3::NG transport events/minute
anterograde
retrograde
8
6
4
2
0
56
18
18
pre
regen
post

Figure 27. IDA3 is transported by anterograde IFT in regenerating cilia.

(A) Bright field (a,d) and TIRF images (b, e) and corresponding kymograms (c, f) of full-length (a-c) and regenerating (d-f) *ida3; IDA3::NG* cilia. Selected IDA3::NG transports are marked with arrowheads in (c). Bars = 2 s and 2 μm. **(B)** Bar diagram showing the frequency of IDA3::NG transport events per minute in full-length (pre; n=18 cilia), regenerating (regen; n=56 cilia), and post-regeneration cilia (post; n=18 cilia of ~10 μm to 12 μm in length). Error bars = SD.

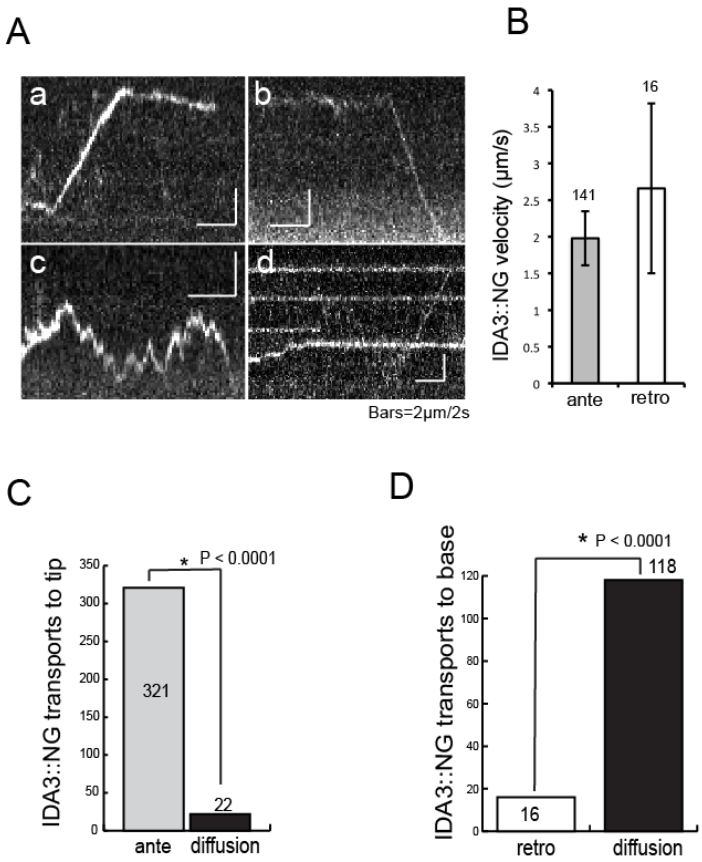
A
a
b
c
d
Bars=2µm/2s
B
IDA3::NG velocity (µm/s)
141
16
ante
retro
C
IDA3::NG transports to tip
* P < 0.0001
321
22
ante
diffusion
D
IDA3::NG transports to base
* P < 0.0001
118
16
retro
diffusion

Figure 28. Characterization of IDA3 behavior in the regenerating cilium

(A) Kymograms of IDA3::NG transport in regenerating cilia. (a) anterograde transport of IDA3::NG, (b) retrograde transport of IDA3::NG, (c) diffusion of IDA3::NG throughout the cilium, (d) stationary IDA3::NG. Bars = 2 s and 2 μm, T: tip, B: base. **(B)** Velocity of IDA3::NG transport in the cilium. Processive anterograde IDA3::NG moves at a velocity of 1.98 μm/s (n=141). Retrograde IDA3::NG transport moves at 2.66 μm/s (n=16). Error bars = SD. **(C)** Number of IDA3::NG anterograde IFT vs. diffusion events from base to tip. Two-tailed binomial test reveals a significant difference in the quantity of IDA3::NG anterograde transport events compared to diffusion ($P<0.0001$). **(D)** Quantity of IDA3::NG retrograde IFT transport vs. diffusion. IDA3::NG seldom binds retrograde IFT (n=16) and instead diffuses through the cilium (n=118). Two-tailed binomial test reveals a significant difference in IDA3::NG retrograde transport events compared to diffusion ($P<0.0001$).

ida3; IDA3::NG photobleaching

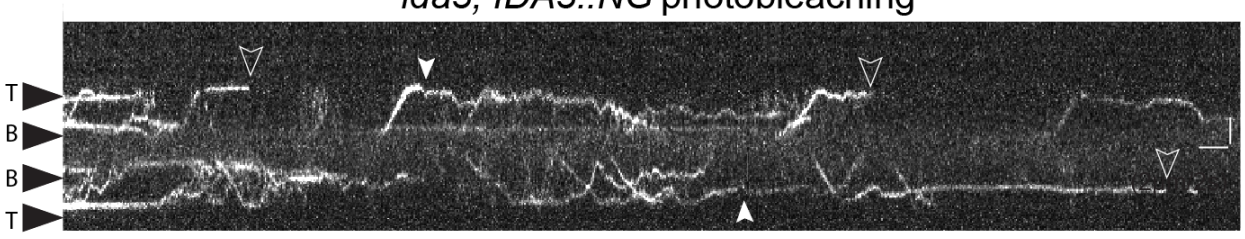

Figure 29. Single particles of IDA3 are transported by IFT to the tip of the cilium

Photobleaching analysis of IDA3::NG in *ida3; IDA3::NG* cilia. Photobleaching analysis reveals a single IDA3::NG particle is transported in by anterograde IFT at one time (open arrows). At times, multiple IDA3::NG particles accumulate at the tip of the cilium (white arrows) likely when IDA3::NG has detached from IFT and has yet to diffuse throughout the cilium. Bar = 2 s and 2 μm.

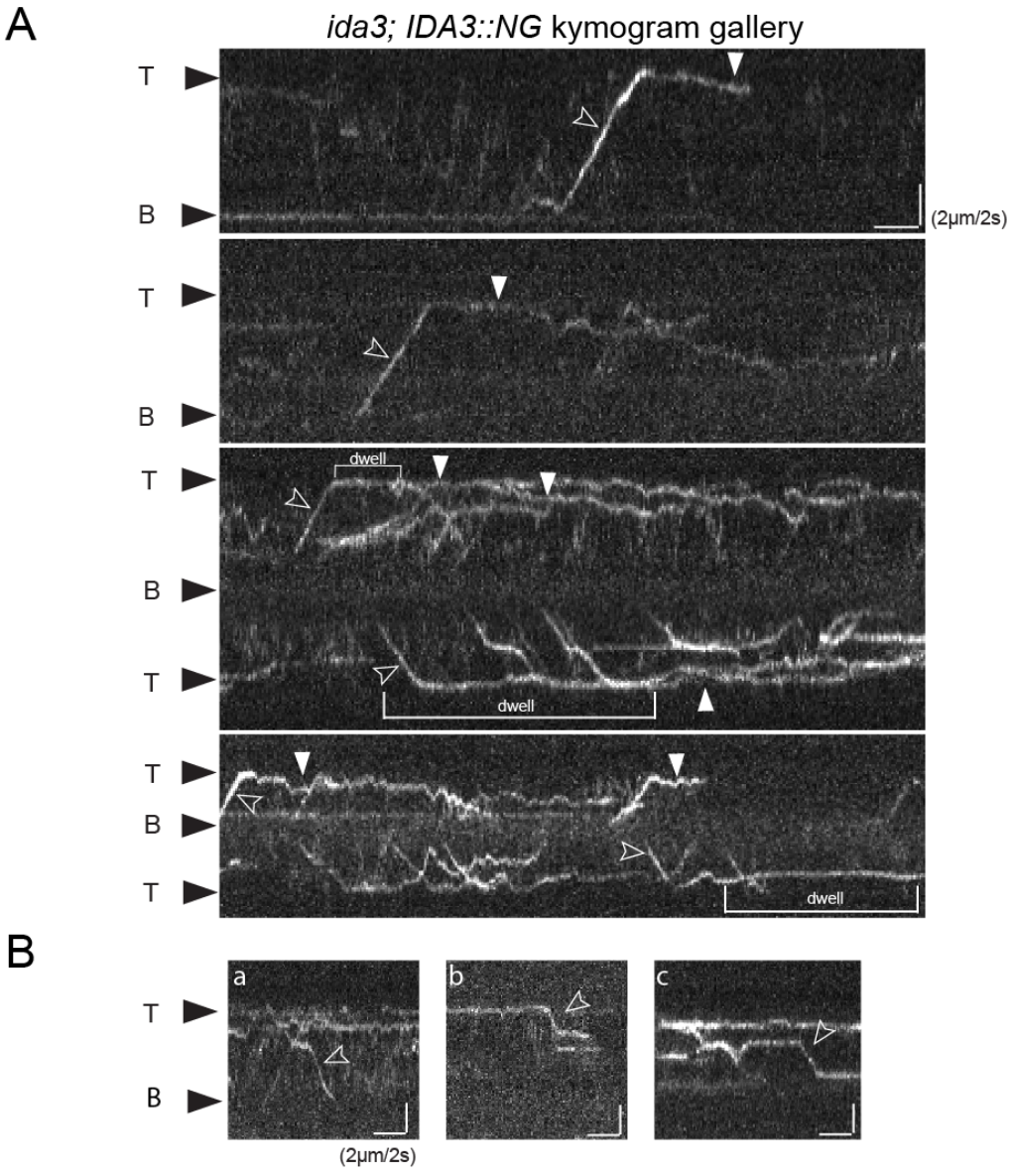
A
ida3; IDA3::NG kymogram gallery
T
B
(2µm/2s)
dwell
B
(2µm/2s)

Figure 30. Kymogram gallery of IDA3 behavior in the cilium

(A) Gallery of kymograms of IDA3::NG behavior in *ida3; IDA3::NG* cilia. Anterograde IFT transport of IDA3::NG (open arrow heads), diffusion (solid arrowheads), and dwell times (indicated by brackets) can be observed within the kymogram gallery. Bars = 2 s and 2 μm. **(B)** Gallery of kymograms representing retrograde transport of IDA3::NG. IDA3::NG interaction with retrograde IFT is transient. (a) IDA3::NG diffuses from the cilium prior to transport by retrograde IFT. (b) IDA3::NG is briefly transported by retrograde IFT prior to diffusion. (c) IDA3::NG is transported by retrograde IFT. Retrograde IFT then appears to stall while in transit.

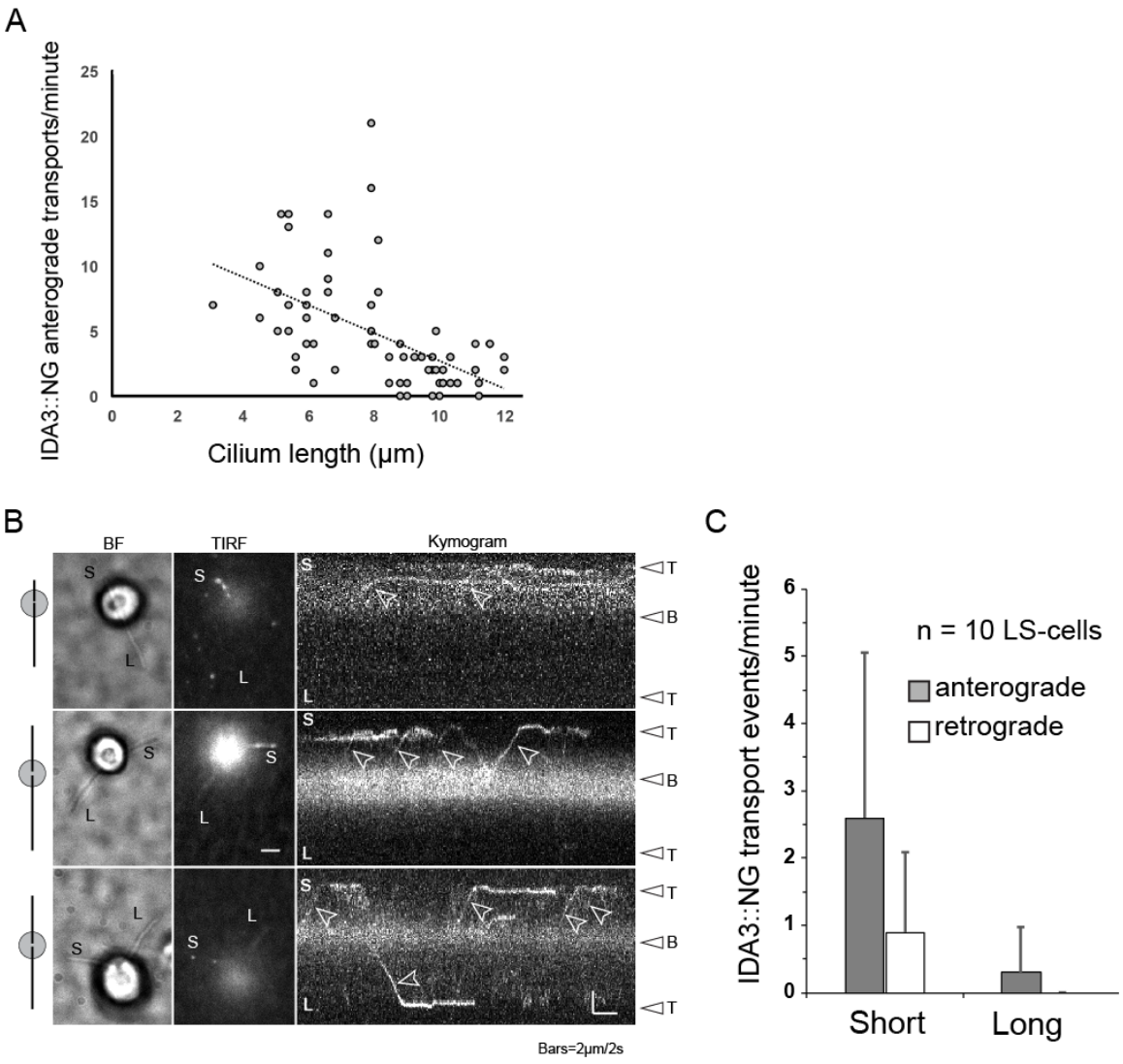
A
IDA3::NG anterograde transports/minute
25
20
15
10
5
0
0
2
4
6
8
10
12
Cilium length (μm)
B
BF
TIRF
Kymogram
S
L
T
B
Bars=2μm/2s
C
IDA3::NG transport events/minute
6
5
4
3
2
1
0
n = 10 LS-cells
anterograde
retrograde
Short
Long

Figure 31. IDA3 transport by anterograde IFT is regulated by ciliary length.

(A) The frequency of IDA3::NG anterograde transport events compared to cilium length. As the length of the cilium increases, the quantity of IDA3::NG transported by anterograde IFT decreases. **(B)** Still frames and kymograms of IDA3::NG transport in *ida3; IDA3::NG* cilia of long-short (LS) cells. Frequent anterograde IFT transport of IDA3::NG only occurs in the regenerating cilium (open arrowheads). Bar = 2 s and 2 μm **(C)** Quantification of IDA3::NG transport frequency in the short and long cilia of LS cells (n=10 cells). Error bars = SD.

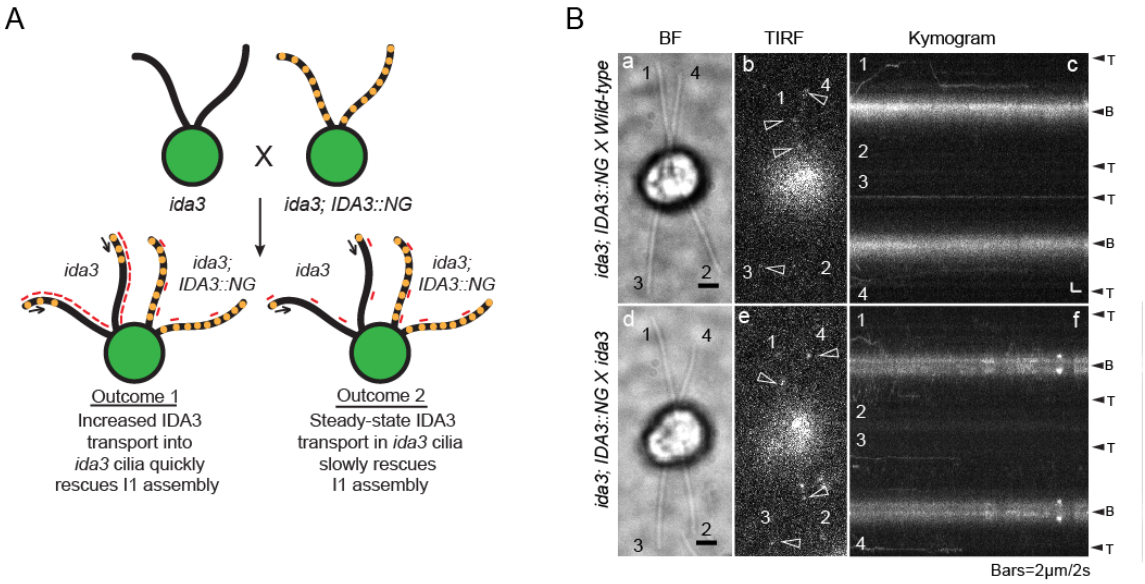
A
X
ida3
ida3; IDA3::NG
ida3
ida3; IDA3::NG
ida3
ida3; IDA3::NG
Outcome 1
Increased IDA3 transport into ida3 cilia quickly rescues I1 assembly
Outcome 2
Steady-state IDA3 transport in ida3 cilia slowly rescues I1 assembly
B
BF
TIRF
Kymogram
ida3; IDA3::NG X Wild-type
ida3; IDA3::NG X ida3
Bars=2μm/2s

Figure 32. IDA3 transport is regulated by changes in cilium length and not the need to assemble I1 dynein in the axoneme

(A) Schematic representation of dikaryon rescue experiment that results in *ida3 x ida3; IDA3::NG* zygotes. Orange dots indicate I1 docked in axoneme. Red dashes indicated IDA3 transport by IFT. **(B)** Bright field (a,d), TIRF images (b, e), and corresponding kymograms (c, f) of *ida3; IDA3::NG* x wild-type dikaryon (a-c) and *ida3; IDA3::NG* x *ida3* dikaryons (d-f). IDA3::NG transport is rare in all four full-length cilia, regardless of I1 absence in the axoneme. Bar = 2 s and 2 μm.

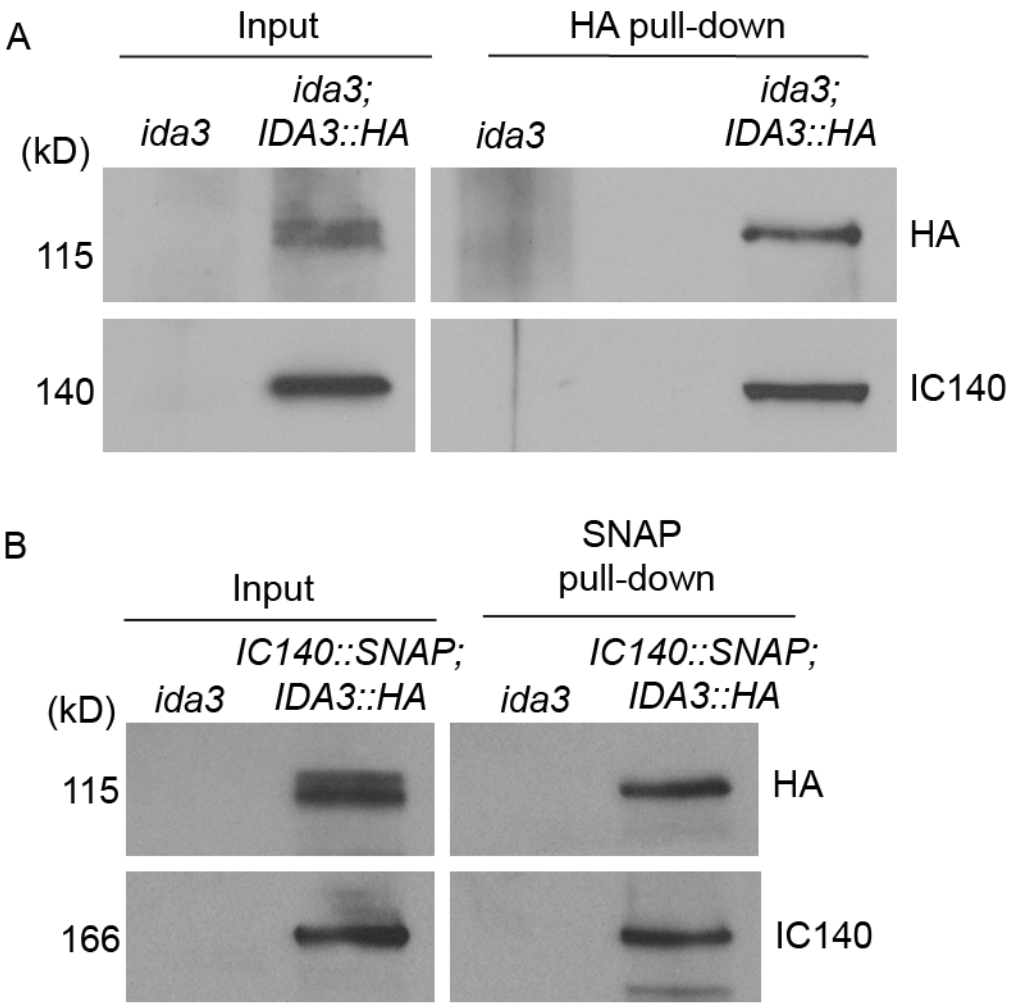
A
Input
HA pull-down
ida3
ida3; IDA3::HA
ida3
ida3; IDA3::HA
(kD)
115
HA
140
IC140
B
Input
SNAP pull-down
IC140::SNAP; IDA3::HA
ida3
IC140::SNAP; IDA3::HA
ida3
(kD)
115
HA
166
IC140

Figure 33. IDA3 interacts with IC140 of the I1 dynein complex in the matrix of the regenerating cilium.

(A) IDA3::HA was immunoprecipitated from matrix of regenerating cilia from *ida3; IDA3::HA*. Both IDA3::HA and IC140 were detected in the IP fraction. **(B)** IC140::SNAP pull-downs from matrix of regenerating *ida3* and *ida3; IDA3::HA; ida7; IC140::SNAP* cilia. Both IC140::SNAP and IDA3::HA were detected in SNAP pull-down samples. IC140 runs at 166 kD due to the addition of SNAP.

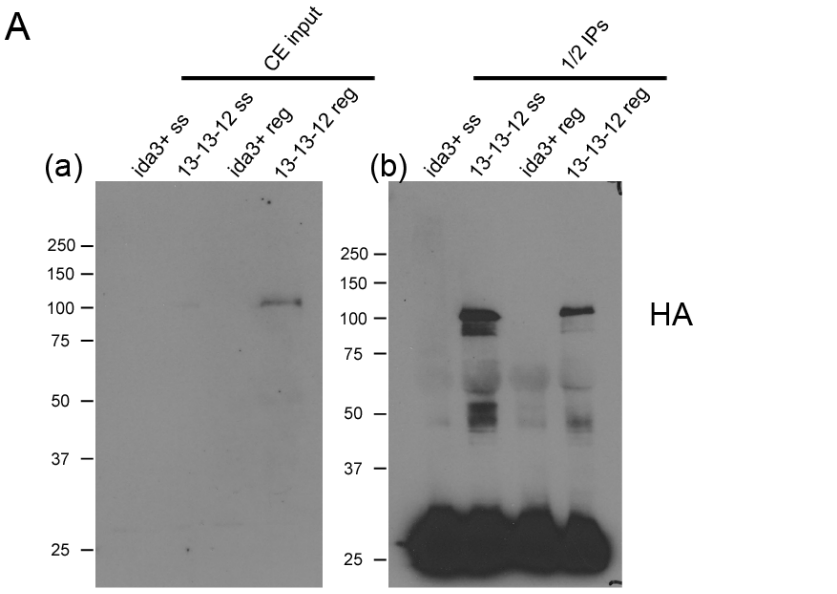
A
CE input
1/2 IPs
ida3+ ss
13-13-12 ss
ida3+ reg
13-13-12 reg
(a)
(b)
250
150
100
75
50
37
25
HA
13-13-12 = ida3; IDA3::HA

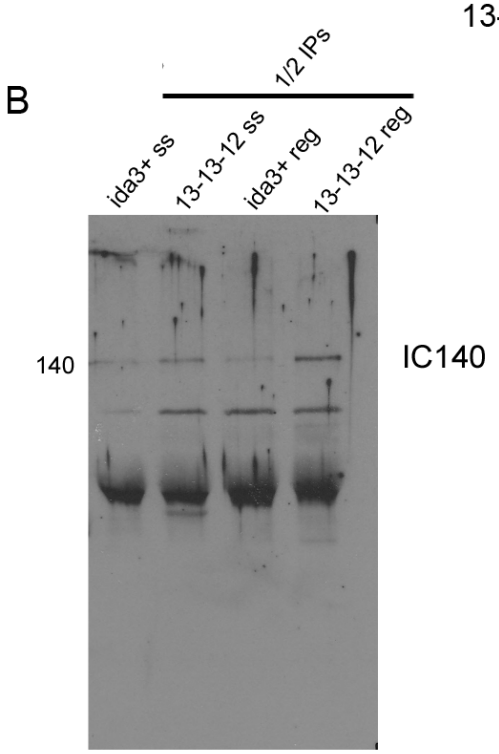
B
1/2 IPs
ida3+ ss
13-13-12 ss
ida3+ reg
13-13-12 reg
140
IC140

Figure 34. IDA3 interacts with IC140 in the cytoplasm

(A) Pull-down of IDA3::HA from cytoplasm of steady-state and regenerating *ida3;IDA3::HA* (13-13-12) cells. **(a)** Immunoblot analysis of cytoplasmic extract input of *ida3* and *ida3;IDA3::HA* steady-state and regenerating fractions. Immunoblot was probed with HA antibody. IDA3::HA is detected in both steady-state and regenerating *ida3;IDA3::HA* cytoplasmic extract but appears more prominent in the regenerating cytoplasmic extract. **(b)** IDA3::HA was immunoprecipitated from *ida3;IDA3::HA* steady-state and regenerating cytoplasm. Immunoblot analysis of pull-down fractions probed with HA antibody detect IDA3::HA in both steady-state and regenerating IP samples. **(B)** IC140 was detected in both steady-state and regenerating IDA3::HA IP samples. IDA3 and IC140 interact in the cytoplasm of cells with either full-length or regenerating cilia.

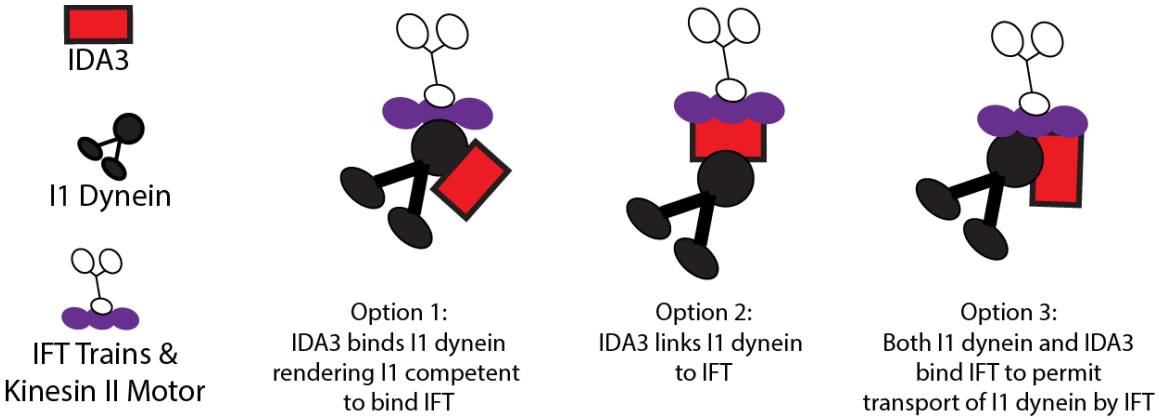
IDA3
I1 Dynein
IFT Trains &
Kinesin II Motor
Option 1:
IDA3 binds I1 dynein
rendering I1 competent
to bind IFT
Option 2:
IDA3 links I1 dynein
to IFT
Option 3:
Both I1 dynein and IDA3
bind IFT to permit
transport of I1 dynein by IFT

‘

Figure 35. Modeling IDA3-mediated I1 dynein interaction with IFT

IDA3 acts as an adapter to mediate IFT interaction with the I1 dynein cargo but how IDA3 mediates this interaction remains unclear. IDA3 may bind I1 dynein and render I1 competent to bind IFT (Option 1). Alternatively, IDA3 may link I1 dynein to IFT (Option 2) or both IDA3 and I1 dynein may interaction with IFT to permit transport of I1 dynein by IFT (Option 3).

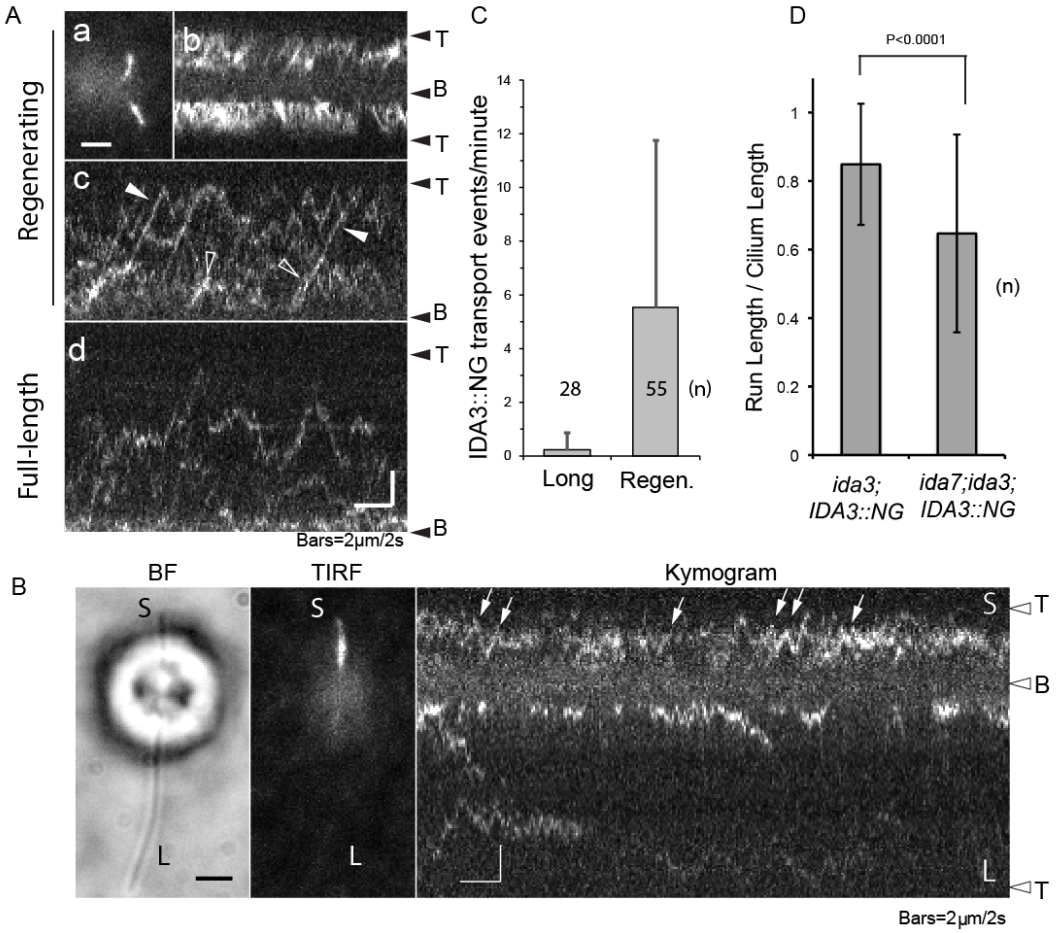
A
Regenerating
Full-length
a
b
c
d
T
B
Bars=2μm/2s
C
IDA3::NG transport events/minute
28
55
(n)
Long
Regen.
D
P<0.0001
Run Length / Cilium Length
(n)
ida3; IDA3::NG
ida7;ida3; IDA3::NG
B
BF
TIRF
Kymogram
S
L
Bars=2μm/2s

Figure 36. Efficient IFT transport of IDA3 requires I1 dynein.

(A) *ida7; ida3; IDA3::NG* cells, lacking I1 dynein, imaged by TIRF. (a) Still frame of regenerating *ida7; ida3; IDA3::NG* cilia and (b-c) kymograms of IDA3::NG transport in regenerating *ida7; ida3; IDA3::NG* cilia. IDA3::NG both undergoes anterograde IFT (white arrowheads) and diffuses (open arrowheads) in the absence of I1 dynein. (d) Kymogram of IDA3::NG diffusion in full-length *ida7; ida3; IDA3::NG* cilia. IDA3::NG processive motion is rarely observed. Bars = 2 s and 2 μm **(B)** Still frames and kymogram of an *ida7; ida3; IDA3::NG* short-long cell. IDA3::NG transport is restricted to regenerating cilium. Bar = 2 s and 2 μm. **(C)** Quantification of IDA3::NG transport events per minute in long and regenerating *ida7; ida3; IDA3::NG* cilia. Error bars = SD. **(D)** Analysis of IDA3 transport efficiency in the presence and absence of I1. The length of IDA3::NG anterograde IFT tracks were compared to the length of the cilium in *ida3; IDA3::NG* (n=96) and *ida7; ida3; IDA3::NG* (n=74) cilia. IDA3::NG transport is less processive in the absence of I1. A two-tailed unpaired t-test confirms a significant difference in the length of anterograde IFT tracks in *ida3; IDA3::NG* and *ida7; ida3; IDA3::NG* cells ($P<0.0001$). Error bars = SD.

Chapter IV

Implications of IDA3 and Future Directions

In Chapter IV, we explore how IDA3 has changed our understanding of IFT adapters while considering future studies that arise from my work. After a brief discussion of the immediate experimentation that will follow my present study of IDA3, I will focus on analysis of IDA3 in the cytoplasm and at the tip of the cilium. In addition to potential experiments, I will discuss the implications of this work and how these next studies can contribute to a broader understanding of ciliary assembly and basic principles of cell biology. I will then transition to a discussion of IDA3 as compared to previously defined IFT adapters and argue we must re-define the *in vivo* properties that describe a component of IFT versus an adapter to IFT. I will conclude my discussion by proposing *ODA8* and *PF27* may encode additional specialized IFT adapter that may be responsible for mediating IFT transport and assembly of the outer dynein arm and radial spoke, respectively.

Summary: Model of IDA3-Mediated I1 Dynein Assembly

I have identified a novel IFT adapter protein, known as IDA3, that mediates IFT entry and transport of the 20S I1 dynein complex into the cilium and to the distal tip of the cilium for docking in the axoneme (Fig. 37A). During assembly of the cilium, IDA3, along with I1 dynein, attaches to IFT in the cytoplasm prior to IFT-mediated entry into the ciliary compartment (Fig. 37A (a-b)). IDA3 and I1 are then transported by IFT to the distal tip of the cilium (Fig. 37A (c)). At this point IFT remodeling occurs and IDA3 and I1 dynein detach from IFT machinery and begin to diffuse throughout the ciliary

compartment (Fig. 37 A (d-e)). I1 dynein will diffuse until docked in the axoneme while IDA3 will continue to diffuse throughout the cilium (Fig. 37 (e)). We predict IDA3 will eventually re-enter the cell body. Transport of I1 dynein and IDA3 by IFT is regulated by changes in cilium length and transport of IDA3 occurs in a cilium-autonomous manner (Fig. 37 B).

Our initial characterization of IDA3 provides the framework to understand IDA3 behavior in relation to I1 dynein transport by IFT but many questions remain. The next step is to perform dual-label live-cell imaging to directly visualize co-incident transport of IDA3 and I1 dynein by IFT in the growing cilium. At this time, I have generated an IC140::mScarlet construct and have isolated *ida7;IC140::mScarlet;ida3;IDA3::NG* transformants that successfully express both IDA3::NG and IC140::mScarlet. Transformation of *ida7* with IC140::mScarlet will be used to enhance our visualization of I1 dynein transport in steady-state and regenerating cilia as the IC140::mScarlet protein will be much brighter than our current IC140::GFP. Transformation of *ida7;ida3;IDA3::NG* with IC140::mScarlet will allow direct visualization of IDA3::NG and I1 dynein (marked by IC140::mScarlet) transport by IFT. In addition to observing co-incident transport of IDA3 and I1 dynein from the base to the tip of the cilium, the dual-label live-cell imagining will also provide us the opportunity to observe how IDA3 and I1 dynein behave once detached from IFT machinery at the tip of the cilium. At this time we do not know if IDA3 and I1 dynein remain attached once free from IFT, diffusing together until I1 dynein docks the axoneme, or if IDA3 and I1 separate during IFT unloading. If IDA3 remains attached to I1 dynein after release from IFT, it is possible IDA3 is also required to retain I1 dynein in an inactive state until the dynein motor docks

the axoneme. Additionally, we do not understand how IFT trains loaded with IDA3 and I1 dynein pass through the selection barrier at the base of the cilium. Both analysis of our IDA3::NG cell line and dual-label live-cell imaging of IDA3 and I1 dynein will allow the visualization of I1 and IDA3 entry into the cilium.

Another question yet to be addressed is the mechanism of targeting and docking of I1 dynein in the axoneme. Working with Maureen Wirschell (University of Mississippi Medical Center), we have begun a BioID (using BirA; Roux, Kim et al., 2012, JCB; Kim, Roux et al 2016 MBC) approach to both define axonemal proteins that interact with IC140 and to further test the hypothesis that IC140 plays a role in docking I1 dynein in the axoneme. Currently, Maureen has transformants expressing IC140-BirA and ready to proceed on analysis of the axoneme.

In the following sub-sections I will focus my discussion on future study of IDA3 in the cytoplasm and at the tip of the cilium. Woven throughout is an emphasis on use of live-cell imagining to address questions of IDA3 transport within the cytoplasm, regulation of IDA3 attachment to IFT and I1 dynein in both the cytoplasm and at the distal tip of the cilium, and the role IDA3 diffusion may play in differential cilia cargo loading and cilium length regulation. Overall, the following sections explore, what I feel, are the most pressing and intriguing new questions to arise from the IDA3 study.

Understanding IDA3 Behavior and Interactions in the Cytoplasm

My study of IDA3 focused exclusively on the requirement of IDA3 for I1 dynein attachment to IFT, entry into the cilium, and transport to the distal tip of the cilium. For this reason, my analysis predominately pertains to characterization of IDA3 once attached

to IFT and in transit within the cilium. Thus, our analysis fails to address questions pertaining to IDA3 in the cytoplasm. Preliminary IDA3 pull-down analyses, using a HA-tagged IDA3, confirm IDA3 and IC140 interact in cytoplasmic extracts isolated from steady-state and regenerating cells (Fig. 34). How and when this I1 dynein/ IDA3 interaction occurs remains unstudied. I predict IDA3 and IC140 first interact shortly after translation and IDA3 interaction with IC140 does not require deflagellation to initiate the IC140/ IDA3 interaction. Alternatively, IDA3 could interact with IC140 following preassembly of I1 dynein. Sequential pull-down of IDA3 prior to and during deflagellation will provide a more definitive time course as to when IDA3 and IC140 interact and whether the quantity of IDA3 bound to IC140 changes during ciliary assembly. Sucrose-gradient fractionation of both steady-state and regenerating cytoplasmic extracts will be required to determine if IDA3 interaction with IC140 is indicative of IDA3 interaction with the fully-assembled 20S I1 dynein complex. Dual-label live-cell imagining of IDA3::NG and IC140::mScarlet will provide an alternative method to confirm IDA3 and IC140 interaction in the cytoplasm.

If we assume that IDA3 interacts with I1 dynein in the cytoplasm of steady-state cells prior to transport towards the basal bodies, then we must ask how IDA3 recognizes the I1 dynein complex with such specificity in an environment that is so diverse in protein composition. After all, IDA3 is only required for the transport of I1 dynein and is therefore highly specific to the I1 dynein cargo. While speculative at this time, I believe the conserved N-terminal region of the IDA3 protein is critical for recognition of the I1 dynein complex. Insertion of the p3xHA tag approximately 89 base pairs within exon 1 of *IDA3* prevents rescue of I1 dynein in the axoneme, suggesting this region is absolutely

essential for IDA3 function as an I1 dynein/ IFT adapter. A structure-function analysis of IDA3 is required to definitively determine the IDA3 domains responsible for carrying out the I1 dynein-IFT adapter function.

Serendipitously, during the cloning of *IDA3* from BAC4E5, I amplified a clone containing a single base change ~1,071 bases within the gene. This mutation results in the conversion of a TGG codon to a TGA codon, which can be used as a stop codon in *Chlamydomonas*. This new stop codon falls in the middle of exon 3. We can take advantage of the *IDA3* clone by transforming this construct into *ida3; oda2* cells (the double mutant is paralyzed) and screen for rescue of paralysis. If we isolate *ida3; oda2* transformants capable of swimming, it will be necessary to analyze both cytoplasmic extract and regenerating matrix fractions by immunoblot using our IDA3 antibody to confirm IDA3 is in fact truncated. If IDA3 is truncated, we will confirm the N-terminal half of IDA3 is capable of carrying out IDA3 function. This preliminary analysis will help us refine the truncated constructs designed for a more precise analysis of IDA3 structure and function. Detailed chemical crosslinking and / or structural analysis will be required to determine the I1 dynein subunit(s) and the IFT protein(s) responsible for directly binding IDA3.

While these analyses will vastly enhance our understanding of I1 dynein/ IDA3 interaction, as discussed above, I predict additional, unidentified proteins are required to successfully target IDA3 to I1 dynein. Mass-spectrometry of IDA3::HA pull-down fractions can identify additional factors required for binding I1 to IDA3. Not only will this list provide us an interesting collection of novel proteins required for I1 dynein assembly in the cytoplasm, the analysis may even provide us the identify of the protein

that requires translation to rescue I1 assembly in the *ida3* x *ida7* dikaryon. Moreover, the identification of additional conserved genes important for ciliary and dynein assembly may reveal novel genes that when defective result in PCD in humans.

IDA3: A Model for Addressing New Questions about Ciliary Assembly

The above analyses, while informative, will only provide insight into the interaction between IDA3 and I1 dynein assembly. Can IDA3 be used as a model to understand broader principles for regulation of cilia biogenesis? In subsequent sub-sections, I will discuss how study of IDA3 can be used to understand transport of ciliary proteins from the cytoplasm to the basal body, regulation of IFT cargo loading and unloading, and the mechanisms required for cilium length regulation.

How Are Ciliary Proteins Transported to the Basal Body?

Much of the research on cilia focuses on ciliary assembly steps that occur after ciliary proteins arrive at the basal body region, but how components destined to enter the cilium are transported to the basal body is under-studied. A study in 2014 by Wood and Rosenbaum suggests both IFT components and axonemal components, such as the radial spoke protein RSP3, attach to the outer surface of cytoplasmic vesicles for transport to the transition fibers at the base of the cilium (Wood et al., 2014). Very little has been done to further test the hypothesis that axonemal proteins hitchhike on vesicles destined to the cilium or other means of transport of the pre-assembled large axonemal complexes.

One possibility is proteins destined for the cilium are actively transported along the rootlet microtubules that extend from the basal bodies. The rootlet microtubules

define four specialized bundles of microtubules, two of which contain four microtubules and two of which contain two microtubules (Dutcher, 2003; Dutcher et al., 2016; Lechtreck et al., 2002). The rootlet microtubules attach directly to the basal bodies and have been shown to be crucial for positioning organelles such as the eye spot in addition to playing a role in cytokinesis (Dutcher, 2003; Dutcher et al., 2016). The rootlet microtubules might provide specialized microtubule tracks that direct transport of ciliary proteins towards the basal bodies. For instance, IFT74 has been shown to co-localize with rootlet microtubules, suggesting IFT proteins or IFT protein complexes use rootlet microtubules for transport to the basal bodies (Richey et al., 2012).

Through live-cell imaging of IDA3::NG, we have observed processive transport of IDA3::NG along the rootlet microtubules towards the basal body region of the cilium. The X-shaped structure shown in Figure 38 represents IDA3::NG along the rootlet microtubules (FIG. 38). Karl Lechtreck obtained the images by slight backing the focal plane in the TIRF microscope to examine the basal body region of the cell. Although not yet studied in detail, live-cell video imaging reveals directional transport of IDA3::NG along the rootlets towards the basal body region. Dual-label live-cell imagining can further enhance this study by looking at the transport of both IDA3 and I1 dynein on rootlet microtubules. Imaging of co-transport of IDA3 and I1 along the rootlet microtubules will provide the first direct observation of an axonemal cargo in transit to the cilium in complex with its specialized IFT adapter. While transport along the rootlet microtubules addresses how ciliary proteins are transported from the cytoplasm to the basal body, it does not address how ciliary complexes, such as the axonemal components, are targeted to the cilium. To date, ciliary targeting sequences have not been identified

for components of the motile cilium. It is possible that the co-transport of the axonemal cargo with specialized adapters is required to target the axonemal component to the basal body region.

How is Cargo-Loading Regulated?

As has been found for axonemal components, including the N-DRC and tubulin, and for the non-axonemal component IDA3, the quantity of cargo transported per minute decreases linearly as flagella lengthen during regeneration (Figure 31A) (Craft et al., 2015; Wren et al., 2013). It remains unknown how the cell controls the quantity of cargo transported at any given time during regeneration. One possibility is that the quantity of axonemal cargo transported by IFT is regulated by the ability of the cargo to bind IFT. As mentioned above, we suspect numerous axonemal components require highly specialized and transient adapters for entry into the cilium and transport by IFT. Considering this hypothesis, we would then predict the quantity of axonemal cargos transported at any given moment would depend upon the quantity of individual IFT adapters available to mediate the interaction between IFT and the axonemal cargo. Thus, by regulating the quantity of IFT adapters competent to bind IFT and transport cargos, the cell can mediate the quantity of axonemal cargo transported at any given time. What mechanisms can the cell use to regulate the quantity of adapters available for transit? Possibly, the cell may regulate the quantity of adapter present in the cytoplasm and/or regulate whether the adapter is competent to bind IFT. Both possibilities will be explored in greater detail below.

If the cell regulates the quantity of an IFT adapter available in the cytoplasm for transport, how is this controlled? This question can be addressed using IDA3 as a model. Perhaps, IDA3 abundance in the cytoplasm is controlled at the translational level over the course of ciliary regeneration. Analysis of cytoplasmic extracts isolated from regenerating cells in the presence and absence of cyclohexamide can determine if IDA3 abundance, at least in part, is regulated at the translational level. The quantity of IDA3 available in the cytoplasm may also be determined by that rate at which IDA3 re-enters the cell body after transit within the cilium. Thus, the quantity of IDA3 in the cytoplasm would depend upon the amount of time required for IDA3 to diffuse from the tip of the cilium into the cell body. In a short cilium, IDA3 would diffuse quickly from tip to cell body allowing the cytoplasmic pool of IDA3 to be replenished rapidly (Fig. 39A). As the cilium lengthens, the time required for IDA3 diffusion will increase, thereby limiting the quantity of IDA3 available in the cytoplasm to transport I1 dynein, ultimately decreasing the quantity of IDA3 and I1 dynein transported as the cilium regenerates (FIG. 39B). For the above predictions, we assume IDA3 re-enters the cell body post-diffusion from tip to base. At this time, we do not have direct evidence to support this assumption. In addition, if IDA3 does recycle into the cytoplasm, we do not know if IDA3 is actively transported across the selection barrier or if IDA3 passively diffuses through the barrier into the cytoplasm. One way to directly test whether IDA3 re-enters the cell body is to tag IDA3 with a photoactivatable fluorophore (Lukyanov et al., 2005). IDA3 fluorescence can be activated at the base of the cilium prior to exit into the cytoplasm. By tracking fluorescent IDA3 using live-cell imaging, we can determine if IDA3 is

actively transported through the ciliary barrier. This study can provide some of the first evidence as to how proteins pass from the cilium into the cytoplasm.

The dependence on diffusion is not novel to IDA3. The kinesin-2 motor, required for anterograde IFT, diffuses from the tip of the cilium towards the cell body (Chien et al., 2017; Engel et al., 2009a; Engel et al., 2012; Liang et al., 2014). Once returned to the cell body, kinesin-2 is recycled and used once again for anterograde IFT transport (Liang et al., 2014). It appears that passive diffusion of essential IFT machinery may play a critical role in regulating the quantity of cargo loaded onto IFT for transport in the assembling cilium. Therefore, under this model, cilium-length regulates the quantity of cargo transported by IFT and, in turn, the quantity of cargo transported restricts the length of the cilium.

In addition to regulating the quantity of adapter available for transport at any given time, the cell may also regulate whether the adapter is competent to bind IFT. Regulation of adapters would most likely occur through post-translational modifications. This hypothesis is founded on study of kinesin-2 in which the FLA8 subunit of kinesin 2 is phosphorylated at S663 by a calcium-dependent kinase at the distal tip of the *Chlamydomonas* cilium (Liang et al., 2014). Phosphorylation of S336 disrupts kinesin interaction with IFT and results in kinesin diffusion within the cilium (Liang et al., 2014). Once returned to the cell body, dephosphorylation of kinesin activates kinesin binding to IFT and subsequent anterograde transit within the cilium (Liang et al., 2014).

Given IDA3 appears to be modified in the matrix of the regenerating cilium (Fig. 25B) and treatment of *ida3; IDA3::HA* regenerating matrix with calf intestinal phosphatase collapses the IDA3 doublet (Fig. 40), IDA3 is an excellent model to test

whether post-translational modification regulates the ability of the adapter to bind IFT. Based on the study of kinesin-2, I suspect IDA3 dephosphorylation is required for IDA3 to bind IFT in the cytoplasm, while phosphorylation at the tip of the cilium is required for unloading of IDA3 at the distal tip of the cilium (Fig. 41). To test this model, after identifying the residues modified in IDA3 using mass-spectrometry (currently underway), we can generate both a phosphomimetic IDA3 mutant and a phosphorylation-null IDA3 mutant, both of which would be tagged with NeonGreen for analysis using live-cell imagining.

The phosphomimetic IDA3 mutant will act as if the IDA3 protein is always phosphorylated. Given our hypothesis, I predict phosphomimetic IDA3 will be unable to bind IFT and thus will not enter the regenerating cilium (Fig. 42A). Therefore, I1 dynein will not be transported to the tip of the cilium and the phosphomimetic IDA3 would exhibit an *ida3* phenotype, lacking I1 dynein in the axoneme.

In contrast to the phosphomimetic IDA3 mutant, the phosphorylation-null IDA3 mutant will be unable to be phosphorylated. Given our hypothesis, IDA3 binds IFT when de-phosphorylated. Therefore, I predict the phosphorylation-null mutant would bind IFT and enter the regenerating cilium. At the tip of the cilium, the phosphorylation null-mutant would no longer be phosphorylated and would be unable to detach from IFT machinery (Fig. 42B). Thus, I predict IDA3 would remain bound to IFT, returning to the cell body by retrograde IFT (Fig. 42B). If I1 dynein unloading depends on IDA3, I1 dynein will be prevented from unloading at the tip of the cilium and the mutant will again exhibit an *ida3* phenotype. It is possible I1 dynein unloading occurs independent of

IDA3 and thus the phosphorylation-null IDA3 mutant may be able to dock I1 dynein in the axoneme.

While the potential outcomes described above are the most likely given our hypothesis, alternative outcomes exist. For instance, our hypothesis assumes modification of IDA3 regulates IDA3 interaction with IFT. Alternatively, IDA3 modification may be required to regulate IDA3 interaction with I1 dynein. Biochemical pull-downs of the IDA3 phosphorylation mutants from the cytoplasm and regenerating matrix can be used to determine if IDA3 modification is required for IDA3 attachment to IFT or to I1 dynein. Overall, the above analyses take advantage of IDA3 to address a number of crucial questions, including how ciliary proteins are transported to the basal body, how IFT cargo loading and unloading is regulated, and elude to potential mechanisms of cilium length regulation. Ultimately, further study of IDA3 may provide the foundation for understanding how the cell regulates IFT cargo loading and has the potential to reveal novel components localized to the base of each cilium that regulate IFT cargo loading in a cilium-autonomous manner. Detailed analyses of the barrier composition and structure throughout regeneration will be required to understand how IFT trains, loaded with cargos, transverse the barrier of the cilium.

IDA3: A New Way to Think About IFT Adapters

The use of adapters in biology is common. As mentioned briefly in the introduction, cytoplasmic dynein uses adapters proteins to bind a large number of distinct cargos in the cytoplasm while kinesin motors use adapters in neurons to transport distinct cargos within the axon (Chua et al., 2012; Cianfrocco et al., 2015; Fu et al., 2014; Huynh

et al., 2017; McKenney et al., 2014; Schroeder et al., 2016). In cilia, adapters have been defined as peripheral IFT components that are not necessary for the assembly or overall function of IFT (Lechtreck et al., 2009). It is logical that IFT machinery would require adapter proteins, as the 22 known IFT proteins must bind hundreds of unique polypeptides. As described in the introduction, the BBSome and the outer dynein arm adapter ODA16 are the best-defined IFT adapters (Ahmed et al., 2008; Desai et al., 2018; Liu et al., 2018). While the BBSome is an adapter required for retrograde transport of various signaling and membrane components, ODA16 is more similar to IDA3 in that ODA16 is required for IFT transport of the outer dynein arm (Ahmed et al., 2005; Ahmed et al., 2008; Lechtreck et al., 2009). However, ODA16 and IDA3 differ in their behavior. In the following sub-section, I will compare and contrast IDA3 and ODA16 behavior. I will argue that ODA16 should be considered a *bona fide* component of IFT. I believe IDA3 provides the first insight into defining a novel class of axonemal adapter proteins that are both highly specific and transient in nature.

ODA16 v. IDA3

As scientists, our ability to precisely and succinctly define properties and events within the cell is restricted by both the vernacular and our ability to view a single event within the broader perspective of the cell. Therefore, science must be an iterative process in which concepts and terminology are continually refined to ensure precision in the wording used to discuss cellular processes and define cellular components. Study of IDA3 is a prime example of how discovery of a novel protein with unique behaviors can alter the way in which we define previously characterized proteins. Our new

understanding of IDA3 behavior has altered the way in which we consider the concept of IFT adapter proteins, and I believe results in re-definition of ODA16 as a *bona fide* component of IFT. All information on ODA16 described in the next paragraph is taken from Ahmed et al., 2008.

Both ODA16 and IDA3 are required for IFT transport of specific axonemal components. The ODA16 adapter transports the outer dynein arm while IDA3 is required for the transport of the I1 dynein complex. While the ODA16 adapter co-localizes with IFT in both full-length and regenerating cilia, IDA3 is only transported by IFT during ciliary assembly. In addition, pull-down analyses reveal ODA16 interacts with IFT proteins, specifically IFT46, but ODA16 does not co-purify with the outer dynein arm. In contrast, our pull-down analyses reveal IDA3 interacts with IC140 of the I1 dynein complex but rarely co-purifies with IFT proteins. Both ODA16 and IDA3 can be transported by IFT in the absence of their axonemal cargos. However, the interaction of IDA3 with IFT is unstable in the absence of I1 dynein. Were ODA16 transport to be imaged in live-cells, I predict the ODA16 adapter would remain tightly bound to IFT46 in the absence of the outer dynein arm cargo (Hou et al., 2017; Taschner et al., 2017), and remain bound to IFT during anterograde and retrograde transport. Thus, based on these studies, ODA16 attachment to IFT and processive transport by IFT occurs independently of cilium-length and the outer dynein arm cargo. In contrast, IDA3 attachment to IFT is dependent on changes in cilium length and processive transport of IDA3 depends on the presence of the I1 dynein cargo.

Should ODA16 still be considered an IFT adapter given our analysis of IDA3? Currently, any protein that, when defective, disrupts the transport of select cargos, but

does not inhibit IFT transport and cilium assembly, is considered an IFT adapter (Lechtreck et al., 2009). In my opinion, this definition lacks precision as it encompasses proteins with distinct behaviors and characteristics. For ODA16, the ODA16 cellular and flagellar distribution is identical to known IFT components. In addition, ODA16 co-purifies with IFT particles, but the authors ultimately define ODA16 as an adapter because ODA16 is only required to assemble the outer dynein arm. In spite of these data, my study of IDA3 now offers an alternative view of an IFT adapter in which interaction with IFT and the specific axonemal cargo is transient and temporary. Crucial to this definition is the transient nature of the adapter, as it interacts with IFT only when axonemal cargos are transported for assembly in the growing cilium, as is observed with IDA3. Thus, I believe ODA16 should now be considered a *bona fide* IFT component while IDA3 should be considered an adapter to IFT machinery.

From a biological standpoint, there could be a number of reasons why the outer dynein arm would require a direct IFT binding site while I1 dynein requires an adapter to bind IFT. The outer dynein arm binds the axoneme once every 24 nm while I1 dynein binds once every 96 nm (Ishikawa, 2013; Nicastro et al., 2006). For this reason, a higher quantity of outer dynein arms must be assembled in the axoneme as compared to I1 dynein and a definitive binding site would allow transport of a large quantity of outer dynein arms. Alternatively, ODA16 may be the IFT component that an unidentified outer dynein arm adapter binds to in order to mediate interaction between the outer dynein arm and IFT.

I predict other axonemal components such as the radial spoke and the N-DRC also require highly specialized and transient adapters to mediate entry and transport of the

axonemal components in the growing cilium. I suspect individual IFT trains will be comprised of a unique composition and quantity of axonemal components. I would be curious to use multi-color spectral imaging to tag a number of axonemal cargos, IFT, IDA3 and ODA16 and quantify the number of trains carrying each cargo and quantity of each cargo present per train. In this way we can begin to appreciate the unique composition of cargo bound to individual IFT trains throughout ciliogenesis.

Identification of Additional IFT Adapters

As emphasized above, I suspect other axonemal complexes require specialized and transient adapters to load IFT and be transported into and within the ciliary compartment. Two *Chlamydomonas* mutants, *oda8* (defective in outer dynein arm assembly in the axoneme) and *pf27* (defective in radial spoke assembly in the axoneme) may be additional IFT adapters. The *oda8* mutant was previously studied by David Mitchell's lab at SUNY Upstate Medical Center while I studied *pf27* in collaboration with Dr. Lea Alford when I first started in the Sale Laboratory. In both cases, the mutants properly assemble their respective axonemal components in the cytoplasm but fail to assemble these components in the axoneme. In this way, characterization of both mutants is highly similar to our initial characterization of IDA3. For this reason, I offer the hypothesis that *ODA8* and *PF27* encode highly specialized, transient IFT adapter proteins.

ODA8 as a candidate ODA Adapter

ODA8, which is a leucine-rich protein, has currently been defined as an outer dynein arm assembly factor (Desai et al., 2015). As with I1 dynein, the outer dynein arm pre-assembles in the cytoplasm before IFT transport into the cilium (Fowkes et al., 1998). ODA8 is required to convert an assembled, yet unstable, outer dynein arm into a stable outer dynein arm that is competent to bind IFT (Desai et al., 2015). Interestingly, the role of ODA8 in outer dynein arm assembly does not end in the cytoplasm and instead ODA8 is also transported into the cilium, presumably along with the outer dynein arm (Desai et al., 2015). It does not seem that ODA8 is a component of the outer dynein arm itself as ODA8 and the outer dynein arm intermediate chain IC2 do not always co-localize (Desai et al., 2015). Therefore, the authors state "…this protein may also function during IFT-dependent outer dynein arm assembly steps which could include attachment of outer dynein arm to IFT complexes at the flagellar base as well as co-transport with outer dynein arms during IFT-dependent entry into the flagellum" (Desai et al., 2015). Additionally, the authors note they are uncertain what happens to ODA8 once detached from IFT and believe it is possible ODA8 diffuses through the cilium, very similarly to IDA3 (Desai et al., 2015). Given some similarity to IDA3, I believe it is possible *ODA8* encodes an outer dynein arm- IFT adapter. Further study of ODA8 would greatly benefit from live-cell imagining.

PF27 as a Potential Radial Spoke IFT Adapter

The radial spoke is known to assemble into a 12S complex in the cytoplasm that then enters the cilium and is transported by IFT to the distal tip for conversion into a 20S

radial spoke complex and final docking in the axoneme (Qin et al., 2004). In *Chlamydomonas,* the radial spoke docks twice every 96 nm and, like I1 dynein, the radial spokes dock the lumen of the axoneme (Barber et al., 2012; Oda et al., 2014b; Pigino et al., 2011). When beginning my dissertation research in the Sale Laboratory, I worked in collaboration with Dr. Lea Alford to characterize the *Chlamydomonas* radial spoke mutant *pf27*. The *pf27* mutant exhibits a paralyzed flagellar phenotype because *pf27* only assembles radial spokes in the proximal 2 μm of the axoneme (Alford et al., 2013). Similar to our initial characterization of *ida3*, we found that the 12S radial spoke is properly preassembled in the cytoplasm and that the 20S radial spokes that docks the proximal region of the *pf27* axoneme are also fully assembled. Therefore, we predicted the *PF27* gene encodes a protein extrinsic to the radial spoke complex, and postulated *PF27* encodes a radial spoke-IFT adapter protein required for efficient transport. To date, identification and characterization of the *PF27* gene has not been published.

If PF27 is an adapter required to mediate interaction between the radial spoke and IFT, then how do the radial spokes assemble in the first 2 μm of the *pf27* axoneme? Taking advantage of *Chlamydomonas* regeneration, axoneme isolation, and immunoblot analyses, we determined in *pf27* the proximal radial spokes incorporate sporadically as the cilium lengthens while all other axonemal components assemble at a consistent rate, indicative of anterograde IFT transport (Fig. 43A-F). We concluded the proximal spokes assembled in *pf27* axonemes enter the cilium by diffusion.

As described in Chapter III, a small fraction (3%) of *ida3* axonemes do incorporate I1 dynein suggesting the 20S I1 dynein complex, as times, can diffuse throughout the cilium barrier and assemble in the axoneme in the absence of IFT (Fig.

14B). Thus, if the 20S I1 dynein complex is capable of diffusing through the barrier, it is reasonable to assume the 12S radial spoke is also able to diffuse through the barrier. Thus diffusion alone could account for the proximal radial spoke assembly in the *pf27* proximal axoneme. As mentioned above, the gene defective in the *pf27* mutant has yet to be characterized. Given our characterization of the *pf27* mutant mimics that of *ida3*, I believe *PF27* will encode a highly specialized, transient IFT adapter for the radial spoke and PF27 transport by IFT will be regulated by cilium length. Karl Lechtreck is currently using live-cell imaging to study radial spoke assembly and can begin to test theses ideas directly.

Concluding Remarks:

The above chapter emphasizes, what I think, are the most pressing questions in the field of ciliary assembly that result from my studies. IDA3 provides an exceptional model for study of transport of ciliary proteins to the basal body region and regulation of IFT-cargo loading and unloading. A more detailed analysis of IDA3 diffusion may further our understanding of how the cell controls the quantity of cargo transported by IFT and provides an alternative means of regulating cilium length. Together, these studies will provide insight into how differential IFT cargo loading occurs and may provide initial clues as to how cargo loading is regulated in a cilium-autonomous manner. With the tools generated during our initial analysis of IDA3, we are now poised to address these long-standing, elusive questions and discern new and vastly unexplored facets of ciliary assembly.

Chapter IV Figures

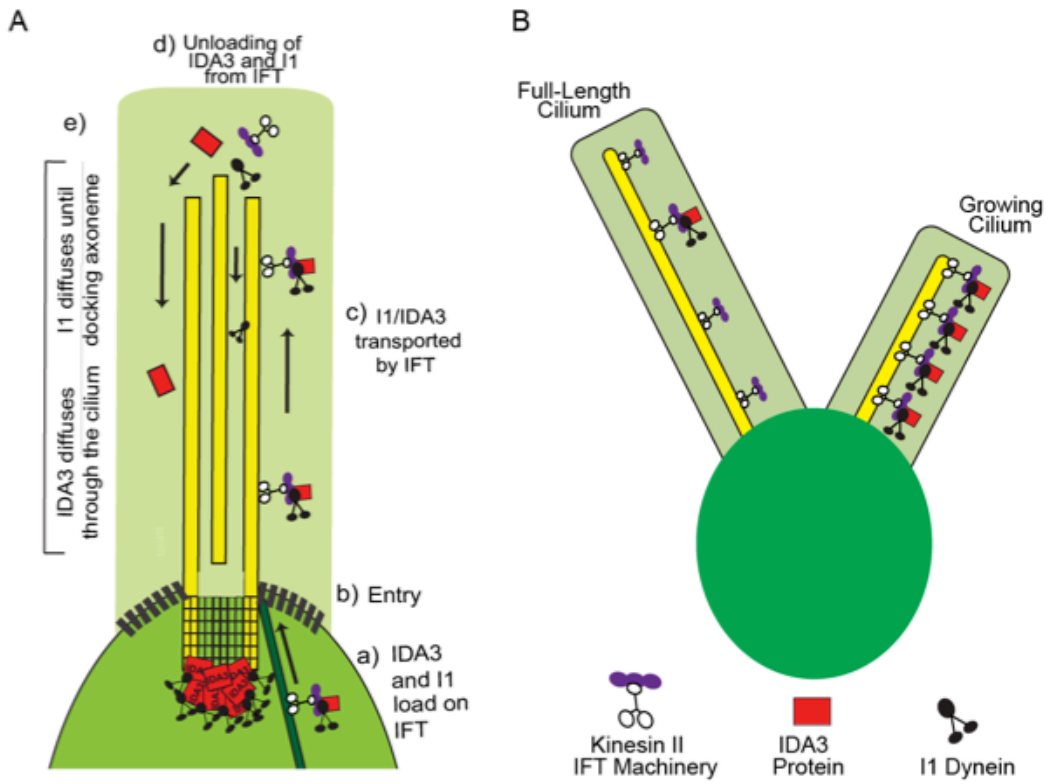

Figure 37. IDA3 mediates IFT entry and transport of the I1 dynein complex in a cilium-autonomous manner.

(A) Model of IDA3-mediated IFT transport of I1 dynein. IDA3 and I1 dynein load onto IFT (a) for entry (b) and transport (c) in the growing cilium. At the distal tip, IDA3 and I1 dynein unload from IFT (d). IDA3 diffuses through the cilium while I1 docks in the axoneme (e). **(B)** IDA3 transport occurs in a cilium-autonomous manner. IDA3 entry and transport predominately occurs in the growing cilium.

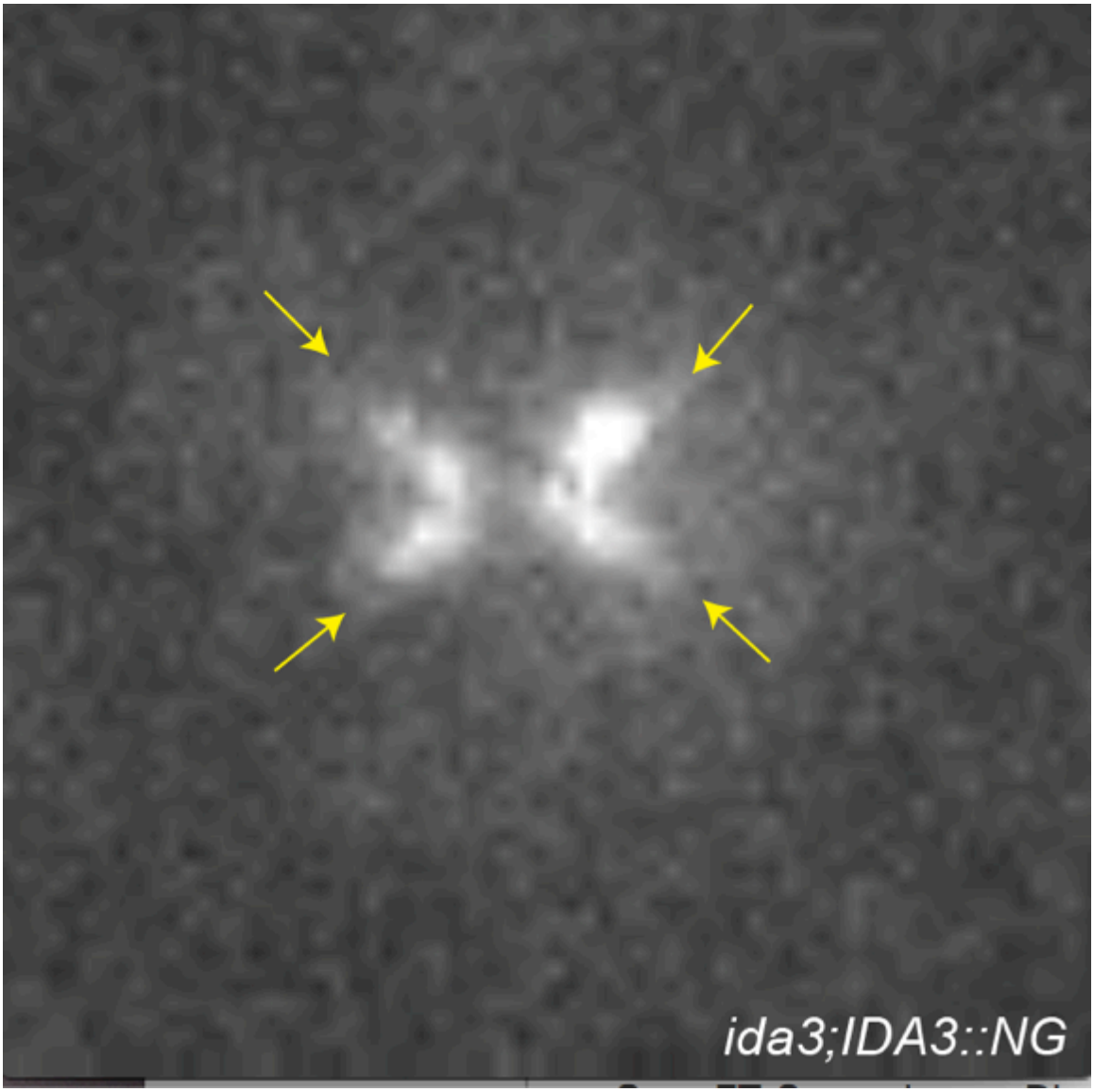
ida3;IDA3::NG

Figure 38. IDA3 is transported along the rootlet microtubules.

Still frame of live-cell TIRF imaging of *ida3;IDA3::NG* cells. IDA3::NG is transported along the rootlet microtubules towards the basal body. Yellow arrows indicate X shape of the rootlet microtubules.

A

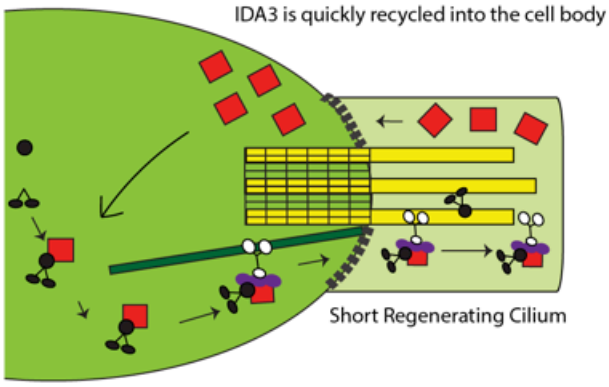
IDA3 is quickly recycled into the cell body
Short Regenerating Cilium

B

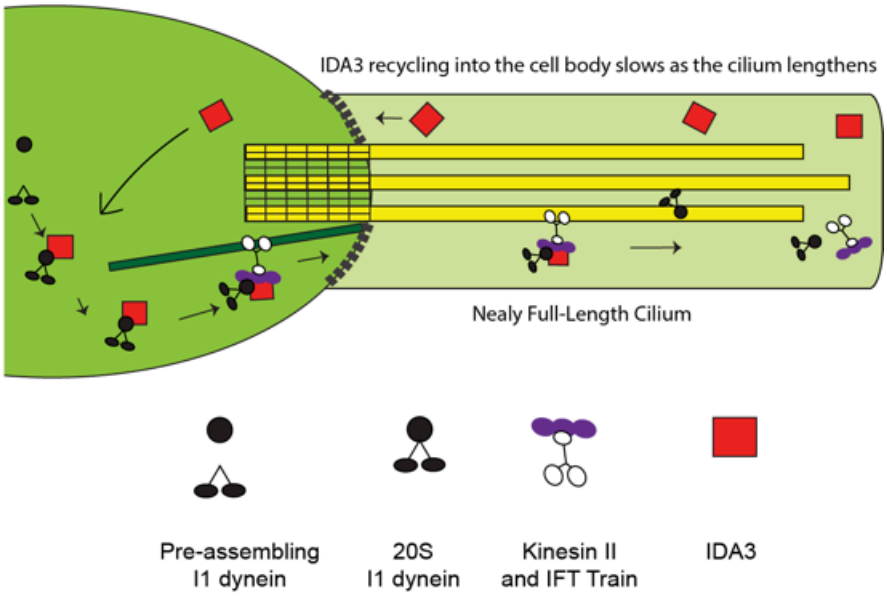
IDA3 recycling into the cell body slows as the cilium lengthens
Nealy Full-Length Cilium
Pre-assembling I1 dynein
20S I1 dynein
Kinesin II and IFT Train
IDA3

Figure 39. The potential role of IDA3 diffusion in IFT-cargo loading and cilium length regulation

(A) In a short cilium, large quantities of IDA3 are transported by IFT to the tip of the cilium. IDA3 re-entry into the cell body will occur quickly as IDA3 will only need to diffuse a short distance. **(B)** When the cilium is approaching full-length, IDA3 must diffuse farther before re-enter the cell body. This in turn will limit the quantity of IDA3 present in the cytoplasm to mediate I1 dynein transport.

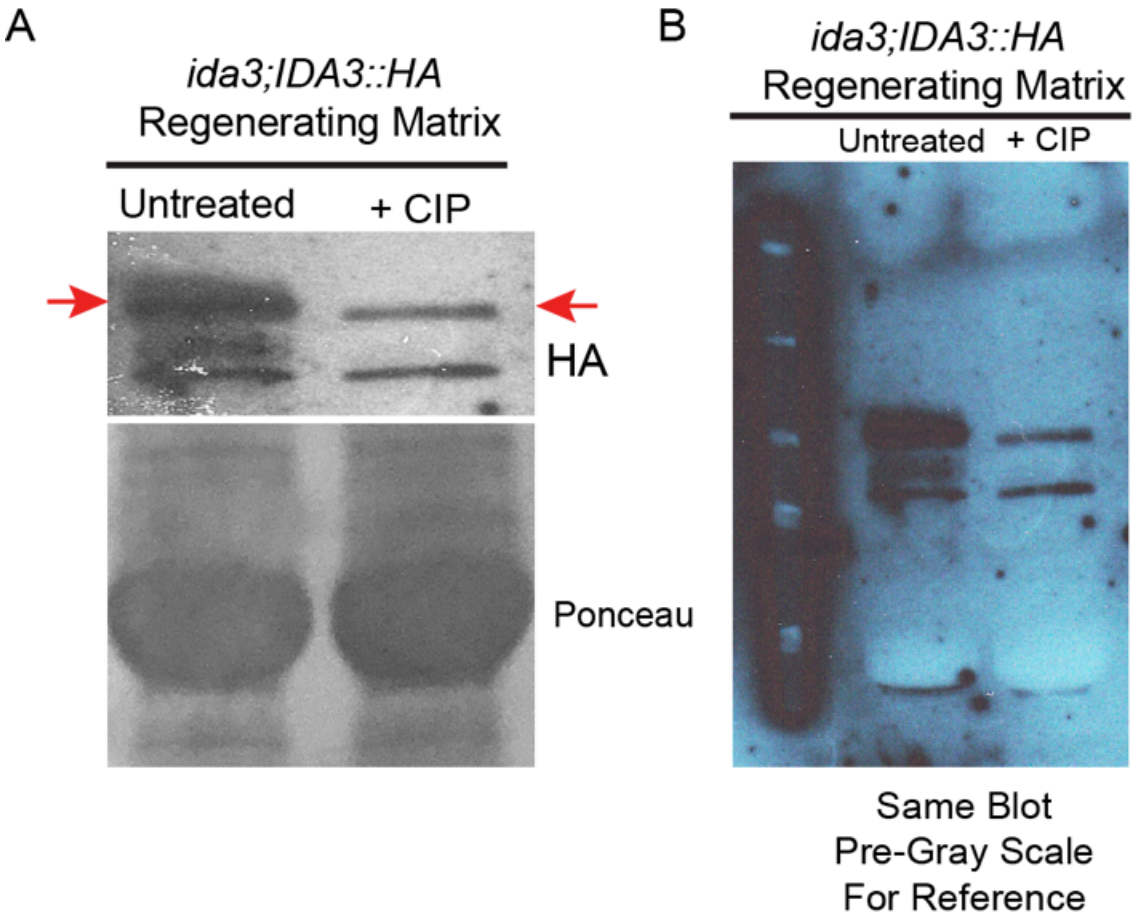
A
ida3;IDA3::HA
Regenerating Matrix
Untreated
+ CIP
HA
Ponceau
B
ida3;IDA3::HA
Regenerating Matrix
Untreated + CIP
Same Blot
Pre-Gray Scale
For Reference

Figure 40. IDA3 is phosphorylated in the regenerating matrix

(A) Regenerating *ida3;IDA3::HA* matrix was isolated and either left untreated or treated with calf-intestinal phosphatase (+CIP). Samples were analyzed by immunoblot and probed with HA antibody. The IDA3::HA double is collapsed in the presence of CIP (red arrows), indicating IDA3 is phosphorylated. Ponceau staining acts as a load control. **(B)** Full-blot, pre-gray scale for future reference. The collapsed IDA3 band is distinct.

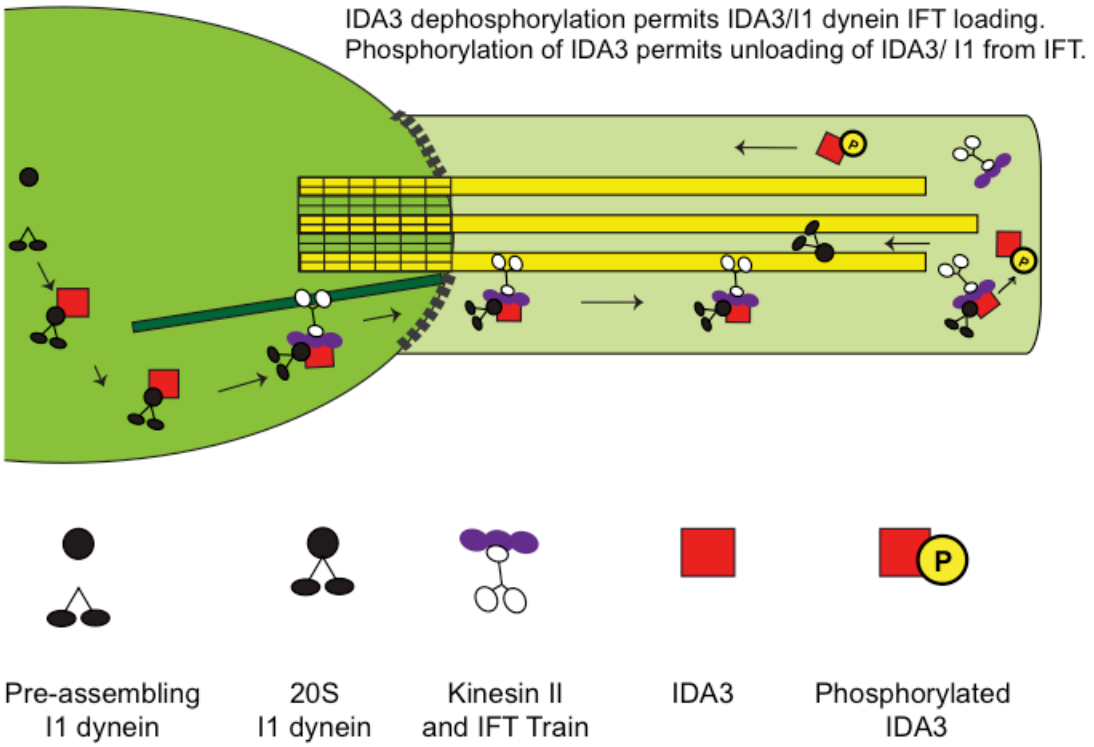
IDA3 dephosphorylation permits IDA3/I1 dynein IFT loading.
Phosphorylation of IDA3 permits unloading of IDA3/ I1 from IFT.
P
P
Pre-assembling I1 dynein
20S I1 dynein
Kinesin II and IFT Train
IDA3
Phosphorylated IDA3

Figure 41. IDA3 attachment to IFT may be regulated by phosphorylation

Model proposing IDA3 dephosphorylation is required to permit IDA3 loading onto IFT. IDA3 phosphorylation at the distal tip releases IDA3 from IFT machinery and phosphorylated IDA3 diffuses throughout the cilium. This hypothesis is founded on the Liang et al., 2014 study of the Kinesin II motor.

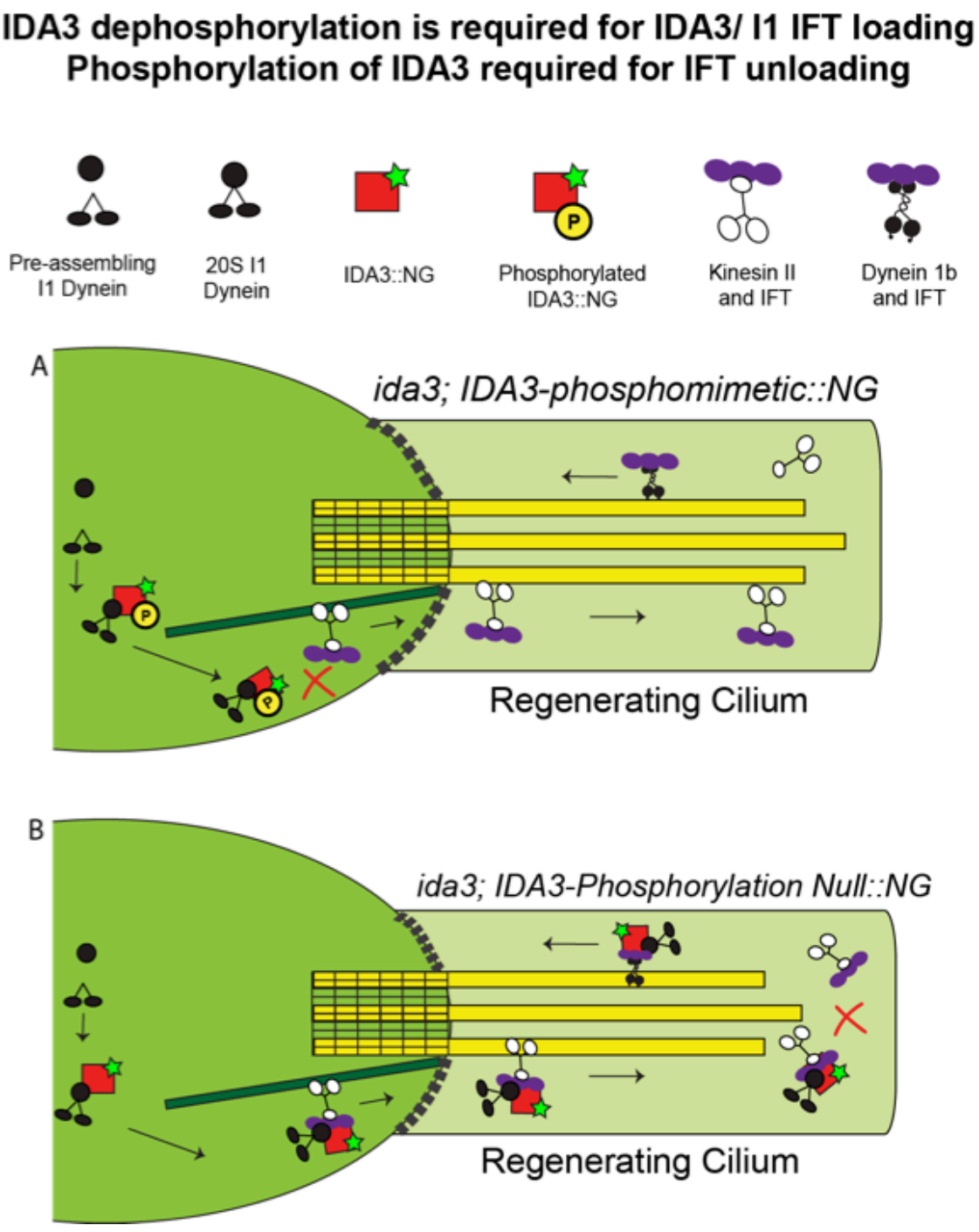
IDA3 dephosphorylation is required for IDA3/ I1 IFT loading
Phosphorylation of IDA3 required for IFT unloading
Pre-assembling I1 Dynein
20S I1 Dynein
IDA3::NG
Phosphorylated IDA3::NG
Kinesin II and IFT
Dynein 1b and IFT
A
ida3; IDA3-phosphomimetic::NG
Regenerating Cilium
B
ida3; IDA3-Phosphorylation Null::NG
Regenerating Cilium

Figure 42. Potential outcomes for study of *IDA3* phosphorylation mutants

Hypothesis: IDA3 dephosphorylation is required for IDA3 attachment to IFT. IDA3 phosphorylation permits IDA3 detachment from IFT. **(A) Prediction:** Phosphomimetic IDA3 will be unable to enter the ciliary compartment as IDA3 will be unable to bind IFT. **(B) Prediction:** The IDA3 phosphorylation null mutant will bind IFT and enter the regenerating cilium as in wild-type. At the distal tip the IDA3-phosphorylation null mutant will not be phosphorylated and therefore will remain attached to IFT. Live-cell imagining of IDA3-phosphorylation null::NG will reveal IDA3 attached to retrograde IFT as IDA3 returns to the cell body.

Figure 6

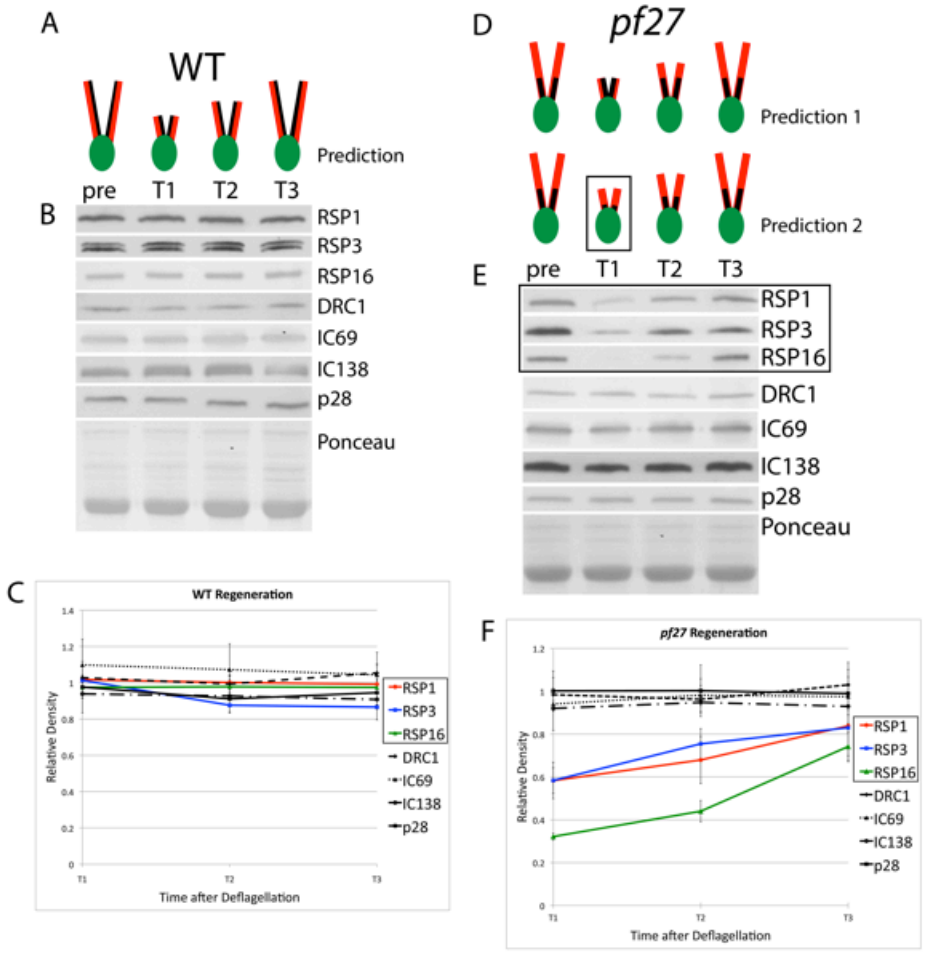
A
WT
Prediction
pre
T1
T2
T3
B
RSP1
RSP3
RSP16
DRC1
IC69
IC138
p28
Ponceau
C
WT Regeneration
Relative Density
Time after Deflagellation
RSP1
RSP3
RSP16
DRC1
IC69
IC138
p28
D
pf27
Prediction 1
Prediction 2
E
pre
T1
T2
T3
RSP1
RSP3
RSP16
DRC1
IC69
IC138
p28
Ponceau
F
pf27 Regeneration
Relative Density
Time after Deflagellation
RSP1
RSP3
RSP16
DRC1
IC69
IC138
p28

Figure 43. The proximal radial spokes in the *pf27* axoneme assemble asynchronously from the rest of the axoneme during ciliary regeneration

(**A**) Schematic model of axonemal assembly in regenerating wild-type cilia. After deflagellation, wild-type axonemal components are predicted to assemble concurrently during regeneration. Specifically, the radial spokes (black) assemble at the same rate as other axonemal components (red). (**B**) Immunoblot analysis of regenerating wild-type cilia. Axonemes isolated before and three time points after deflagellation were probed for radial spoke proteins 1, 3, and 16. Other axonemal components including the dynein regulatory complex (DRC1), outer dynein arm (IC69), I1 dynein (IC138), and single-headed inner dynein arms (p28) were also examined. Band intensity for each of these axonemal components remains unchanged during regeneration. Consistent with the model, axonemal components assembled in the regenerating cilium at the same rate as quantified by densitometry (graph in C). Ponceau staining was used as a load control for densitometry. (**C**) Quantification graph of band density over time illustrates concurrent assembly of axonemal components in wild-type. (**D**) Schematic model of axonemal assembly in regenerating *pf27* cilia. Since *pf27* axonemes have less radial spokes than wild-type, we present two predictions for *pf27* axonemal radial spoke assembly relative to other axonemal components. Prediction 1 illustrates radial spoke (black) assembly concurrent with other axonemal components (red) in the early stages of regeneration. At about 2 μm, radial spoke assembly ceases while other axonemal components continue to assemble. Prediction 2 illustrates a progressive and independent assembly of *pf27* axonemal radial spokes (black) compared to other axonemal components (red). (**E**) Immunoblot analysis of regenerating *pf27* cilia support prediction 2. Band intensity

for radial spoke proteins 1, 3, and 16 increased progressively during regeneration while band intensity for other axonemal components (DRC1, IC69, IC138, and p28) remained unchanged. Densitometry confirmed the independent assembly of *pf27* axonemal radial spokes from other axonemal components as in prediction 2 (graph in F). (**F**) Quantification of band density illustrates progressive and independent assembly of *pf27* axonemal radial spokes compared to other axonemal components. (Figure 6, Alford et al. 2013).

Appendix I: Materials and Methods

Strains and Culture Conditions

Chlamydomonas reinhardtii strains used include wild-type (CC-124, CC-125, CC-620, CC-621), *ida3* (CC-2668), *ida3; oda2, ida7* (CC-3921), *ida3; IDA3::HA, ida3; IDA3::NG, ida7; ida3; IDA3::NG, ida3; IDA3::HA; ida7; IC140::SNAP, ida7; IC140::GFP, oda6; ida7; IC140::GFP* and the polymorphic strain CC-1952 (S1C5). Cells were cultured in either tris-acetate-phosphate (TAP) medium, L medium, or M medium (Harris, 2009) with aeration on a 14:10h light/dark cycle or under constant light. Wild-type, *ida7,* CC-1952 (S1C5) and *ida3* were acquired through the *Chlamydomonas* Resource Center (University of Minnesota, St. Paul, MN). All other strains were generated specifically for this publication. Details on strains and methods used in study of *ida3* in Chapter II are detailed in Viswanadha et al., 2014. Details on strains used for study of the radial spoke (i.e. *pf27*) and details on methods used to analyze radial spoke assembly are described in detail in Alford et al., 2013.

Generation of *ida7; IC140::SNAP*

A GFP-tagged IC140 construct, containing the *APHVIII* selection cassette (Sizova et al., 1996), was generated from clone pCP3 (Perrone et al., 1998). The *APHVIII* cassette was inserted into pCP3 with *Sma*l and *Kpn*I to produce the plasmid *IC140::GFP-AphVIII*. The 3.28-kb *Nru*I – *EcoR*I fragment from *IC140::GFP-APHVIII* was excised and subcloned into plasmid pSE280 to produce pCS5.1. A 2.068-kb *Nru*I-*Rsr*II fragment containing the SNAP tag in place of GFP in exon 2 was synthesized and cloned into the pUC57-Kan vector (Genscript, Piscataway, NJ) to make clone pCS17. The *Nru*I-*Rsr*II

fragment from pCS17 was excised and subcloned into the pCS5.1 plasmid to produce pCS18. A 2.71-kb *Psp*XI-*EcoR*V fragment from pCS18 was subcloned into the *IC140::GFP-AphVIII* clone to produce pCS20, which contains the *IC140* gene fused to SNAP in exon 2. Plasmid pCS20 was used to transform the *ida7* strain using the glass bead method (Kindle, 1990). Paromomycin-resistant colonies were selected and examined for assembly of the SNAP::IC140 fusion protein in axonemes and for motility. Several transformants were selected that display wild-type like motility.

Generation of *oda6; ida7; IC140::GFP*

To visualize the IC140 movement in cilia, a rescued strain of *oda6; ida7* expressing exogenous IC140::GFP molecules was generated (*oda6; ida7R::GFP*), and used for the TIRF analyses. To generate the *oda6; ida7R::GFP* strain, *oda6; ida7* mutants were transformed with the vector *pCP3-GFP-APHVIII*, which had the pBlueScript backbone and contained an *Xba*I-*Sma*I *Chlamydomonas* genomic fragment covering all the IC140 genomic region with a GFP tag at the first exon of the IC140 gene. *pCP3-GFP-APHVIII* also had the *APHVIII*-gene cassette, which confers paromomycin resistance to transformants. Transformation was carried out by the electroporation method. We also used TIRF microscopy to observe I1 dynein transport analyzed *ida7;* IC140:: GFP obtained from Oda et al., (Oda et al., 2015).

Constructing double, triple, and quadruple mutants

Strains (e.g. *ida3;oda2, ida7; ida3::IDA3-NG, and ida3; IDA3::HA; ida7; IC140::SNAP*) were generated by transformation were crossed by standard protocols

(Dutcher, 1995). To generate the *ida3; oda2* mutant, cells were treated with dbcAMP and IBMX (Pasquale et al., 1987) for 30 min to allow mating of a strain with short or no flagella. Markers were determined by PCR with the following primers: *ida7* via pMN24 sequences (AAT ACG CAA ACC GCC TCT C and TGG CGT AAT CAT GGT CAT AGC), IDA3::HA (ATC GAT CCG GAC GAC CGT ACC C and GTG GTG ACG TAG TCC AGC AG), IC140::SNAP via the SNAP tag (ATC AAG CTG CTG GGC AA and GAT CAC CTC GCC CAA CTT). Loss of I1 dynein, indicative of the *ida7* mutation, was confirmed by immunoblot analysis of isolated axonemes.

Dikaryons between *ida3* and *ida3; IDA3::NG* were generated by differentiating each cell type for 6-16 h in M-N/5 medium prior to mixing the gametes of each cell type (Harris, 2009)and the zygotes with full-length, steady-state cilia were observed by TIRF microscopy.

Molecular mapping and whole genome sequencing

Strain CC-2668 (*ida3*) was backcrossed to wild-type cells (CC-125) five times. The backcrossed *ida3* strain was crossed to CC-1952 (S1C5) and 230 progeny were used in mapping. Crude DNA preparation, PCR and enzymatic digestion of DNA from individual progeny were performed as previously described (Lin et al., 2015). The single *ida3* progeny was subjected to whole genome sequencing (Lin et al., 2013a; Lin et al., 2015). The NCBI accession number for the raw sequencing reads of *ida3* is SRX525037. We had 40x coverage of the *Chlamydomonas* genome (Lin et al., 2013a). The *ida3* nonsense mutation was confirmed in both *ida3* and *ida3; oda2* by PCR (Primers: ACT

TGC TTT CTC ACG GCA CT and CCA TGA GAC TCC TTC CGT GT) and Sanger sequencing.

Reversion Analysis

UV light at 750 microJoules was used to mutagenize *ida3 ;oda2* (Lin et al., 2015). UV mutagenized *ida3; oda2* plates were incubated in dark overnight. After 1-2 days cells were scraped into a tube containing 20 mL of R liquid medium. After 1.5 days the top 5 mL of medium were moved to a new tube. Medium was transferred once every three days until swimmers were observed. *ida3; oda2* swimmers were visually scored for motility rescue and were analyzed by immunoblot for rescue of the intermediate chains IC140/IC138 as a marker for I1 dynein assembly in the axoneme. Sanger sequencing confirmed the intragenic reversion within *ida3* of the *ida3; oda2* cells exhibiting a rescue phenotype. Extragenic suppressors were also isolated by above method.

Cloning of *IDA3* and transformation and rescue of *ida3* mutants

All cloning and tagging of *IDA3* was completed at the custom cloning core facility at Emory University. Briefly, the *IDA3* gene (~4.2kB) was PCR amplified from the BAC (4E5) clone containing the Cre03.g205000 gene. *Chlamydomonas*-codon optimized p3xHA (Silflow et al., 2001) or NeonGreen (Craft et al., 2015; Harris et al., 2016) were inserted into either the N-terminus or C-terminus of IDA3 or embedded within the first or second exon of the *IDA3* gene. All *IDA3*-tagged constructs were inserted into the PUCBM20 vector containing a *Chlamydomonas* Hygromycin B selection marker (pHyg3) (Berthold et al., 2002). The resulting constructs were

transformed into the *ida3* mutant by electroporation and placed on TAP+Hygromycin plates (final concentration at 10 μg/mL) for selection of single colonies expressing Hygromycin-resistance. Surviving colonies were visually scored for motility rescue of wild-type speed and isolated axonemes from each colony were analyzed by immunoblot for rescue of IC140/IC138 as a marker of I1 dynein assembly in the axoneme.

Preparation of Matrix Fractions

C. reinhardtii cells grown on constant light in L medium were collected by centrifugation and resuspended in chilled deciliation buffer (10 mM Tris, pH 7.5, 5% sucrose, 1 mM $CaCl_2$) and kept on ice. *C. reinhardtii* cells were deciliated by pH shock (Alford et al., 2013; Hunter et al., 2016). Cells were resuspended in room temperature L medium and aerated for 35 min at room temperature on constant light to regenerate cilia to approximately half length (Hunter et al., 2016). Regeneration of cilia was observed by phase contrast microscopy. Cells were collected by centrifugation (3,000 rpm for 5 min) and again resuspended in chilled deciliation buffer. A second deciliation was induced on ice by pH shock and flagella were collected by subsequent centrifugation.

To isolate the matrix fraction, cilia were resuspended in HMDE + 25 mM NaCl (10 mM HEPES, 5 mM $MgSO_4$, 1 mM DTT, 0.5 mM EDTA, 25 mM NaCl, protease inhibitors, pH 7.4). EDTA was omitted from HMDE + 25 mM NaCl buffer for all SNAP pull-down experiments. Cilia were flash frozen in liquid nitrogen and thawed at room temperature prior to centrifugation to remove remaining axonemes and membranes from the matrix fraction (Cole et al., 1998; Lucker et al., 2005; Pazour et al., 2005). Matrix fractions were either stored at 4°C prior to use in immunoprecipitation / pull-down

analyses or denatured with Laemmli sample buffer for immunoblot analysis. For matrix fractions of full-length cilia the regeneration step was omitted and cilia were isolated by pH shock and centrifugation prior to matrix isolation through identical freeze-thaw methods.

Membrane + Matrix Isolation

C. reinhardtii cells grown 2 nights on constant light in TAP medium were collected by centrifugation and resuspended in chilled deciliation buffer (10 mM Tris, pH 7.5, 5% sucrose, 1 mM $CaCl_2$) and kept on ice. *C. reinhardtii* cells were deciliated by pH shock (Alford et al., 2013; Hunter et al., 2016). Cells were resuspended in room temperature L medium and aerated for 35 min at room temperature on constant light to regenerate cilia to approximately half length (Hunter et al., 2016). Regeneration of cilia was observed by phase contrast microscopy. Cells were collected by centrifugation (3,000 rpm for 5 min) and again re-suspended in chilled deciliation buffer. A second deciliation was induced on ice by pH shock and flagella were collected by subsequent centrifugation.

To isolate the membrane + matrix fraction, cilia were isolated by centrifugation and re-suspended in 200 µl HMDE + 25 mM NaCl (10 mM HEPES, 5 mM $MgSO_4$, 1 mM DTT, 0.5 mM EDTA, 25 mM NaCl, protease inhibitors, pH 7.4). NP-40 Alternative Protein Grade Detergent (#492018-50 mL, EMD Millipore Corp., Billerica, MA, USA) was added to the flagellar sample (final concentration 1% of total volume) (Craige et al., 2013). The sample was incubated on ice for 10 minutes prior centrifugation at 13,200 rpm for 15 minutes. After centrifugation, the supernatant was isolated (membrane +

matrix fraction) and samples were denatured with Laemmli sample buffer for immunoblot analysis. For membrane + matrix fractions of full-length cilia the regeneration step was omitted and cilia were isolated by pH shock and centrifugation prior to membrane-matrix isolation through identical detergent methods. Please note inclusion of detergent in membrane + matrix samples disrupted SDS-PAGE analysis of proteins ~100 KD or larger making immunoblot analysis of membrane + matrix challenging.

CIP Treatment of Regenerating Matrix

Regenerating matrix from *ida3;IDA3::HA* cells was prepared by freeze-thaw method. Isolated flagella were suspended in 200 µl HMD + 25 mM NaCl (10 mM HEPES, 5 mM $MgSO_4$, 1 mM DTT, 25 mM NaCl, protease inhibitors, pH 7.4). Note EDTA was omitted from buffer for CIP treatment. After freeze thaw, ~250 µl of matrix was isolated and divided equally into two 1.5 mL eppendorf tubes. One sample was left untreated while 2 µl (2 units) of calf-intestinal alkaline phosphatase (M182A, Promega, Madison, WI, USA) was added to the second sample. The matrix samples were left at room temperature for 30 minutes prior to addition of Laemmli sample buffer for immunoblot analysis. 60 µl of each sample was loaded onto a 4-20% BioRad Criterion and probed with anti-HA (12CA5) at a 1:1,000 dilution. Goat anti-mouse secondary was used at 1:10,000 and blot was developed using ECL prime with a 2 h exposure.

Antibodies and Immunoblot Analyses

SDS-PAGE and immunoblotting were performed using standard procedures. Primary antibodies used in this study include: mouse monoclonal antibody against HA (Clone 12CA5, Roche, Mannheim, Germany), rat monoclonal antibody against HA (Clone 3f10, Sigma-Aldrich, Dermstadt, Germany) and IFT57 (Cole et al., 1998; Hou et al., 2007). Rabbit polyclonal antibodies include IC140 (Yang et al., 1998), IC138 (Hendrickson et al., 2004), IDA3 1B Affinity Purified (unpublished) and RSP3 (Wirschell et al., 2008). Secondary antibodies goat anti-mouse (#1706516) and goat anti-rabbit (#1706515) were purchased from Biorad (Hercules, CA). Goat anti-rat secondary (#31474) was purchased from Thermo Scientific (Rockford, IL, USA). Secondary antibodies used for immunofluorescence included Alexa Fluor 488 anti-rat IgG and Alexa Fluor 488 anti-rabbit IgG.

Generation of IDA3 Antibody

The N-terminal 416 bp of *IDA3* cDNA was cloned into pET-28a(+) vector to generate a 6xHIS-tagged construct. The completed construct was transformed into BL21 (DE3) pLysS cells for induction. Cells were induced with 0.4mM IPTG at RT (~20°C) overnight on shaker. The next morning cells were spun down and lysed with BugBuster protein extraction reagent (Novagen). Since the expressed His-tagged IDA3 protein is insoluble, the inclusion bodies were resuspended in BugBuster protein extraction reagent (Novagen) with 8M urea for purification. His-tagged IDA3 proteins were purified using HisTALON Gravity Columns (Clontech). The purified proteins were then concentrated using Microcon YM-30 columns (Millipore). Purified His-tagged IDA3 proteins were used to inject rabbits to produce antibodies against IDA3 (Spring Valley Laboratories

Inc., Woodbine, MD, USA). Rabbit 1B produced the most promising serum. Therefore, the final bleed was affinity-purified using HisTALON Gravity Columns (Clontech) with antigens attached to resin. This antibody is stored under IDA3 1B AP.

Generation of IDA3 Peptide Antibody

The first 150 amino acids of IDA3 were synthesized by GenScript USA Inc. (Piscataway, NJ, USA) and used at an antigen to generate an IDA3 antibody under the standard affinity purified antibody antigen polyclonal package. This antibody is stored under the name IDA3_Gen in the -20°C chest freezer. To date, the IDA3_Gen antibody has not been proven useful. Further characterization of the antibody on concentrated matrix of regenerating cilia may be useful in the future, though the antibody generated against the IDA3 fusion proteins appears more promising at this time. (See *ida3* P.2 notebook for additional information on antibody characterization).

Isolation of Axonemes

Cells were grown to mid-log phase and deciliated either by pH shock (Hunter et al., 2016; Lefebvre, 1995) or by treating the cells with dibucaine (Witman, 1986). After centrifugation to separate cilia from cell bodies, the cilia were demembranated by final 1% Nonidet P-40 (EMD Millipore, Darmstadt, Germany) in HMDE +25 mM NaCl (10 mM HEPES, 5 mM $MgSO_4$, 1 mM DTT, 0.5 mM EDTA, 25 mM NaCl, protease inhibitors, pH 7.4). Post centrifugation, the axoneme pellet was resuspended in HMDE +25 mM NaCl + protease inhibitors and denatured for immunoblot analyses in Laemmli sample buffer at a final concentration of 1mg/mL.

Isolation of Cytoplasmic Extracts

Glass beads were used to lyse cells cultured for 3 days (Ahmed et al., 2008). Broken cells were clarified by centrifugation at 10,000 rpm in the Sorval SA600 rotor for 10 min. The supernatant was then further clarified at 22.5K rpm for 2 h (Type-40 fixed angle rotor, Beckman Coulter, Fullerton, CA). Clarified supernatant was collected and denatured with Laemmli sample buffer for immunoblot analysis. For regenerating cytoplasmic extract samples, cells were deflagellated and regenerated according to standard methods (Alford et al., 2013; Hunter et al., 2016). After 30 m post-deflagellation, cells were lysed using the glass bead method and regenerating cytoplasmic extracts were isolated as described above.

Electron Microscopy

Conventional electron microscopy was performed on axonemes isolated from CC125, *ida3,* and *ida3; IDA3::HA* cells as previously described (Kamiya et al., 1991).

Cryo-Electron Tomography

Axoneme preparation for cryo–ET

Strains of *C. reinhardtii* were first grown on solid agar plates made with Tris-acetate-phosphate (TAP) medium for 5-7 days (Harris, 2009) and then a small amount of cells were transferred to liquid TAP growth medium for 3-4 days culturing under 12:12 h light: dark regime and flask shaking with the speed of 120 rpm. Cells were harvested by centrifugation (2,200 rpm) and resuspended in 10 mM HEPES buffer, pH 7.4 (1 mM

$SrCl_2$, 4% sucrose and 1 mM DTT). Cilia were isolated using the pH shock method (Witman et al., 1972); in brief cell pellets were resuspended in HEPES buffer (4% Sucrose, 1 mM $SrCl_2$, 10 mM HEPES, 1% DTT, pH 7.4) and the pH lowered to 4.5 by adding 0.5 M acetate acid. After 80 s, the pH value was brought back to 7.4 by adding 1 M KOH. After detachment of the cilia from the cell bodies the following solution was added to the buffer (5 mM $MgSO_4$, 1 mM EGTA, 0.1 mM EDTA and 100 μl protease inhibitor cocktails) (Sigma-Aldrich). Cilia were washed two times over a 20% sucrose cushion and then demembranated with 0.1% IGEPAL CA-630 (Sigma-Aldrich). Axonemes were collected by centrifugation at 10,000 *g* for 10 min and resuspended in HMEEK buffer (30 mM HEPES, 25 mM KCl, 5 mM $MgSO_4$, 0.1 mM EDTA and 0.2 mM EGTA). Cilia isolation and all steps thereafter were performed on ice or at 4°C.

Cryo-sample preparation, cryo-electron tomography and image processing

Freshly prepared axonemes were plunge-frozen on glow discharged (for 30 s at -35 mA) grids with holy-carbon film (copper; R2/2; 200 meshes; Quantifoil Micro Tools GmbH, Jena, Germany) using a homemade plunge-freezer to achieve sample vitrification, as previously described (Heuser et al., 2009). In brief, 3 μl of axoneme sample was applied to the grid and gently mixed with 1 μl of 10 times concentrated 10 nm colloidal gold solution. The gold particles were pre-coated with 5% (w/v) BSA solution to help prevent their aggregation (Iancu et al., 2006). Grids were blotted with Whatman filter paper from the backside for 1.5-2.5 s and rapidly plunged into liquid ethane. Sample grids were stored in liquid nitrogen until used.

Vitrified axonemes were imaged on a Tecnai F30 transmission electron microscope (Thermo-Fisher/FEI, Hillsboro, OR) operated at 300 kV. Tilt series (from -

60˚ to 60˚; 1.5-2.5˚ tilting increments) were recorded with a 2k x 2k charge-coupled device camera (Gatan, Pleasanton, CA) after energy filtering (Gatan) in zero-loss mode (20 eV slit width). Using the low dose mode in the microscope control and data acquisition software SerialEM (Mastronarde, 2005) the total electron dose per tilt series was limited to ~100 e/Å^2 to avoid radiation damage. A magnification of 13,500 (pixel size of 1 nm) and a defocus of -8 μm were used for imaging.

For image processing, the tilt series images were aligned using the 10 nm gold as fiducial markers. Both alignment and tomogram reconstruction by weighted back-projection were performed using the IMOD software package (Kremer et al., 1996). The axonemal 96 nm repeats were picked from the raw tomograms, aligned and subtomogram averaged using the PEET software (Nicastro et al., 2006). 3D visualization of the averaged structures by isosurface rendering was performed with UCSF Chimera package (Pettersen et al., 2004). Automated classification analyses of the I1 inner dynein arm were carried out with a PCA (principle component analysis) clustering approach (Heumann et al., 2011).

TIRF Microscopy

For TIRF imaging, we used a Eclipse Ti-U microscope (Nikon) equipped with 60× NA1.49 TIRF objective and through-the-objective TIRF illumination provided by a 40-mW 488-nm diode laser (Spectraphysics) (Lechtreck, 2013). Excitation and emission were filtered using the Nikon GFP/mCherry TIRF filter and the emission was separated using an Image Splitting Device (Photometrics DualView2 with filter cube 11-EM). Observation chambers for live cell imaging were assembled by inverting a 22 × 22 mm no. 1.5 cover glass with ~10 μl of 5 mM Hepes, pH 7.3, 6.25 mM EGTA onto an equal

volume of cells in M medium on a 24 × 60 mm no. 1.5 cover glass. Images were recorded at 10 fps using an iXON3 (Andor) and the NIS-Elements Advanced Research software (Nikon). FIJI (ImageJ plugin bundle, National Institutes of Health) was used to generate kymograms (Lechtreck, 2016). Individual frames were copied into Photoshop (Adobe) and adjusted for contrast and brightness; figures were assembled in Illustrator (CS6 version 16.0.3; Adobe). To generate videos, stacks were saved in avi format. For photo-bleaching of the entire cilia, the intensity of the 488-nm laser was increased to 10% or more for 4–12 s (Wingfield et al., 2017).

To examine regenerating cilia, cells were deflagellated by a pH shock, washed into fresh M medium, and incubated with agitation in bright light; to delay regeneration, cells were stored on ice until needed. For long-short experiments, cells were passaged 4-6 times through a 26G ^{x} 1/2 needle using a1-mL syringe. This treatment resulted in a small percentage (~1%) of long-zero cells that were imaged using TIRF microscopy after allowing flagellar regeneration for ~10-20 minutes.

Immunofluorescence Methods

Basal Body Staining

ida3; IDA3::HA (10-6-5) steady-state cells were in 100 mL L-bubblers one night on constant light with aeration. On day of prep, 50mL of fresh autolysin was generated as is done for transformation protocol. 50mL of *ida3;IDA3::HA* cells were spun at 2,000 rpm for 5 minutes. Cells were resuspended in 15mL fresh autolysin and incubated at room temperature for 30 min to remove cell walls. Cells were spun at 1,500 rpm for 5 minutes to remove cell wall ghosts. Cells were mounted on glass coverslips using 1%

PEI and fixed 5 minutes at -20°C in cold methanol (see Sale Lab immunofluorescence protocol). IF was completed following typical methods (see Sale Lab immunofluorescence protocol). Cells were stained with IDA3 1B (AP) antibody at a 1:25 dilution and HA (3f10) antibody at a 1:50 dilution. Anti-rabbit and anti-rat alexa-fluor secondary antibodies were used a 1:1,000 dilution. Cells were imaged using Olympus FV1000 inverted microscope and images were processed using ImageJ (FIJI) software.

Immunofluorescence of regenerating cytoskeletons

ida3 and *ida3; IDA3::HA* (10-6-5 and 11-5-12) cells were grown in 100 mL L-bubblers one night constant light with aeration. 100 mL of cells were spun down at 3,500 rpm for 2 min and brought up in 50 mL of chilled deflagellation buffer on ice. 1mL of 0.5M glacial acetic acid was added to lower the pH and cells were examined for deflagellation (Hunter et al., 2016). Upon confirmation of deflagellation, 0.5M potassium-hydroxide was added to neutralize the pH. Deflagellated cells were spun at 2,000 rpm x 5 minutes and brought up in ~15 mL L-media for regenerating at room temperature for ~30 minutes. Cilia were ~ ½ to ¾ in length. Cytoskeleton prep was then performed on regenerating cells (See Sale Lab protocol: Isolated cytoskeletal prep provided by Branch Craige). During preparation, I noted permeabilization of cells was not efficient for the regenerating cells. I later tried regenerating in autolysin to remove cell walls prior to permeabilization but cells became cranky and died during regeneration. Cells were stained with anti-HA (3f10) and 1:100 and anti-rat alexa fluor 488 secondary. Cells were imaged by epifluorescence microscopy using the microscope of Maureen Powers.

Immunofluorescence for puncta staining

ida3;IDA3::HA (10-3-13) cells were grown 1 night constant light in 100 mL L-bubbler with aeration. Cells were mounted on coverslips using 1% PEI and fixed in chilled acetone 10 minutes at -20°C. Following fixation, coverslips were washed 3 times with 1X PBS. Cells were blocked and stained with anti-HA (3f10) at 1:100 and goat anti-rat alexa fluor 488 secondary at a 1:1,000 dilution. Cells were imaged by epifluorescence using the microscope of Maureen Powers.

Immunoprecipitation of IDA3::HA from Matrix

All immunoprecipitation experiments were performed in matrix fractions isolated from regenerating cilia (as described above). To perform HA immunoprecipitation analyses, matrix fractions were isolated from regenerating cilia of *ida3* (CC-2688) and *ida3; IDA3::HA* strains. Immunoprecipitation (IP) buffer consists of 10 mM HEPES (pH 7.4), 5 mM $MgSO_4$, 1 mM DTT, 0.1 mM EDTA, 25 mM KCl, 75 mM NaCl, and 0.05% Triton X-100. Part of matrix fractions was denatured with Laemmli sample buffer for analysis of input by immunoblotting. The rest of the matrix fractions was pre-incubated with protein A agarose beads (Invitrogen) for 1 h at 4°C with slight agitation to pre-clear the matrix fractions. Prior to immunoprecipitation, 3F10-crosslinked beads (Roche) were blocked with 3% BSA in IP buffer by rocking for 1h at 4°C. Pre-cleared matrix fractions and pre-blocked 3F10-crosslinked beads were collected by centrifugation and combined for immunoprecipitation overnight at 4°C with slight agitation. Immunoprecipitates were washed with IP buffer the next day and denatured with 2x Laemmli sample buffer. Input samples and immunoprecipitates were resolved by SDS-PAGE and analyzed by immunoblotting.

Cytoplasmic extract IP

Isolation of cytoplasmic extract (both steady-state and regenerating) was performed as described above. The same number of *ida3* (CC-2688) and *ida3::IDA3-HA* cells was used to collect cytoplasmic fractions during steady-state and regeneration. Immunoprecipitation (IP) buffer consists of 10mM HEPES (pH 7.4), 5mM $MgSO_4$, 1mM DTT, 0.1mM EDTA, 25mM KCl, 75mM NaCl, and 0.05% Triton X-100. Part of cytoplasmic extracts was fixed with Laemmli sample buffer for input analysis by immunoblotting. The rest of the cytoplasmic extract fractions was pre-incubated with protein A agarose beads (Invitrogen) for 1hr at 4°C with slight agitation for pre-clearing. Prior to immunoprecipitation, 3F10-crosslinked beads (Roche) were blocked with 3% BSA in IP buffer by rocking for 1hr at 4°C. Pre-cleared cytoplasmic extract fractions and pre-blocked 3F10-crosslinked beads were collected by centrifugation and combined for immunoprecipitation overnight at 4°C with slight agitation. Immunoprecipitates were washed with IP buffer the next day and fixed with 2x Laemmli sample buffer. Input samples and immunoprecipitates were resolved by SDS-PAGE and analyzed by immunoblotting.

SNAP Affinity Purification

Matrix fractions were prepared by freeze-thaw, stored at 4°C, and supplemented with 0.5% Triton X-100 prior to use. For affinity purification we used a modified protocol from Zlatic et al. (Zlatic et al., 2013). SNAP magnetic beads (Cat No. S9145S, New England Biolabs) were prepared as follows: for each strain, 40 µl of the SNAP magnetic beads were spun down at room temperature using a bench-top mini-centrifuge

at top speed (14,000 x g) for 1 min. The clarified supernatant was removed and the beads were incubated overnight in an end over end rocker at 4°C in a buffer containing 3% BSA, 10 mM HEPES, 5 mM $MgSO_4$, 1 mM DTT, 25 mM NaCl, protease inhibitors, pH 7.4. Fresh DTT and protease inhibitors were added to the buffer solution every day prior to use. The next day, the beads were washed twice in a buffer containing 10 mM HEPES, 5 mM $MgSO_4$, 1 mM DTT, 0.5 mM EDTA, 25 mM NaCl, 0.5% Triton X-100, protease inhibitors, pH 7.4 using the magnetic holder. Matrix fractions were then added to the SNAP beads and the mixture was incubated at 4°C in an end-over-end rotor overnight. The magnetic beads were then washed 6 times in a buffer containing 10 mM HEPES, 5 mM $MgSO_4$, 1 mM DTT, 0.5 mM EDTA, 25 mM NaCl, 0.5% Triton X-100, protease inhibitors, pH 7.4. The beads were then resuspended in 2x Laemmli sample buffer and denatured at 95° C for 5 min for immunoblot analysis.

Analysis of processive IDA3 movement in *ida7; ida3; IDA3::NG*

TIRF microscopy was used to visualize IDA3 transport in regenerating *ida3; IDA3::NG* and *ida7; ida3; IDA3::NG* cells. Both cell types were imaged when cilia were approximately the same length (roughly 7-9 μm). Subsequent kymograms were generated. The length of the cilium and the length of anterograde IFT tracks were measured using Image J Software (National Institutes of Health, Bethesda, MD). Any kymograms in which the tip of the cilium could not be clearly distinguished were excluded from the analysis. The ratio of anterograde IFT track length to cilium length was then determined.

Statistical analysis

To determine whether a statistical difference between anterograde IFT (or retrograde transport) vs. diffusion of IDA3 exists, a two-tailed binomial test was performed in Graphpad software (La Jolla California USA, www.graphpad.com) as described before (Lechtreck, 2013). To determine if a statistical difference exists between IDA3 IFT transport in the presence or absence of I1, a two-tailed unpaired t-test was performed in Graphpad software. The graphs were drawn Adobe Illustrator and Excel.

Appendix II: IDA3 Construction Information

Truncated IDA3 Construct: IDA3 Accutaq Attempt #2 P.139 ida3#1 notebook. Glycerol stock: IDA3 Accu#2B- Topo2.1 (9/16/14). Emily's -80 box. Predicted premature stop at 1,071 within gene.

All WS-labeled constructs were generated through the Emory Cloning Core and unless otherwise specified are ampR and HygR.

WS8: N-term HA-tagged IDA3. This HA-tag is not *Chlamydomonas* codon optimized and this construct should not be used. Glycerol stocks: Emily's -80°C box under the names: IDA3HA N-term A 12/14/14 Top10 and IDA3HA N-term B 12/14/14 Top 10.

WS9: C-term HA-tagged IDA3. This HA-tag is not *Chlamydomonas* codon optimized and this construct should not be used. Glycerol stocks: Emily's -80°C box under names: IDA3HA C-term A 12/14/14 Top10 and IDA3HA C-term B 12/14/14 Top 10.

WS10: p3xHA-N-terminally tagged IDA3. This construct contains the *Chlamydomonas* codon-optimized HA-tag. Glycerol Stock: Emily's -80°C box under name: P3xHA (N-term) IDA3 (WS10) 5/19/14.

WS11: p3xHA-C-terminally tagged IDA3. This construct contains the *Chlamydomonas* codon-optimized HA-tag. Glycerol Stock: Emily's -80°C box under name: IDA3-p3xHA C-term (WS11) 06/09/15.

WS12: p3xHA inserted within the first exon of IDA3. WS12 did not rescue I1 dynein assembly when transformed into *ida3*. Glycerol Stock: Emily's -80°C box under name: WS12A and WS12B (2/20/16).

WS13: p3xHA inserted within second exon of IDA3. WS13 provided excellent rescue of I1 dynein assembly when transformed into *ida3*. WS13 is the construct present in all

HA-transformations in the Hunter et al., 2018 MBoC publication. Key *ida3* transformant containing this construct include 13-13-12 (used for MBoC publication). Note: 13-13-19 appears to have a truncated IDA3::HA and may be useful in the future. Glycerol Stock: Emily's -80°C box under name: WS13A and WS13B (2/20/16).

WS14: NeonGreen-tag attached to the N-terminus of IDA3. WS14 rescues I1 dynein assembly when transformed into *ida3*. Key *ida3* transformant imaged include 14-16-5. Glycerol Stock: Emily's -80°C box under name: WS14 (5/28/16).

WS15: NeonGreen-tag embedded in the second exon. WS15 provides excellent I1 dynein rescue of the *ida3* mutant. One key *ida3* transformant that contain WS15 is 15-3-14, used by Karl Lechtreck for live-cell imaging. Glycerol Stock: Emily's -80°C box under name: WS15 (5/28/16).

WS16: IC140::NG construct. I believe the NG tag replaced GFP in Ryosuke's IC140::GFP construct (pCP3-GFP AphVIII IC140-GFP Ryosuke: Emily's -80°C box: IC140-GFP Ryosuke 1A (1B) 2/1/2017). The construct did not rescue *ida7* and did not express paromomycin resistance as it was supposed to. Now believe there was a mix-up with IC140-GFP constructs. May be necessary to sequence this construct to confirm. Glycerol stock: Emily's -80°C box under name: IC140-NG #1 (#2) WS16 2/10/17 Top10.

WS24: IC140:mScarlett embedded within the second exon of IC140. Starting plasmids for generation include: **mScarlet::IFT54** (Gift of Karl Lechtreck-Glycerol Stock: Emily's -80°C box: mScarlet IFT54 1 (2) 10/20/17 Top10) and **PCS20.C1 IC140::SNAP** (gift from Maureen Wirschell-Glycerol Stock: Emily's -80°C box under name PCS20.C1 IC140-SNAP 10/25/17 Top10). This construct contains a paromomycin resistance marker

and is not hygromycin resistant. Work with this construct is currently underway. WS24 does rescue I1 dynein assembly when transformed into *ida7*.

References

Ahmed, N.T., and D.R. Mitchell. 2005. ODA16p, a Chlamydomonas flagellar protein needed for dynein assembly. *Mol Biol Cell*. 16:5004-5012.

Ahmed, N.T., C. Gao, B.F. Lucker, D.G. Cole, and D.R. Mitchell. 2008. ODA16 aids axonemal outer row dynein assembly through an interaction with the intraflagellar transport machinery. *J Cell Biol*. 183:313-322.

Alford, L.M., A.L. Mattheyses, E.L. Hunter, H. Lin, S.K. Dutcher, and W.S. Sale. 2013. The Chlamydomonas mutant pf27 reveals novel features of ciliary radial spoke assembly. *Cytoskeleton (Hoboken)*. 70:804-818.

Alford, L.M., D. Stoddard, J.H. Li, E.L. Hunter, D. Tritschler, R. Bower, D. Nicastro, M.E. Porter, and W.S. Sale. 2016. The nexin link and B-tubule glutamylation maintain the alignment of outer doublets in the ciliary axoneme. *Cytoskeleton (Hoboken)*. 73:331-340.

Awata, J., K. Song, J. Lin, S.M. King, M.J. Sanderson, D. Nicastro, and G.B. Witman. 2015. DRC3 connects the N-DRC to dynein g to regulate flagellar waveform. *Mol Biol Cell*. 26:2788-2800.

Bangs, F., and K.V. Anderson. 2017. Primary Cilia and Mammalian Hedgehog Signaling. *Cold Spring Harb Perspect Biol*. 9.

Barber, C.F., T. Heuser, B.I. Carbajal-Gonzalez, V.V. Botchkarev, Jr., and D. Nicastro. 2012. Three-dimensional structure of the radial spokes reveals heterogeneity and interactions with dyneins in Chlamydomonas flagella. *Mol Biol Cell*. 23:111-120.

Bayly, P.V., B.L. Lewis, P.S. Kemp, R.B. Pless, and S.K. Dutcher. 2010. Efficient spatiotemporal analysis of the flagellar waveform of Chlamydomonas reinhardtii. *Cytoskeleton (Hoboken)*. 67:56-69.

Bayly, P.V., B.L. Lewis, E.C. Ranz, R.J. Okamoto, R.B. Pless, and S.K. Dutcher. 2011. Propulsive forces on the flagellum during locomotion of Chlamydomonas reinhardtii. *Biophys J*. 100:2716-2725.

Behal, R.H., M.S. Miller, H. Qin, B.F. Lucker, A. Jones, and D.G. Cole. 2012. Subunit interactions and organization of the Chlamydomonas reinhardtii intraflagellar transport complex A proteins. *J Biol Chem*. 287:11689-11703.

Belzile, O., C.I. Hernandez-Lara, Q. Wang, and W.J. Snell. 2013. Regulated membrane protein entry into flagella is facilitated by cytoplasmic microtubules and does not require IFT. *Curr Biol*. 23:1460-1465.

Berthold, P., R. Schmitt, and W. Mages. 2002. An engineered Streptomyces hygroscopicus aph 7" gene mediates dominant resistance against hygromycin B in Chlamydomonas reinhardtii. *Protist*. 153:401-412.

Bhogaraju, S., L. Cajanek, C. Fort, T. Blisnick, K. Weber, M. Taschner, N. Mizuno, S. Lamla, P. Bastin, E.A. Nigg, and E. Lorentzen. 2013. Molecular basis of tubulin transport within the cilium by IFT74 and IFT81. *Science*. 341:1009-1012.

Bloodgood, R.A. 1995. Flagellar surface motility: gliding and microsphere movements. *Methods Cell Biol*. 47:273-279.

Bower, R., D. Tritschler, K. Vanderwaal, C.A. Perrone, J. Mueller, L. Fox, W.S. Sale, and M.E. Porter. 2013. The N-DRC forms a conserved biochemical complex that maintains outer doublet alignment and limits microtubule sliding in motile axonemes. *Mol Biol Cell*. 24:1134-1152.

Braun, D.A., and F. Hildebrandt. 2017. Ciliopathies. *Cold Spring Harb Perspect Biol*. 9.

Brazelton, W.J., C.D. Amundsen, C.D. Silflow, and P.A. Lefebvre. 2001. The bld1 mutation identifies the Chlamydomonas osm-6 homolog as a gene required for flagellar assembly. *Curr Biol*. 11:1591-1594.

Brokaw, C.J., and R. Kamiya. 1987. Bending patterns of Chlamydomonas flagella: IV. Mutants with defects in inner and outer dynein arms indicate differences in dynein arm function. *Cell Motil Cytoskeleton*. 8:68-75.

Brown, J.M., and G.B. Witman. 2014. Cilia and Diseases. *Bioscience*. 64:1126-1137.

Brown, J.M., D.A. Cochran, B. Craige, T. Kubo, and G.B. Witman. 2015. Assembly of IFT trains at the ciliary base depends on IFT74. *Curr Biol*. 25:1583-1593.

Bui, K.H., H. Sakakibara, T. Movassagh, K. Oiwa, and T. Ishikawa. 2009. Asymmetry of inner dynein arms and inter-doublet links in Chlamydomonas flagella. *J Cell Biol*. 186:437-446.

Bui, K.H., T. Yagi, R. Yamamoto, R. Kamiya, and T. Ishikawa. 2012. Polarity and asymmetry in the arrangement of dynein and related structures in the Chlamydomonas axoneme. *J Cell Biol*. 198:913-925.

Chien, A., S.M. Shih, R. Bower, D. Tritschler, M.E. Porter, and A. Yildiz. 2017. Dynamics of the IFT machinery at the ciliary tip. *Elife*. 6.

Chua, J.J., E. Butkevich, J.M. Worseck, M. Kittelmann, M. Gronborg, E. Behrmann, U. Stelzl, N.J. Pavlos, M.M. Lalowski, S. Eimer, E.E. Wanker, D.R. Klopfenstein, and R. Jahn. 2012. Phosphorylation-regulated axonal dependent transport of syntaxin 1 is mediated by a Kinesin-1 adapter. *Proc Natl Acad Sci U S A*. 109:5862-5867.

Cianfrocco, M.A., M.E. DeSantis, A.E. Leschziner, and S.L. Reck-Peterson. 2015. Mechanism and regulation of cytoplasmic dynein. *Annu Rev Cell Dev Biol*. 31:83-108.

Cole, D.G., D.R. Diener, A.L. Himelblau, P.L. Beech, J.C. Fuster, and J.L. Rosenbaum. 1998. Chlamydomonas kinesin-II-dependent intraflagellar transport (IFT): IFT particles contain proteins required for ciliary assembly in Caenorhabditis elegans sensory neurons. *J Cell Biol*. 141:993-1008.

Cole, D.G. 2003. The intraflagellar transport machinery of Chlamydomonas reinhardtii. *Traffic*. 4:435-442.

Craft, J.M., J.A. Harris, S. Hyman, P. Kner, and K.F. Lechtreck. 2015. Tubulin transport by IFT is upregulated during ciliary growth by a cilium-autonomous mechanism. *J Cell Biol*. 208:223-237.

Craige, B., J.M. Brown, and G.B. Witman. 2013. Isolation of Chlamydomonas flagella. *Curr Protoc Cell Biol*. Chapter 3:Unit 3 41 41-49.

Deane, J.A., D.G. Cole, E.S. Seeley, D.R. Diener, and J.L. Rosenbaum. 2001. Localization of intraflagellar transport protein IFT52 identifies basal body transitional fibers as the docking site for IFT particles. *Curr Biol*. 11:1586-1590.

Dentler, W. 2005. Intraflagellar transport (IFT) during assembly and disassembly of Chlamydomonas flagella. *J Cell Biol*. 170:649-659.

Desai, P.B., J.R. Freshour, and D.R. Mitchell. 2015. Chlamydomonas axonemal dynein assembly locus ODA8 encodes a conserved flagellar protein needed for cytoplasmic maturation of outer dynein arm complexes. *Cytoskeleton (Hoboken)*. 72:16-28.

Desai, P.B., A.B. Dean, and D.R. Mitchell. 2018. Cytoplasmic preassembly and trafficking of axonemal dyneins. *In* Dynein: Structure, Biology, and Disease. Vol. 1. S. King, editor. Academic Press (Elsevier). 141-162.

Diener, D.R., P. Yang, S. Geimer, D.G. Cole, W.S. Sale, and J.L. Rosenbaum. 2011. Sequential assembly of flagellar radial spokes. *Cytoskeleton (Hoboken)*. 68:389-400.

Dougherty, G.W., N.T. Loges, J.A. Klinkenbusch, H. Olbrich, P. Pennekamp, T. Menchen, J. Raidt, J. Wallmeier, C. Werner, C. Westermann, C. Ruckert, V. Mirra, R. Hjeij, Y. Memari, R. Durbin, A. Kolb-Kokocinski, K. Praveen, M.A. Kashef, S. Kashef, F. Eghtedari, K. Haffner, P. Valmari, G. Baktai, M. Aviram, L. Bentur, I. Amirav, E.E. Davis, N. Katsanis, M. Brueckner, A. Shaposhnykov, G. Pigino, B. Dworniczak, and H. Omran. 2016. DNAH11 Localization in the Proximal Region of Respiratory Cilia Defines Distinct Outer Dynein Arm Complexes. *Am J Respir Cell Mol Biol*. 55:213-224.

Duquesnoy, P., E. Escudier, L. Vincensini, J. Freshour, A.M. Bridoux, A. Coste, A. Deschildre, J. de Blic, M. Legendre, G. Montantin, H. Tenreiro, A.M. Vojtek, C. Loussert, A. Clement, D. Escalier, P. Bastin, D.R. Mitchell, and S. Amselem. 2009. Loss-of-function mutations in the human ortholog of Chlamydomonas reinhardtii ODA7 disrupt dynein arm assembly and cause primary ciliary dyskinesia. *Am J Hum Genet*. 85:890-896.

Dutcher, S.K. 1995. Mating and tetrad analysis in *Chlamydomonas reinhardtii*. *Methods Cell Biol*. 47:531-540.

Dutcher, S.K. 2003. Elucidation of basal body and centriole functions in Chlamydomonas reinhardtii. *Traffic*. 4:443-451.

Dutcher, S.K. 2014. The awesome power of dikaryons for studying flagella and basal bodies in Chlamydomonas reinhardtii. *Cytoskeleton (Hoboken)*. 71:79-94.

Dutcher, S.K., and E.T. O'Toole. 2016. The basal bodies of Chlamydomonas reinhardtii. *Cilia*. 5:18.

Eguether, T., J.T. San Agustin, B.T. Keady, J.A. Jonassen, Y. Liang, R. Francis, K. Tobita, C.A. Johnson, Z.A. Abdelhamed, C.W. Lo, and G.J. Pazour. 2014. IFT27 links the BBSome to IFT for maintenance of the ciliary signaling compartment. *Dev Cell*. 31:279-290.

Elam, C.A., M. Wirschell, R. Yamamoto, L.A. Fox, K. York, R. Kamiya, S.K. Dutcher, and W.S. Sale. 2011. An axonemal PP2A B-subunit is required for PP2A localization and flagellar motility. *Cytoskeleton (Hoboken)*. 68:363-372.

Engel, B.D., K.F. Lechtreck, T. Sakai, M. Ikebe, G.B. Witman, and W.F. Marshall. 2009a. Total internal reflection fluorescence (TIRF) microscopy of Chlamydomonas flagella. *Methods Cell Biol*. 93:157-177.

Engel, B.D., W.B. Ludington, and W.F. Marshall. 2009b. Intraflagellar transport particle size scales inversely with flagellar length: revisiting the balance-point length control model. *J Cell Biol*. 187:81-89.

Engel, B.D., H. Ishikawa, K.A. Wemmer, S. Geimer, K. Wakabayashi, M. Hirono, B. Craige, G.J. Pazour, G.B. Witman, R. Kamiya, and W.F. Marshall. 2012. The role of retrograde intraflagellar transport in flagellar assembly, maintenance, and function. *J Cell Biol*. 199:151-167.

Fagerberg, L., B.M. Hallstrom, P. Oksvold, C. Kampf, D. Djureinovic, J. Odeberg, M. Habuka, S. Tahmasebpoor, A. Danielsson, K. Edlund, A. Asplund, E. Sjostedt, E. Lundberg, C.A. Szigyarto, M. Skogs, J.O. Takanen, H. Berling, H. Tegel, J. Mulder, P. Nilsson, J.M. Schwenk, C. Lindskog, F. Danielsson, A. Mardinoglu, A. Sivertsson, K. von Feilitzen, M. Forsberg, M. Zwahlen, I. Olsson, S. Navani, M. Huss, J. Nielsen, F. Ponten, and M. Uhlen. 2014. Analysis of the human tissue-specific expression by genome-wide integration of transcriptomics and antibody-based proteomics. *Mol Cell Proteomics*. 13:397-406.

Fowkes, M.E., and D.R. Mitchell. 1998. The role of preassembled cytoplasmic complexes in assembly of flagellar dynein subunits. *Mol Biol Cell*. 9:2337-2347.

Fu, M.M., and E.L. Holzbaur. 2014. Integrated regulation of motor-driven organelle transport by scaffolding proteins. *Trends Cell Biol*. 24:564-574.

Gao, C., G. Wang, J.D. Amack, and D.R. Mitchell. 2010. Oda16/Wdr69 is essential for axonemal dynein assembly and ciliary motility during zebrafish embryogenesis. *Dev Dyn*. 239:2190-2197.

Garcia-Gonzalo, F.R., and J.F. Reiter. 2017. Open Sesame: How Transition Fibers and the Transition Zone Control Ciliary Composition. *Cold Spring Harb Perspect Biol*. 9.

Gibbons, B.H., and I.R. Gibbons. 1972. Flagellar movement and adenosine triphosphatase activity in sea urchin sperm extracted with triton X-100. *J Cell Biol*. 54:75-97.

Gokhale, A., M. Wirschell, and W.S. Sale. 2009. Regulation of dynein-driven microtubule sliding by the axonemal protein kinase CK1 in Chlamydomonas flagella. *J Cell Biol*. 186:817-824.

Goncalves, J., and L. Pelletier. 2017. The Ciliary Transition Zone: Finding the Pieces and Assembling the Gate. *Mol Cells*. 40:243-253.

Goodenough, U.W., and J.E. Heuser. 1982. Substructure of the outer dynein arm. *J Cell Biol*. 95:798-815.

Grimes, D.T., and R.D. Burdine. 2017. Left-Right Patterning: Breaking Symmetry to Asymmetric Morphogenesis. *Trends Genet*. 33:616-628.

Harris, E.H. 2009. The *Chlamydomonas* Sourcebook: Introduction to *Chlamydomonas and its laboratory use*. Academic Press (Elsevier). 444 pp.

Harris, J.A., Y. Liu, P. Yang, P. Kner, and K.F. Lechtreck. 2016. Single-particle imaging reveals intraflagellar transport-independent transport and accumulation of EB1 in Chlamydomonas flagella. *Mol Biol Cell*. 27:295-307.

Haycraft, C.J., B. Banizs, Y. Aydin-Son, Q. Zhang, E.J. Michaud, and B.K. Yoder. 2005. Gli2 and Gli3 localize to cilia and require the intraflagellar transport protein polaris for processing and function. *PLoS Genet*. 1:e53.

He, M., S. Agbu, and K.V. Anderson. 2017. Microtubule Motors Drive Hedgehog Signaling in Primary Cilia. *Trends Cell Biol*. 27:110-125.

Hendrickson, T.W., C.A. Perrone, P. Griffin, K. Wuichet, J. Mueller, P. Yang, M.E. Porter, and W.S. Sale. 2004. IC138 is a WD-repeat Dynein Intermediate Chain Required for Light Chain Assembly and Regulation of Flagellar Bending. *Mol Biol Cell*. 12:5431-5442.

Heumann, J.M., A. Hoenger, and D.N. Mastronarde. 2011. Clustering and variance maps for cryo-electron tomography using wedge-masked differences. *J Struct Biol*. 175:288-299.

Heuser, T., M. Raytchev, J. Krell, M.E. Porter, and D. Nicastro. 2009. The dynein regulatory complex is the nexin link and a major regulatory node in cilia and flagella. *J Cell Biol*. 187:921-933.

Heuser, T., C.F. Barber, J. Lin, J. Krell, M. Rebesco, M.E. Porter, and D. Nicastro. 2012. Cryoelectron tomography reveals doublet-specific structures and unique interactions in the I1 dynein. *Proc Natl Acad Sci U S A*. 109:E2067-2076.

Hilton, L.K., K. Gunawardane, J.W. Kim, M.C. Schwarz, and L.M. Quarmby. 2013. The kinases LF4 and CNK2 control ciliary length by feedback regulation of assembly and disassembly rates. *Curr Biol*. 23:2208-2214.

Horani, A., T.W. Ferkol, S.K. Dutcher, and S.L. Brody. 2016. Genetics and biology of primary ciliary dyskinesia. *Paediatr Respir Rev*. 18:18-24.

Hou, Y., H. Qin, J.A. Follit, G.J. Pazour, J.L. Rosenbaum, and G.B. Witman. 2007. Functional analysis of an individual IFT protein: IFT46 is required for transport of outer dynein arms into flagella. *J Cell Biol*. 176:653-665.

Hou, Y., and G.B. Witman. 2017. The N-terminus of IFT46 mediates intraflagellar transport of outer arm dynein and its cargo-adaptor ODA16. *Mol Biol Cell*. 28:2420-2433.

Huang, B., M.R. Rifkin, and D.J. Luck. 1977. Temperature-sensitive mutations affecting flagellar assembly and function in Chlamydomonas reinhardtii. *J Cell Biol*. 72:67-85.

Huangfu, D., A. Liu, A.S. Rakeman, N.S. Murcia, L. Niswander, and K.V. Anderson. 2003. Hedgehog signalling in the mouse requires intraflagellar transport proteins. *Nature*. 426:83-87.

Hunter, E.L., W.S. Sale, and L.M. Alford. 2016. Analysis of Axonemal Assembly During Ciliary Regeneration in Chlamydomonas. *Methods Mol Biol*. 1454:237-243.

Huynh, W., and R.D. Vale. 2017. Disease-associated mutations in human BICD2 hyperactivate motility of dynein-dynactin. *J Cell Biol*. 216:3051-3060.

Iancu, C.V., W.F. Tivol, J.B. Schooler, D.P. Dias, G.P. Henderson, G.E. Murphy, E.R. Wright, Z. Li, Z. Yu, A. Briegel, L. Gan, Y. He, and G.J. Jensen. 2006. Electron cryotomography sample preparation using the Vitrobot. *Nat Protoc*. 1:2813-2819.

Ishikawa, H., and W.F. Marshall. 2017. Testing the time-of-flight model for flagellar length sensing. *Mol Biol Cell*. 28:3447-3456.

Ishikawa, T. 2013. 3D structure of eukaryotic flagella/cilia by cryo-electron tomography. *Biophysics (Nagoya-shi)*. 9:141-148.

Ishikawa, T. 2017. Axoneme Structure from Motile Cilia. *Cold Spring Harb Perspect Biol*. 9.

Ishikawa, T. 2018. Organization of dyneins in the axoneme. *In* Dyneins: Structure, Biology, and Disease. Vol. 1. S. King, editor. Academic Press (Elsevier). 203-218.

Jensen, V.L., and M.R. Leroux. 2017. Gates for soluble and membrane proteins, and two trafficking systems (IFT and LIFT), establish a dynamic ciliary signaling compartment. *Curr Opin Cell Biol*. 47:83-91.

Johnson, K.A., and J.L. Rosenbaum. 1992. Polarity of flagellar assembly in Chlamydomonas. *J Cell Biol*. 119:1605-1611.

Jonassen, J.A., J. San Agustin, J.A. Follit, and G.J. Pazour. 2008. Deletion of IFT20 in the mouse kidney causes misorientation of the mitotic spindle and cystic kidney disease. *J Cell Biol*. 183:377-384.

Kamiya, R., E. Kurimoto, and E. Muto. 1991. Two types of Chlamydomonas flagellar mutants missing different components of inner-arm dynein. *J Cell Biol*. 112:441-447.

Kamiya, R., and T. Yagi. 2014. Functional diversity of axonemal dyneins as assessed by in vitro and in vivo motility assays of Chlamydomonas mutants. *Zoolog Sci*. 31:633-644.

Kee, H.L., J.F. Dishinger, T.L. Blasius, C.J. Liu, B. Margolis, and K.J. Verhey. 2012. A size-exclusion permeability barrier and nucleoporins characterize a ciliary pore complex that regulates transport into cilia. *Nat Cell Biol*. 14:431-437.

Kindle, K.L. 1990. High-frequency nuclear transformation of *Chlamydomonas reinhardtii*. *Proc Natl Acad Sci U S A*. 87:1228-1232.

King, S. 2018. Composition and assembly of axonemal dyneins. *In* Dyneins: Structure, Biology, and Disease. Vol. 1. S. King, editor. Academic Press (Elsevier). 163-202.

King, S.J., and S.K. Dutcher. 1997. Phosphoregulation of an inner dynein arm complex in Chlamydomonas reinhardtii is altered in phototactic mutant strains. *J Cell Biol*. 136:177-191.

King, S.M. 2016. Axonemal Dynein Arms. *Cold Spring Harb Perspect Biol*. 8.

Klena, N.T., B.C. Gibbs, and C.W. Lo. 2017. Cilia and Ciliopathies in Congenital Heart Disease. *Cold Spring Harb Perspect Biol*. 9.

Klink, B.U., E. Zent, P. Juneja, A. Kuhlee, S. Raunser, and A. Wittinghofer. 2017. A recombinant BBSome core complex and how it interacts with ciliary cargo. *Elife*. 6.

Knowles, M.R., L.A. Daniels, S.D. Davis, M.A. Zariwala, and M.W. Leigh. 2013. Primary ciliary dyskinesia. Recent advances in diagnostics, genetics, and characterization of clinical disease. *Am J Respir Crit Care Med*. 188:913-922.

Knowles, M.R., M. Zariwala, and M. Leigh. 2016. Primary Ciliary Dyskinesia. *Clin Chest Med*. 37:449-461.

Kobayashi, D., and H. Takeda. 2012. Ciliary motility: the components and cytoplasmic preassembly mechanisms of the axonemal dyneins. *Differentiation*. 83:S23-29.

Kotani, N., H. Sakakibara, S.A. Burgess, H. Kojima, and K. Oiwa. 2007. Mechanical properties of inner-arm dynein-f (dynein I1) studied with in vitro motility assays. *Biophys J*. 93:886-894.

Kozminski, K.G., P.L. Beech, and J.L. Rosenbaum. 1995. The Chlamydomonas kinesin-like protein FLA10 is involved in motility associated with the flagellar membrane. *J Cell Biol*. 131:1517-1527.

Kremer, J.R., D.N. Mastronarde, and J.R. McIntosh. 1996. Computer visualization of three-dimensional image data using IMOD. *J Struct Biol*. 116:71-76.

Kubo, T., H.A. Yanagisawa, T. Yagi, M. Hirono, and R. Kamiya. 2010. Tubulin polyglutamylation regulates axonemal motility by modulating activities of inner-arm dyneins. *Curr Biol*. 20:441-445.

Kubo, T., T. Yagi, and R. Kamiya. 2012. Tubulin polyglutamylation regulates flagellar motility by controlling a specific inner-arm dynein that interacts with the dynein regulatory complex. *Cytoskeleton (Hoboken)*. 69:1059-1068.

Kubo, T., J.M. Brown, K. Bellve, B. Craige, J.M. Craft, K. Fogarty, K.F. Lechtreck, and G.B. Witman. 2016. Together, the IFT81 and IFT74 N-termini form the main module for intraflagellar transport of tubulin. *J Cell Sci*. 129:2106-2119.

Kubo, T., and T. Oda. 2017. Electrostatic interaction between polyglutamylated tubulin and the nexin-dynein regulatory complex regulates flagellar motility. *Mol Biol Cell*. 28:2260-2266.

Kurkowiak, M., E. Zietkiewicz, and M. Witt. 2015. Recent advances in primary ciliary dyskinesia genetics. *J Med Genet*. 52:1-9.

Lechtreck, K.F., J. Rostmann, and A. Grunow. 2002. Analysis of Chlamydomonas SF-assemblin by GFP tagging and expression of antisense constructs. *J Cell Sci*. 115:1511-1522.

Lechtreck, K.F., E.C. Johnson, T. Sakai, D. Cochran, B.A. Ballif, J. Rush, G.J. Pazour, M. Ikebe, and G.B. Witman. 2009. The Chlamydomonas reinhardtii BBSome is an IFT cargo required for export of specific signaling proteins from flagella. *J Cell Biol*. 187:1117-1132.

Lechtreck, K.F. 2013. In vivo imaging of IFT in Chlamydomonas flagella. *Methods Enzymol*. 524:265-284.

Lechtreck, K.F., J.M. Brown, J.L. Sampaio, J.M. Craft, A. Shevchenko, J.E. Evans, and G.B. Witman. 2013. Cycling of the signaling protein phospholipase D through cilia requires the BBSome only for the export phase. *J Cell Biol*. 201:249-261.

Lechtreck, K.F. 2015. IFT-Cargo Interactions and Protein Transport in Cilia. *Trends Biochem Sci*. 40:765-778.

Lechtreck, K.F. 2016. Methods for Studying Movement of Molecules Within Cilia. *Methods Mol Biol*. 1454:83-96.

Lechtreck, K.F., J.C. Van De Weghe, J.A. Harris, and P. Liu. 2017. Protein transport in growing and steady-state cilia. *Traffic*. 18:277-286.

Lefebvre, P.A. 1995. Flagellar amputation and regeneration in Chlamydomonas. *Methods Cell Biol*. 47:3-7.

Li, Y., N.T. Klena, G.C. Gabriel, X. Liu, A.J. Kim, K. Lemke, Y. Chen, B. Chatterjee, W. Devine, R.R. Damerla, C. Chang, H. Yagi, J.T. San Agustin, M. Thahir, S. Anderton, C. Lawhead, A. Vescovi, H. Pratt, J. Morgan, L. Haynes, C.L. Smith, J.T. Eppig, L. Reinholdt, R. Francis, L. Leatherbury, M.K. Ganapathiraju, K. Tobita, G.J. Pazour, and C.W. Lo. 2015. Global genetic analysis in mice unveils central role for cilia in congenital heart disease. *Nature*. 521:520-524.

Liang, Y., Y. Pang, Q. Wu, Z. Hu, X. Han, Y. Xu, H. Deng, and J. Pan. 2014. FLA8/KIF3B phosphorylation regulates kinesin-II interaction with IFT-B to control IFT entry and turnaround. *Dev Cell*. 30:585-597.

Liew, G.M., F. Ye, A.R. Nager, J.P. Murphy, J.S. Lee, M. Aguiar, D.K. Breslow, S.P. Gygi, and M.V. Nachury. 2014. The intraflagellar transport protein IFT27 promotes BBSome exit from cilia through the GTPase ARL6/BBS3. *Dev Cell*. 31:265-278.

Lin, H., M.L. Miller, D.M. Granas, and S.K. Dutcher. 2013a. Whole genome sequencing identifies a deletion in protein phosphatase 2A that affects its stability and localization in Chlamydomonas reinhardtii. *PLoS Genet*. 9:e1003841.

Lin, H., N.P. Nauman, A.J. Albee, S. Hsu, and S.K. Dutcher. 2013b. New mutations in flagellar motors identified by whole genome sequencing in Chlamydomonas. *Cilia*. 2:14.

Lin, H., and S.K. Dutcher. 2015. Genetic and genomic approaches to identify genes involved in flagellar assembly in Chlamydomonas reinhardtii. *Methods Cell Biol*. 127:349-386.

Lin, J., W. Yin, M.C. Smith, K. Song, M.W. Leigh, M.A. Zariwala, M.R. Knowles, L.E. Ostrowski, and D. Nicastro. 2014. Cryo-electron tomography reveals ciliary defects underlying human RSPH1 primary ciliary dyskinesia. *Nat Commun*. 5:5727.

Lin, Y.C., P. Niewiadomski, B. Lin, H. Nakamura, S.C. Phua, J. Jiao, A. Levchenko, T. Inoue, R. Rohatgi, and T. Inoue. 2013c. Chemically inducible diffusion trap at cilia reveals molecular sieve-like barrier. *Nat Chem Biol*. 9:437-443.

Liu, A., B. Wang, and L.A. Niswander. 2005. Mouse intraflagellar transport proteins regulate both the activator and repressor functions of Gli transcription factors. *Development*. 132:3103-3111.

Liu, P., and K.F. Lechtreck. 2018. The Bardet-Biedl syndrome protein complex is an adapter expanding the cargo range of intraflagellar transport trains for ciliary export. *Proc Natl Acad Sci U S A*.

Lucker, B.F., R.H. Behal, H. Qin, L.C. Siron, W.D. Taggart, J.L. Rosenbaum, and D.G. Cole. 2005. Characterization of the intraflagellar transport complex B core: direct interaction of the IFT81 and IFT74/72 subunits. *J Biol Chem*. 280:27688-27696.

Lukyanov, K.A., D.M. Chudakov, S. Lukyanov, and V.V. Verkhusha. 2005. Innovation: Photoactivatable fluorescent proteins. *Nat Rev Mol Cell Biol*. 6:885-891.

Marshall, W.F., and J.L. Rosenbaum. 2001. Intraflagellar transport balances continuous turnover of outer doublet microtubules: implications for flagellar length control. *J Cell Biol*. 155:405-414.

Marshall, W.F., H. Qin, M. Rodrigo Brenni, and J.L. Rosenbaum. 2005. Flagellar length control system: testing a simple model based on intraflagellar transport and turnover. *Mol Biol Cell*. 16:270-278.

Mastronarde, D.N. 2005. Automated electron microscope tomography using robust prediction of specimen movements. *J Struct Biol*. 152:36-51.

McKenney, R.J., W. Huynh, M.E. Tanenbaum, G. Bhabha, and R.D. Vale. 2014. Activation of cytoplasmic dynein motility by dynactin-cargo adapter complexes. *Science*. 345:337-341.

Mueller, J., C.A. Perrone, R. Bower, D.G. Cole, and M.E. Porter. 2005. The FLA3 KAP subunit is required for localization of kinesin-2 to the site of flagellar assembly and processive anterograde intraflagellar transport. *Mol Biol Cell*. 16:1341-1354.

Myster, S.H., J.A. Knott, E. O'Toole, and M.E. Porter. 1997. The Chlamydomonas Dhc1 gene encodes a dynein heavy chain subunit required for assembly of the I1 inner arm complex. *Mol Biol Cell*. 8:607-620.

Myster, S.H., J.A. Knott, K.M. Wysocki, E. O'Toole, and M.E. Porter. 1999. Domains in the 1alpha dynein heavy chain required for inner arm assembly and flagellar motility in Chlamydomonas. *J Cell Biol*. 146:801-818.

Nguyen, R.L., L.W. Tam, and P.A. Lefebvre. 2005. The LF1 gene of Chlamydomonas reinhardtii encodes a novel protein required for flagellar length control. *Genetics*. 169:1415-1424.

Nicastro, D., C. Schwartz, J. Pierson, R. Gaudette, M.E. Porter, and J.R. McIntosh. 2006. The molecular architecture of axonemes revealed by cryoelectron tomography. *Science*. 313:944-948.

Nicastro, D., X. Fu, T. Heuser, A. Tso, M.E. Porter, and R.W. Linck. 2011. Cryo-electron tomography reveals conserved features of doublet microtubules in flagella. *Proc Natl Acad Sci U S A*. 108:E845-853.

O'Toole, E.T., T.H. Giddings, Jr., M.E. Porter, and L.E. Ostrowski. 2012. Computer-assisted image analysis of human cilia and Chlamydomonas flagella reveals both similarities and differences in axoneme structure. *Cytoskeleton (Hoboken)*. 69:577-590.

Oda, T., H. Yanagisawa, R. Kamiya, and M. Kikkawa. 2014a. A molecular ruler determines the repeat length in eukaryotic cilia and flagella. *Science*. 346:857-860.

Oda, T., H. Yanagisawa, T. Yagi, and M. Kikkawa. 2014b. Mechanosignaling between central apparatus and radial spokes controls axonemal dynein activity. *J Cell Biol*. 204:807-819.

Oda, T., H. Yanagisawa, and M. Kikkawa. 2015. Detailed structural and biochemical characterization of the nexin-dynein regulatory complex. *Mol Biol Cell*. 26:294-304.

Olcese, C., M.P. Patel, A. Shoemark, S. Kiviluoto, M. Legendre, H.J. Williams, C.K. Vaughan, J. Hayward, A. Goldenberg, R.D. Emes, M.M. Munye, L. Dyer, T. Cahill, J. Bevillard, C. Gehrig, M. Guipponi, S. Chantot, P. Duquesnoy, L. Thomas, L. Jeanson, B. Copin, A. Tamalet, C. Thauvin-Robinet, J.F. Papon, A. Garin, I. Pin, G. Vera, P. Aurora, M.R. Fassad, L. Jenkins, C. Boustred, T. Cullup, M. Dixon, A. Onoufriadis, A. Bush, E.M. Chung, S.E. Antonarakis, M.R. Loebinger, R. Wilson, M. Armengot, E. Escudier, C. Hogg, U.K.R. Group, S. Amselem, Z. Sun, L. Bartoloni, J.L. Blouin, and H.M. Mitchison. 2017. X-linked primary ciliary dyskinesia due to mutations in the cytoplasmic axonemal dynein assembly factor PIH1D3. *Nat Commun*. 8:14279.

Omran, H., D. Kobayashi, H. Olbrich, T. Tsukahara, N.T. Loges, H. Hagiwara, Q. Zhang, G. Leblond, E. O'Toole, C. Hara, H. Mizuno, H. Kawano, M. Fliegauf, T. Yagi, S. Koshida, A. Miyawaki, H. Zentgraf, H. Seithe, R. Reinhardt, Y. Watanabe, R. Kamiya, D.R. Mitchell, and H. Takeda. 2008. Ktu/PF13 is required for cytoplasmic pre-assembly of axonemal dyneins. *Nature*. 456:611-616.

Orozco, J.T., K.P. Wedaman, D. Signor, H. Brown, L. Rose, and J.M. Scholey. 1999. Movement of motor and cargo along cilia. *Nature*. 398:674.

Ostrowski, L.E., S.K. Dutcher, and C.W. Lo. 2011. Cilia and models for studying structure and function. *Proc Am Thorac Soc*. 8:423-429.

Owa, M., A. Furuta, J. Usukura, F. Arisaka, S.M. King, G.B. Witman, R. Kamiya, and K. Wakabayashi. 2014. Cooperative binding of the outer arm-docking complex

underlies the regular arrangement of outer arm dynein in the axoneme. *Proc Natl Acad Sci U S A*. 111:9461-9466.

Pasquale, S.M., and U.W. Goodenough. 1987. Cyclic AMP functions as a primary sexual signal in gametes of Chlamydomonas reinhardtii. *J Cell Biol*. 105:2279-2292.

Pazour, G.J., C.G. Wilkerson, and G.B. Witman. 1998. A dynein light chain is essential for the retrograde particle movement of intraflagellar transport (IFT). *J Cell Biol*. 141:979-992.

Pazour, G.J., B.L. Dickert, and G.B. Witman. 1999. The DHC1b (DHC2) isoform of cytoplasmic dynein is required for flagellar assembly. *J Cell Biol*. 144:473-481.

Pazour, G.J., B.L. Dickert, Y. Vucica, E.S. Seeley, J.L. Rosenbaum, G.B. Witman, and D.G. Cole. 2000a. Chlamydomonas IFT88 and its mouse homologue, polycystic kidney disease gene tg737, are required for assembly of cilia and flagella. *J Cell Biol*. 151:709-718.

Pazour, G.J., and G.B. Witman. 2000b. Forward and reverse genetic analysis of microtubule motors in Chlamydomonas. *Methods*. 22:285-298.

Pazour, G.J., N. Agrin, J. Leszyk, and G.B. Witman. 2005. Proteomic analysis of a eukaryotic cilium. *J Cell Biol*. 170:103-113.

Perrone, C.A., P. Yang, E. O'Toole, W.S. Sale, and M.E. Porter. 1998. The Chlamydomonas IDA7 locus encodes a 140-kDa dynein intermediate chain required to assemble the I1 inner arm complex. *Mol Biol Cell*. 9:3351-3365.

Perrone, C.A., S.H. Myster, R. Bower, E.T. O'Toole, and M.E. Porter. 2000. Insights into the structural organization of the I1 inner arm dynein from a domain analysis of the 1beta dynein heavy chain. *Mol Biol Cell*. 11:2297-2313.

Pettersen, E.F., T.D. Goddard, C.C. Huang, G.S. Couch, D.M. Greenblatt, E.C. Meng, and T.E. Ferrin. 2004. UCSF Chimera--a visualization system for exploratory research and analysis. *J Comput Chem*. 25:1605-1612.

Pigino, G., K.H. Bui, A. Maheshwari, P. Lupetti, D. Diener, and T. Ishikawa. 2011. Cryoelectron tomography of radial spokes in cilia and flagella. *J Cell Biol*. 195:673-687.

Piperno, G., Z. Ramanis, E.F. Smith, and W.S. Sale. 1990. Three distinct inner dynein arms in Chlamydomonas flagella: molecular composition and location in the axoneme. *J Cell Biol*. 110:379-389.

Piperno, G., K. Mead, and S. Henderson. 1996. Inner dynein arms but not outer dynein arms require the activity of kinesin homologue protein KHP1(FLA10) to reach the distal part of flagella in Chlamydomonas. *J Cell Biol*. 133:371-379.

Piperno, G., and K. Mead. 1997. Transport of a novel complex in the cytoplasmic matrix of Chlamydomonas flagella. *Proc Natl Acad Sci U S A*. 94:4457-4462.

Porter, M.E., J. Power, and S.K. Dutcher. 1992. Extragenic suppressors of paralyzed flagellar mutations in Chlamydomonas reinhardtii identify loci that alter the inner dynein arms. *J Cell Biol*. 118:1163-1176.

Porter, M.E., R. Bower, J.A. Knott, P. Byrd, and W. Dentler. 1999. Cytoplasmic dynein heavy chain 1b is required for flagellar assembly in Chlamydomonas. *Mol Biol Cell*. 10:693-712.

Porter, M.E., and W.S. Sale. 2000. The 9 + 2 axoneme anchors multiple inner arm dyneins and a network of kinases and phosphatases that control motility. *J Cell Biol*. 151:F37-42.

Porter, M.E. 2018. Ciliary and flagellar motility and he nexin-dynein regulatory complex. *In* Dyneins: Structure, Biology, and Disease. Vol. 1. S. King, editor. Academic Press (Elsevier). 203-218.

Qin, H., D.R. Diener, S. Geimer, D.G. Cole, and J.L. Rosenbaum. 2004. Intraflagellar transport (IFT) cargo: IFT transports flagellar precursors to the tip and turnover products to the cell body. *J Cell Biol*. 164:255-266.

Qin, H., Z. Wang, D. Diener, and J. Rosenbaum. 2007. Intraflagellar transport protein 27 is a small G protein involved in cell-cycle control. *Curr Biol*. 17:193-202.

Reiter, J.F., and M.R. Leroux. 2017. Genes and molecular pathways underpinning ciliopathies. *Nat Rev Mol Cell Biol*. 18:533-547.

Richey, E.A., and H. Qin. 2012. Dissecting the sequential assembly and localization of intraflagellar transport particle complex B in Chlamydomonas. *PLoS One*. 7:e43118.

Rosenbaum, J.L., and F.M. Child. 1967. Flagellar regeneration in protozoan flagellates. *J Cell Biol*. 34:345-364.

Rosenbaum, J.L., J.E. Moulder, and D.L. Ringo. 1969. Flagellar elongation and shortening in Chlamydomonas. The use of cycloheximide and colchicine to study the synthesis and assembly of flagellar proteins. *J Cell Biol*. 41:600-619.

Satir, P., T. Heuser, and W.S. Sale. 2014. A Structural Basis for How Motile Cilia Beat. *Bioscience*. 64:1073-1083.

Schroeder, C.M., and R.D. Vale. 2016. Assembly and activation of dynein-dynactin by the cargo adaptor protein Hook3. *J Cell Biol*. 214:309-318.

Sheffield, V.C. 2004. Use of isolated populations in the study of a human obesity syndrome, the Bardet-Biedl syndrome. *Pediatr Res*. 55:908-911.

Shi, X., G. Garcia, 3rd, J.C. Van De Weghe, R. McGorty, G.J. Pazour, D. Doherty, B. Huang, and J.F. Reiter. 2017. Super-resolution microscopy reveals that disruption of ciliary transition-zone architecture causes Joubert syndrome. *Nat Cell Biol*. 19:1178-1188.

Silflow, C.D., M. LaVoie, L.W. Tam, S. Tousey, M. Sanders, W. Wu, M. Borodovsky, and P.A. Lefebvre. 2001. The Vfl1 Protein in Chlamydomonas localizes in a rotationally asymmetric pattern at the distal ends of the basal bodies. *J Cell Biol*. 153:63-74.

Sizova, I.A., T.V. Lapina, O.N. Frolova, N.N. Alexandrova, K.E. Akopiants, and V.N. Danilenko. 1996. Stable nuclear transformation of Chlamydomonas reinhardtii with a Streptomyces rimosus gene as the selective marker. *Gene*. 181:13-18.

Slough, J., L. Cooney, and M. Brueckner. 2008. Monocilia in the embryonic mouse heart suggest a direct role for cilia in cardiac morphogenesis. *Dev Dyn*. 237:2304-2314.

Smith, E.F., and W.S. Sale. 1991. Microtubule binding and translocation by inner dynein arm subtype I1. *Cell Motil Cytoskeleton*. 18:258-268.

Smith, E.F., and W.S. Sale. 1992a. Structural and functional reconstitution of inner dynein arms in Chlamydomonas flagellar axonemes. *J Cell Biol*. 117:573-581.

Smith, E.F., and W.S. Sale. 1992b. Regulation of dynein-driven microtubule sliding by the radial spokes in flagella. *Science*. 257:1557-1559.

Spassky, N., and A. Meunier. 2017. The development and functions of multiciliated epithelia. *Nat Rev Mol Cell Biol*. 18:423-436.

Stepanek, L., and G. Pigino. 2016. Microtubule doublets are double-track railways for intraflagellar transport trains. *Science*. 352:721-724.

Summers, K.E., and I.R. Gibbons. 1971. Adenosine triphosphate-induced sliding of tubules in trypsin-treated flagella of sea-urchin sperm. *Proc Natl Acad Sci U S A*. 68:3092-3096.

Takao, D., and K.J. Verhey. 2016. Gated entry into the ciliary compartment. *Cell Mol Life Sci*. 73:119-127.

Takao, D., L. Wang, A. Boss, and K.J. Verhey. 2017. Protein Interaction Analysis Provides a Map of the Spatial and Temporal Organization of the Ciliary Gating Zone. *Curr Biol*. 27:2296-2306 e2293.

Tam, L.W., W.L. Dentler, and P.A. Lefebvre. 2003. Defective flagellar assembly and length regulation in LF3 null mutants in Chlamydomonas. *J Cell Biol*. 163:597-607.

Tam, L.W., P.T. Ranum, and P.A. Lefebvre. 2013. CDKL5 regulates flagellar length and localizes to the base of the flagella in Chlamydomonas. *Mol Biol Cell*. 24:588-600.

Tarkar, A., N.T. Loges, C.E. Slagle, R. Francis, G.W. Dougherty, J.V. Tamayo, B. Shook, M. Cantino, D. Schwartz, C. Jahnke, H. Olbrich, C. Werner, J. Raidt, P. Pennekamp, M. Abouhamed, R. Hjeij, G. Kohler, M. Griese, Y. Li, K. Lemke, N. Klena, X. Liu, G. Gabriel, K. Tobita, M. Jaspers, L.C. Morgan, A.J. Shapiro, S.J. Letteboer, D.A. Mans, J.L. Carson, M.W. Leigh, W.E. Wolf, S. Chen, J.S. Lucas, A. Onoufriadis, V. Plagnol, M. Schmidts, K. Boldt, Uk10K, R. Roepman, M.A. Zariwala, C.W. Lo, H.M. Mitchison, M.R. Knowles, R.D. Burdine, J.J. Loturco, and H. Omran. 2013. DYX1C1 is required for axonemal dynein assembly and ciliary motility. *Nat Genet*. 45:995-1003.

Taschner, M., S. Bhogaraju, and E. Lorentzen. 2012. Architecture and function of IFT complex proteins in ciliogenesis. *Differentiation*. 83:S12-22.

Taschner, M., F. Kotsis, P. Braeuer, E.W. Kuehn, and E. Lorentzen. 2014. Crystal structures of IFT70/52 and IFT52/46 provide insight into intraflagellar transport B core complex assembly. *J Cell Biol*. 207:269-282.

Taschner, M., and E. Lorentzen. 2016a. Recombinant Reconstitution and Purification of the IFT-B Core Complex from Chlamydomonas reinhardtii. *Methods Mol Biol*. 1454:69-82.

Taschner, M., and E. Lorentzen. 2016b. The Intraflagellar Transport Machinery. *Cold Spring Harb Perspect Biol*. 8.

Taschner, M., A. Mourao, M. Awasthi, J. Basquin, and E. Lorentzen. 2017. Structural basis of outer dynein arm intraflagellar transport by the transport adaptor protein ODA16 and the intraflagellar transport protein IFT46. *J Biol Chem*. 292:7462-7473.

Toba, S., L.A. Fox, H. Sakakibara, M.E. Porter, K. Oiwa, and W.S. Sale. 2011. Distinct roles of 1alpha and 1beta heavy chains of the inner arm dynein I1 of Chlamydomonas flagella. *Mol Biol Cell*. 22:342-353.

Torisawa, T., M. Ichikawa, A. Furuta, K. Saito, K. Oiwa, H. Kojima, Y.Y. Toyoshima, and K. Furuta. 2014. Autoinhibition and cooperative activation mechanisms of cytoplasmic dynein. *Nat Cell Biol*. 16:1118-1124.

Toropova, K., M. Mladenov, and A.J. Roberts. 2017. Intraflagellar transport dynein is autoinhibited by trapping of its mechanical and track-binding elements. *Nat Struct Mol Biol*. 24:461-468.

VanderWaal, K.E., R. Yamamoto, K. Wakabayashi, L. Fox, R. Kamiya, S.K. Dutcher, P.V. Bayly, W.S. Sale, and M.E. Porter. 2011. bop5 Mutations reveal new roles for the IC138 phosphoprotein in the regulation of flagellar motility and asymmetric waveforms. *Mol Biol Cell*. 22:2862-2874.

Vashishtha, M., Z. Walther, and J.L. Hall. 1996. The kinesin-homologous protein encoded by the Chlamydomonas FLA10 gene is associated with basal bodies and centrioles. *J Cell Sci*. 109 (Pt 3):541-549.

Viswanadha, R., E.L. Hunter, R. Yamamoto, M. Wirschell, L.M. Alford, S.K. Dutcher, and W.S. Sale. 2014. The ciliary inner dynein arm, I1 dynein, is assembled in the cytoplasm and transported by IFT before axonemal docking. *Cytoskeleton (Hoboken)*. 71:573-586.

Viswanadha, R., W.S. Sale, and M.E. Porter. 2017. Ciliary Motility: Regulation of Axonemal Dynein Motors. *Cold Spring Harb Perspect Biol*. 9.

Wakabayashi, K., S. Takada, G.B. Witman, and R. Kamiya. 2001. Transport and arrangement of the outer-dynein-arm docking complex in the flagella of Chlamydomonas mutants that lack outer dynein arms. *Cell Motil Cytoskeleton*. 48:277-286.

Wallmeier, J., H. Shiratori, G.W. Dougherty, C. Edelbusch, R. Hjeij, N.T. Loges, T. Menchen, H. Olbrich, P. Pennekamp, J. Raidt, C. Werner, K. Minegishi, K. Shinohara, Y. Asai, K. Takaoka, C. Lee, M. Griese, Y. Memari, R. Durbin, A. Kolb-Kokocinski, S. Sauer, J.B. Wallingford, H. Hamada, and H. Omran. 2016. TTC25 Deficiency Results in Defects of the Outer Dynein Arm Docking Machinery and Primary Ciliary Dyskinesia with Left-Right Body Asymmetry Randomization. *Am J Hum Genet*. 99:460-469.

Walther, Z., M. Vashishtha, and J.L. Hall. 1994. The Chlamydomonas FLA10 gene encodes a novel kinesin-homologous protein. *J Cell Biol*. 126:175-188.

Wang, Q., J. Pan, and W.J. Snell. 2006. Intraflagellar transport particles participate directly in cilium-generated signaling in Chlamydomonas. *Cell*. 125:549-562.

Wickstead, B., and K. Gull. 2007. Dyneins across eukaryotes: a comparative genomic analysis. *Traffic*. 8:1708-1721.

Wilson, N.F. 2008. Gametic cell adhesion and fusion in the unicellular alga Chlamydomonas. *Methods Mol Biol*. 475:39-51.

Wingfield, J.L., I. Mengoni, H. Bomberger, Y.Y. Jiang, J.D. Walsh, J.M. Brown, T. Picariello, D.A. Cochran, B. Zhu, J. Pan, J. Eggenschwiler, J. Gaertig, G.B. Witman, P. Kner, and K. Lechtreck. 2017. IFT trains in different stages of assembly queue at the ciliary base for consecutive release into the cilium. *Elife*. 6.

Wirschell, M., T. Hendrickson, and W.S. Sale. 2007. Keeping an eye on I1: I1 dynein as a model for flagellar dynein assembly and regulation. *Cell Motil Cytoskeleton*. 64:569-579.

Wirschell, M., F. Zhao, C. Yang, P. Yang, D. Diener, A. Gaillard, J.L. Rosenbaum, and W.S. Sale. 2008. Building a radial spoke: flagellar radial spoke protein 3 (RSP3) is a dimer. *Cell Motil Cytoskeleton*. 65:238-248.

Wirschell, M., H. Olbrich, C. Werner, D. Tritschler, R. Bower, W.S. Sale, N.T. Loges, P. Pennekamp, S. Lindberg, U. Stenram, B. Carlen, E. Horak, G. Kohler, P. Nurnberg, G. Nurnberg, M.E. Porter, and H. Omran. 2013. The nexin-dynein regulatory complex subunit DRC1 is essential for motile cilia function in algae and humans. *Nat Genet*. 45:262-268.

Witman, G.B., K. Carlson, J. Berliner, and J.L. Rosenbaum. 1972. *Chlamydomonas* flagella. I. Isolation and electrophoretic analysis of microtubules, matrix, membranes, and mastigonemes. *J Cell Biol*. 54:507-539.

Witman, G.B. 1975. The site of in vivo assembly of flagellar microtubules. *Ann N Y Acad Sci*. 253:178-191.

Witman, G.B. 1986. Isolation of *Chlamydomonas* flagella and flagellar axonemes. *Method Enzymol*. 134:280-290.

Wood, C.R., and J.L. Rosenbaum. 2014. Proteins of the ciliary axoneme are found on cytoplasmic membrane vesicles during growth of cilia. *Curr Biol*. 24:1114-1120.

Wren, K.N., J.M. Craft, D. Tritschler, A. Schauer, D.K. Patel, E.F. Smith, M.E. Porter, P. Kner, and K.F. Lechtreck. 2013. A differential cargo-loading model of ciliary length regulation by IFT. *Curr Biol*. 23:2463-2471.

Wu, C., J. Li, A. Peterson, K. Tao, and B. Wang. 2017. Loss of dynein-2 intermediate chain Wdr34 results in defects in retrograde ciliary protein trafficking and Hedgehog signaling in the mouse. *Hum Mol Genet*. 26:2386-2397.

Yamamoto, R., T. Yagi, and R. Kamiya. 2006. Functional binding of inner-arm dyneins with demembranated flagella of Chlamydomonas mutants. *Cell Motil Cytoskeleton*. 63:258-265.

Yamamoto, R., K. Song, H.A. Yanagisawa, L. Fox, T. Yagi, M. Wirschell, M. Hirono, R. Kamiya, D. Nicastro, and W.S. Sale. 2013. The MIA complex is a conserved and novel dynein regulator essential for normal ciliary motility. *J Cell Biol*. 201:263-278.

Yamamoto, R., J.M. Obbineni, L.M. Alford, T. Ide, M. Owa, J. Hwang, T. Kon, K. Inaba, N. James, S.M. King, T. Ishikawa, W.S. Sale, and S.K. Dutcher. 2017. Chlamydomonas DYX1C1/PF23 is essential for axonemal assembly and proper morphology of inner dynein arms. *PLoS Genet*. 13:e1006996.

Yang, P., and W.S. Sale. 1998. The Mr 140,000 Intermediate Chain of Chlamydomonas Flagellar Inner Arm Dynein Is a WD-Repeat Protein Implicated in Dynein Arm Anchoring. *Mol. Biol. Cell*. 9:3335-3349.

Yang, P., L. Fox, R.J. Colbran, and W.S. Sale. 2000. Protein phosphatases PP1 and PP2A are located in distinct positions in the Chlamydomonas flagellar axoneme. *J Cell Sci*. 113 (Pt 1):91-102.

Yang, P., C. Yang, and W.S. Sale. 2004. Flagellar radial spoke protein 2 is a calmodulin binding protein required for motility in Chlamydomonas reinhardtii. *Eukaryot Cell*. 3:72-81.

Yang, T.T., J. Su, W.J. Wang, B. Craige, G.B. Witman, M.F. Tsou, and J.C. Liao. 2015. Superresolution Pattern Recognition Reveals the Architectural Map of the Ciliary Transition Zone. *Sci Rep*. 5:14096.

Zariwala, M.A., H. Omran, and T.W. Ferkol. 2011. The emerging genetics of primary ciliary dyskinesia. *Proc Am Thorac Soc*. 8:430-433.

Zlatic, S.A., E.J. Grossniklaus, P.V. Ryder, G. Salazar, A.L. Mattheyses, A.A. Peden, and V. Faundez. 2013. Chemical-genetic disruption of clathrin function spares adaptor complex 3-dependent endosome vesicle biogenesis. *Mol Biol Cell*. 24:2378-2388.